


8-2017

Preclinical Development of Therapeutic Strategies Against Triple-Negative and Inflammatory Breast Cancer

Angie M. Torres-Adorno

Follow this and additional works at: https://digitalcommons.library.tmc.edu/utgsbs_dissertations

 Part of the [Cancer Biology Commons](#), [Cell Biology Commons](#), [Cellular and Molecular Physiology Commons](#), [Laboratory and Basic Science Research Commons](#), [Molecular Biology Commons](#), and the [Translational Medical Research Commons](#)

Recommended Citation

Torres-Adorno, Angie M., "Preclinical Development of Therapeutic Strategies Against Triple-Negative and Inflammatory Breast Cancer" (2017). *The University of Texas MD Anderson Cancer Center UTHealth Graduate School of Biomedical Sciences Dissertations and Theses (Open Access)*. 789.
https://digitalcommons.library.tmc.edu/utgsbs_dissertations/789

This Dissertation (PhD) is brought to you for free and open access by the The University of Texas MD Anderson Cancer Center UTHealth Graduate School of Biomedical Sciences at DigitalCommons@TMC. It has been accepted for inclusion in The University of Texas MD Anderson Cancer Center UTHealth Graduate School of Biomedical Sciences Dissertations and Theses (Open Access) by an authorized administrator of DigitalCommons@TMC. For more information, please contact digitalcommons@library.tmc.edu.

**PRECLINICAL DEVELOPMENT OF THERAPEUTIC STRATEGIES AGAINST
TRIPLE-NEGATIVE AND INFLAMMATORY BREAST CANCER**

by

Angie Marie Torres-Adorno, B.S.

APPROVED:

Naoto T. Ueno, M.D., Ph.D.
Advisory Professor

Bedrich L. Eckhardt, Ph.D.

Wendy A. Woodward, M.D., Ph.D.

Varsha V. Gandhi, Ph.D.

Peiying Yang, Ph.D.

APPROVED:

Dean, The University of Texas
MD Anderson Cancer Center UTHealth Graduate School of Biomedical Sciences

**PRECLINICAL DEVELOPMENT OF THERAPEUTIC STRATEGIES AGAINST
TRIPLE-NEGATIVE AND INFLAMMATORY BREAST CANCER**

A

DISSERTATION

Presented to the Faculty of

The University of Texas

MD Anderson Cancer Center UTHealth

Graduate School of Biomedical Sciences

in Partial Fulfillment

of the Requirements

for the Degree of

DOCTOR OF PHILOSOPHY

by

Angie Marie Torres-Adorno, B.S.

Houston, Texas

August, 2017

DEDICATION

This dissertation is dedicated to
my parents Luis A. Torres Quiñones and María M. Adorno Ríos,
to my siblings Magdaline M. and Luis A. Torres Adorno,
and to my heart's other half John K. Morrow.

Toda mi vida me sentí con la valentía de enfrentar los retos que encontraba en mi camino porque nunca me faltó el amor y apoyo incondicional de ustedes. Hoy, doy gracias una vez más porque aquí conmigo están, logrando junto a mí esta gran hazaña que tanto sacrificio tomó.

Nunca fue fácil estar lejos, pero siempre fue tan fácil sentirlos cerca de mí.

Los amo, y a ustedes les dedico mi disertación doctoral.

ACKNOWLEDGMENTS

First and foremost, I would like to thank my Ph.D. dissertation advisor, Dr. Naoto Tada Ueno, for always seeing and believing in the potential in me to grow as a scientist and human being. Your sincere guidance and support allowed me to learn and become an independent scientist, and I thank you for thrusting in me to lead two very impactful projects as part of your research team. Your kindness, passion and compassion have inspired me to grow in many aspects of my life.

I also thank my current and previous advisory committee members Dr. Bedrich L. Eckhardt, Dr. Wendy A. Woodward, Dr. Varsha V. Gandhi, Dr. Peiying Yang, Dr. James M. Reuben, Dr. Candelaria Gomez-Manzano, Dr. Dihua Yu, Dr. Oliver Bogler, Dr. Pierre McCrea, for their willingness to support me, their patience, and valuable input into my research projects and professional development in the cancer research field.

Additionally, I sincerely thank all the current and past members of the Ueno Lab, for their willingness to help me always, and for providing such an amicable and supportive environment all through my PhD degree development by been excellent colleagues and friends, especially to Dr. Jangsoon Lee, Dr. Xuemei Xie, Dr. Chandra Bartholomeusz, Dr. Bora Lim, Dr. Xiaoping Wang, Larry Coffey II, and Afsaneh Keyhani. I also thank great collaborators and friends that supported multiple aspects of my research, especially Dr. Heidi Vitrac for her time and support educating me about cell membrane fluidity and mass spectrometry analyses, Dr. Geoffrey Bartholomeusz for his support developing the synthetic-lethal siRNA screen, Dr. Yuan Qi for her expert biostatistics support, Mrs. Lin Tan for her support with mass spectrometry

analysis, Dr. Kandice Levental for contributing to the development of membrane fluidity imaging, and Drs. Robert Chapkin and Yang-Yi Fan for their effort and time helping me analyze fatty acid composition of tissue samples.

I would also like to thank my friends, with whom I have had such amazing times during my years of education, always supporting my goals and endeavors, and allowing for so many fun and memorable moments in my life. Thank you!

Finally, I thank my loving family, which have always been by my side all though the great, as well as challenging, moments of my life, my father Luis A. Torres, my mother María M. Adorno, my sister Magdaline M. Torres, and my brother Luis A. Torres. I also thank my heart's other half, John K. Morrow, for loving and supporting me for the last three years, and for filling my days with so much happiness. The unconditional love and support that you all gift me have been crucial for my success, and inspire me to be a better version of myself every day.

PRECLINICAL DEVELOPMENT OF THERAPEUTIC STRATEGIES AGAINST TRIPLE-NEGATIVE AND INFLAMMATORY BREAST CANCER

Angie Marie Torres-Adorno, B.S.

Advisory Professor: Naoto T. Ueno, M.D., Ph.D.

Triple-negative (TNBC) and inflammatory (IBC) breast cancer are the most aggressive forms of breast cancer, accounting for 20% and 10% of cancer-related deaths, respectively. Among IBC cases, 30% are additionally classified with TNBC molecular pathology, a diagnosis that significantly worsens patient's prognosis. The current lack of TNBC and IBC molecular understanding prevents the development of effective therapeutic strategies. To identify effective treatments, we explored aberrant apoptosis pathways and cell membrane fluidity as novel therapeutic targets.

We first identified an effective therapeutic strategy against TNBC and IBC by pro-apoptotic protein NOXA-mediated inhibition of the anti-apoptotic protein MCL1 following inhibition of histone deacetylases (HDAC) in combination with inhibition of the oncogenic MEK pathway. In breast cancer patients, low NOXA/high MCL1 tumor expression is indeed associated to poor survival outcomes, supporting the induction of NOXA expression, and subsequent inhibition of MCL1, for the treatment against TNBC and IBC.

Secondly, we investigated the role of an anti-inflammatory and non-toxic polyunsaturated fatty acid, eicosapentaenoic acid (EPA), for the development of a treatment strategy against TNBC and IBC. Through a synthetic-lethal siRNA high-throughput screen we identified inhibition of EPHA2, an oncogenic protein specifically associated to poor survival in

TNBC patients, to be the top candidate that enhanced EPA cytotoxicity against TNBC and IBC cells. Though functional assays, we identified combination EPA and EPHA2-inhibition to be an effective therapeutic strategy involving the induction of cell death via modulation of cell membrane fluidity by ABCA1 inhibition-mediated intracellular cholesterol accumulation in triple-negative IBC cells.

In summary, here we provide robust preclinical evidence that supports the Phase I clinical development of combination HDAC and MEK inhibitors, and of EPA and EPHA2-inhibition, for the treatment of patients with TNBC and IBC.

TABLE OF CONTENTS

Approval Page	i
Title Page	ii
Dedication	iii
Acknowledgments	iv
Abstract	vi
Table of contents	viii
List of illustrations	xii
List of tables.....	xvi
Abbreviations	xvii
CHAPTER 1: INTRODUCTION.....	1
1.1 Breast cancer.....	1
1.1.1 Breast cancer epidemiology.....	1
1.1.2 Breast cancer molecular subtypes.....	1
1.2 Triple-negative breast cancer	3
1.3 Inflammatory breast cancer.....	3
1.4 Standard of care for triple negative and inflammatory breast cancer	4
1.4.1 Experimental therapeutic approaches for TNBC and IBC	5
1.5 Limitations with current strategies and gaps in knowledge.....	6
1.6 Goal of the project	7
CHAPTER 2: MATERIALS AND METHODS	9
2.1 Breast cancer patient tumor expression analysis	9

2.2	Cell lines	10
2.3	Reagents and antibodies.....	12
2.4	Western blot analysis	13
2.5	Quantitative real-time PCR.....	14
2.6	Annexin V apoptosis assays.....	14
2.7	<i>In vivo</i> xenograft animal models.....	15
2.8	<i>In vitro</i> cell proliferation assay	16
2.9	Soft agar assay	17
2.10	Co-immunoprecipitation	17
2.11	Immunohistochemistry (IHC).....	18
2.12	TUNEL staining.....	18
2.13	Chromatin Immunoprecipitation.....	18
2.14	Synthetic-lethal siRNA screen.....	19
2.15	Cell lines with doxycycline-inducible genes	20
2.16	Xenograft tumor cell sorting	20
2.17	Membrane fluidity assay	21
2.18	Membrane fluidity imaging	22
2.19	Fatty acid analysis.....	22
2.20	Mass spectrometry EPA analysis.....	23
2.21	Cholesterol quantification	23
2.22	Statistical analysis	24

CHAPTER 3: IDENTIFICATION OF AN HDAC AND MEK INHIBITORS

COMBINATION STRATEGY AGAINST TNBC AND IBC	25
--------------------------------------------------------	-----------

3.1	Introduction.....	25
3.1.1	Epigenetic modulation in cancer	25
3.1.2	Histone deacetylase inhibitors.....	26
3.1.3	The BCL-2 family of proteins and apoptosis regulation.....	26
3.1.4	Oncogenic MEK/ERK pathway and TNBC.....	27
3.1.5	Gap in knowledge.....	27
3.2	Results.....	28
3.2.1	NOXA and MCL1 expression are molecularly and clinically relevant to entinostat and pimasertib treatment in IBC and TNBC.	28
3.2.2	Entinostat and pimasertib combination therapy synergize to inhibit the growth of aggressive breast cancer cells that overexpress NOXA after entinostat treatment.	36
3.2.3	NOXA and MCL1 play important roles in regulation of sensitization of IBC and TNBC cells to entinostat and pimasertib treatment.	44
3.2.4	Entinostat and pimasertib combination treatment suppresses tumorigenic potential <i>in vitro</i> and <i>in vivo</i> tumor growth in xenograft models of aggressive breast cancer.....	48
3.3	Discussion	55

CHAPTER 4: IDENTIFICATION OF A COMBINATIONAL THERAPY STRATEGY OF EICOSAPENTAENOIC ACID AND EPHA2-TARGETING AGAINST TN-IBC 59

4.1	Introduction.....	59
4.1.1	Inflammation in cancer.....	59
4.1.2	Inflammation in TN-IBC.....	59
4.1.3	Anti-inflammatory compounds against TN-IBC.....	60
4.1.3.1	Eicosapentaenoic acid (EPA)	60

4.1.4	Ephrin family of receptor tyrosine kinases	62
4.1.4.1	Ephrin type-A receptor 2 (EPHA2)	62
4.1.5	Gap in Knowledge.....	63
4.2	Results.....	64
4.2.1	Eicosapentaenoic acid reduces tumor growth in a TN-IBC xenograft model.....	64
4.2.2	Identification of EPHA2 as a clinically relevant target that can enhance EPA therapy against TN-IBC	64
4.2.3	EPHA2 therapy in combination with EPHA2 inhibition synergistically kills cells through induction of apoptosis.....	68
4.2.4	Combination treatment of EPA and EPHA2 inhibition modifies the cell membrane rigidity status and lipid structure of TN-IBC cell lines.....	77
4.2.5	The cholesterol exporter protein, ABCA1, is a critical mediator of apoptosis in TN-IBC cells response to EPA and EPHA2-inhibition therapy.	84
4.2.6	Inhibition of EPHA2 enhances the therapeutic action of EPA in TN-IBC xenograft models	92
4.3	Discussion	99
CHAPTER 5: CONCLUSIONS AND FUTURE DIRECTIONS.....		103
5.1	Major findings.....	103
5.2	Significance.....	104
5.3	Future directions	105
BIBLIOGRAPHY		109
VITA.....		133

LIST OF ILLUSTRATIONS

Figure 1. Estimated breast cancer incidence and death rates for 2017	1
Figure 2. Clinical appearance of an Inflammatory Breast Cancer patient	4
Figure 3. Illustrated diagram of major topics of interest to be evaluated in this study.....	7
Figure 4. Diagram of histone deacetylases activity in the removal of acetyl groups from histones and silencing of gene expression	25
Figure 5. Entinostat induces increased phosphorylation/activation of the pro-survival ERK pathway in IBC cell lines	31
Figure 6. High MCL1/low NOXA co-expression is associated with poor outcome in breast cancer patients.....	32
Figure 7. Increased <i>NOXA</i> gene promoter acetylation levels following entinostat treatment	33
Figure 8. Entinostat treatment selectively increases expression of <i>NOXA</i> mRNA in TNBC and IBC cell lines.....	34
Figure 9. Basal MCL1 protein expression is present in most TNBC and IBC cell lines.....	35
Figure 10. Entinostat and pimasertib combination treatment enhanced cell death in IBC and TNBC cell lines that overexpressed NOXA after entinostat treatment	38
Figure 11. TNBC and IBC cell lines overexpressing NOXA after entinostat treatment exhibit synergy of combination treatment with pimasertib	39
Figure 12. Mitochondrial apoptosis activated following combination therapy	41
Figure 13. Low-NOXA-inducible HCC1806 cell line did activated mitochondrial apoptosis after entinostat and pimasertib single or combination treatments	42
Figure 14. NOXA binds to MCL1 following combination entinostat and pimasertib treatment	43
Figure 15. NOXA expression plays an important role in the regulation of sensitization of TNBC and IBC cells to treatment.....	46

Figure 16. MCL1 protein expression and activity have a significant role in the sensitivity of TNBC and IBC cells to pimasertib and entinostat combination treatment.....	47
Figure 17. Entinostat and pimasertib combination treatment inhibits colony formation <i>in vitro</i>	49
Figure 18. Entinostat and pimasertib combination treatment inhibits tumor growth <i>in vivo</i>	50
Figure 19. Higher and lower doses of entinostat and pimasertib combination treatment induce tumor regression in IBC and TNBC xenograft models.....	51
Figure 20. No toxicity was observed after entinostat and pimasertib single and combination treatments <i>in vivo</i>	52
Figure 21. Combination entinostat and pimasertib therapy inhibits proliferation, and promotes apoptosis, <i>in vivo</i>	53
Figure 22. Entinostat and pimasertib combination treatment promotes NOXA-mediated apoptosis and decreased expression of MCL1	54
Figure 23. Diagram of EPA activity in cell membrane and intracellular pathways	61
Figure 24. EPA (Vascepa) formulated diet equivalent to daily human dose.....	65
Figure 25. Eicosapentaenoic acid reduced tumor growth in a preclinical model of TN-IBC	66
Figure 26. Diagram of functional high-throughput siRNA screen identifies candidate genes sensitizing TN-IBC cells to EPA therapy	67
Figure 27. Top significant targeting candidates enhance TN-IBC cells sensitivity to EPA.....	70
Figure 28. Basal EPHA2 protein expression is present in most TN and TN-IBC cell lines	71
Figure 29. EPHA2 mRNA expression is predominantly higher in TNBC cell lines.....	72
Figure 30. EPHA2 is a clinically significant target that enhances TN-IBC cells sensitivity to EPA.....	73
Figure 31. Diagram of gene-silencing, and drug targeted, inhibition of EPHA2 strategies to be tested in combination with EPA treatment	74

Figure 32. Gene silencing and targeted EPHA2 inhibition acts synergistically with EPA against TN-IBC in vitro.....	75
Figure 33. EPA in combination incorporates in the plasma membrane, and induces the internalization of EPHA2.....	79
Figure 34. Combination treatment of EPA and EPHA2-inhibition increases plasma cell membrane rigidity on TN-IBC cell lines	80
Figure 35. Phosphatidylcholine plasma membrane lipid profiling of SUM149PT cells after EPA and EPHA2-targeting treatments	81
Figure 36. Combination treatment of EPA and EPHA2-inhibition modifies plasma cell membrane lipid composition of TN-IBC cell lines.....	82
Figure 37. Cholesterol accumulates in plasma membrane fraction following EPA and EPHA2-inhibition treatment.....	83
Figure 38. Diagram for cholesterol modulation techniques used to modify cell membrane fluidity.....	84
Figure 39. Modulation of cholesterol concentration in the membrane fraction of TN-IBC cells	85
Figure 40. Accumulation of intracellular cholesterol plays a role in the induction of apoptosis following combination EPA and EPHA2-targeting therapy in TN-IBC cells.....	86
Figure 41. Diagram of main regulators of cellular cholesterol homeostasis	87
Figure 42. ABCA1 and SREBP-2 are inhibited following combination therapy of EPA and EPHA2-inhibition in TN-IBC cells.....	89
Figure 43. ABCA1 modulation is responsible for the induction of apoptosis following combination EPA and EPHA2-targeting therapy in TN-IBC cells	90
Figure 44. Cholesterol accumulation induces apoptosis following ABCA1-siRNA inhibition ..	91
Figure 45. Establishment of inducible shRNA-RPHA2 TN-IBC cell lines in xenograft models	94

Figure 46. Gene silencing inhibition of EPHA2 acts synergistically with EPA against TN-IBC tumor xenografts	95
Figure 47. Inhibition of EPHA2 following gene silencing and EPA treatment inhibits ABCA1 in TN-IBC tumor xenografts.....	96
Figure 48. Dasatinib EPHA2-targeted inhibition enhances EPA therapy against TN-IBC tumor xenografts.....	97
Figure 49. Inhibition of EPHA2 following dasatinib and EPA treatment inhibits ABCA1 and promotes apoptosis in TN-IBC tumor xenografts.....	98
Figure 50. Summary of mechanistic action of EPA in combination with EPHA2-targeting via ABCA1 inhibition in TN-IBC cells	102
Figure 51. Diagram of major mechanisms of synergy involved in our newly discovered combinational therapies against TNBC and IBC.....	103
Figure 52. Schema of clinical trial for entinostat in combination with selumetinib including details of biological sample collection for biomarker analysis.....	106
Figure 53. Summarized overview of clinical trials and biomarker development for proposed combination therapy strategies in patients with invasive breast cancers	108

LIST OF TABLES

Table 1. Breast cancer cell lines' molecular receptor status and TNBC subtype classification .	11
Table 2. Effect of entinostat on the expression of apoptosis-related gene pathways	30
Table 3. Candidate genes significantly affecting SUM149 TN-IBC cells sensitivity to EPA	69
Table 4. IC ₅₀ values of breast cancer cell lines following EPA and dasatinib single and combination treatments	76

ABBREVIATIONS

ABCA1	ATP-binding cassette sub-family A member 1
BRCA	Breast cancer type 1 susceptibility protein
COX2	Prostaglandin G/H synthase 2
DFS	Disease free survival
DMFS	Distant metastasis free survival
Dox	Doxycycline
EPA	Eicosapentaenoic acid
ER	Estrogen receptor
ERK	Mitogen-activated protein kinase 3
HDAC	Histone deacetylases
HER2	Receptor tyrosine-protein kinase erbB-2
HMGCR	3-hydroxy-3-methylglutaryl-coenzyme A reductase
IBC	Inflammatory breast cancer
Ki67	Proliferation marker protein Ki-67
LDLR	Low-density lipoprotein receptor
MβCD	Methyl- β -cyclodextrin
MCL1	Induced myeloid leukemia cell differentiation protein Mcl-1
MEK	Dual specificity mitogen-activated protein kinase kinase 1
mRNA	Messenger ribonucleic acid
NOXA	Phorbol-12-myristate-13-acetate-induced protein 1
OS	Overall survival
PC	Phosphatidylcholine
PgR	Progesterone receptor
SREPB-2	sterol regulatory element-binding protein 2
siRNA	Small interfering ribonucleic acid
TNBC or TN	Triple-negative breast cancer
TN-IBC	Triple-negative inflammatory breast cancer
TP53	Cellular tumor antigen p53

CHAPTER 1: INTRODUCTION

1.1 Breast cancer

1.1.1 Breast cancer epidemiology

In the United States, breast cancer is the most commonly diagnosed cancer in women, accounting for 252,710 new cases in 2017 (1). Breast cancer is also the second most common cause of cancer related death in women, with an estimated 40,610 deaths, or 15%, in 2017 (Figure 1) (1). While breast cancer death rates have decreased by 32% over the last 90 years, thanks to the continued research and development of therapeutic strategies, its incidence has seen a rise of about 20%, demonstrating an urgent need to continue exploring new therapeutic approaches with increased efficacy against breast cancer.

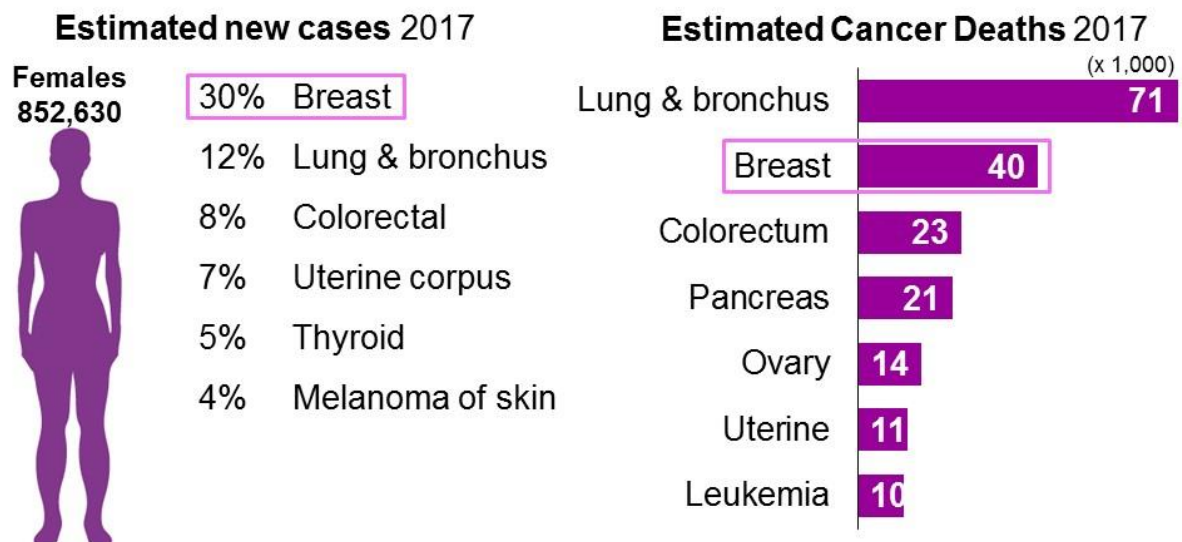


Figure 1. Estimated breast cancer incidence and death rates for 2017.

1.1.2 Breast cancer molecular subtypes

Breast cancer is characterized by its heterogeneity among patients. Breast cancer subtyping is often performed by the assessment of expression of three main proteins: estrogen

receptor (ER), progesterone receptor (PgR), and HER2/*neu* (receptor tyrosine-protein kinase erbB-2, HER2). Gene expression-based techniques, in particular by the use of the PAM50 gene set (2), are often used to identify breast cancer subtypes, although subtyping by use of protein panels of immunohistochemical markers are still widely used in the clinic. Unfortunately, discrepancies between these two subtyping methods exist (2), which leads to different treatment decisions. There are four major intrinsic molecular subtypes of breast cancer, based on their respective protein and gene signatures: Luminal A, Luminal B, HER2-enriched, and Triple-negative (basal-like) (3, 4). Luminal A subtype is characterized by its hormone receptor (ER, 92% agreement between PAM50 and IHC subtyping; and/or PgR, 94% agreement) positivity, together with negativity of the HER2 growth receptor, and low levels of the proliferation marker Ki67 (5). Luminal A breast cancers tend to have the best prognosis due to their inhibited growth rate (6). Luminal B breast cancer subtype is similarly hormone receptor positive (ER, 92% agreement; and/or PgR, 74% agreement), but could be either HER2 receptor positive or negative, with high levels of Ki67 (7). Luminal B breast cancers tend to grow at a faster rate compared to Luminal A, together with worse prognosis (6). HER2-enriched breast cancers are positive for the HER2 receptor, but negative for hormone receptors (77% agreement) (8). This subtype tends to grow at a faster rate compared to luminal subtypes, therefore having a worsened prognosis (9), but HER2 targeted treatment strategies are often highly effective (10). Triple-negative breast cancers are negative for all three growth receptors: hormone (ER and PgR), and HER2 (5, 9), are mainly comprised of basal-like (57% agreement) and HER2 (30% agreement) subtypes. Even with its lack of receptor expression, this subtype is characterized by its high rate of growth, migration, and invasion compared to all other breast cancer subtypes (11).

1.2 Triple-negative breast cancer

Triple-negative breast cancer (TNBC or TN), representing 10-17% of all breast carcinomas, is diagnosed molecularly in terms of its negative ER, PgR, and HER2 receptor status, and is associated with lower survival and a higher risk of local and regional relapse, compared to hormone (ER/PgR)-positive and HER2-positive breast cancers (12, 13). TNBC tumors are classified as basal-like subtypes, due to their expression profiles resembling those of basal epithelial cells with a high expression of basal markers (e.g., keratins 5, 6, 14, 17, EGFR) and proliferation-related genes (5). Approximately 60 to 90 % of basal tumors are triple-negative cases, allowing for the association of basal and TNBC tumors as similar entities (14). This subtype is common in younger women carrying *BRCA1* and *TP53* gene mutations, being even more common among African-American women and pre-menopausal individuals (3, 15). TNBC is a highly heterogeneous disease characterized by its strong metastatic potential and poor prognosis, which can be further sub-classified based by its canonical pathways among the subtypes: basal-like1, basal-like 2, immunomodulatory, mesenchymal-like, mesenchymal stem-like, and luminal androgen receptor (16).

1.3 Inflammatory breast cancer

Inflammatory breast cancer (IBC) is a rare clinical diagnosis representing 1-5% of all breast carcinomas, but disproportionately associated with 10% of breast cancer related deaths (17, 18). Instead of the appearance of a distinct lump, the IBC clinical onset consists of redness (erythema), swelling (edema), pitted skin (peau d'orange), or inverted nipple of the breast, caused by the buildup of lymph in the ducts and skin as a result of cancer cells blockage (tumor emboli) of the lymph vessels, preventing normal lymph flow (**Figure 2**) (19). Similar to TNBC, IBC is characterized by its strong metastatic potential and associated poor prognosis. Among all

breast cancer molecular subtypes, IBC has a worse prognosis when compared to non-inflammatory forms of breast cancer (non-IBC) cases (20). TNBC accounts for about 30% of IBCs molecular subtype, which is a significantly higher proportion when compared to non-TNBCs (17, 21). There is a theory in the breast cancer field that this high percentage of TNBC may be the reason that IBC has been associated with a more aggressive clinical course and decreased breast cancer-specific and overall survival (22, 23).



Figure 2. Clinical appearance of an Inflammatory Breast Cancer patient.

1.4 Standard of care for triple negative and inflammatory breast cancer

Among the triple-negative status of TNBC, conventional targeted therapies are ineffective, with the current standard care of cytotoxic chemotherapy followed by surgery displaying moderate efficacy with a 5-year overall survival of approximately 80% (24). Although TNBC has been observed to be sensitive to conventional chemotherapies, several studies have shown that the poor prognosis for TNBC is mainly due to the lack of additional treatment options available (10).

The standard treatment for IBC consists of chemotherapies known as anthracyclines, and targeted therapies when applicable (HER2-positive cases), followed by surgery and radiation therapy, in this specific order. As the most aggressive form of breast cancer, even after multidisciplinary treatment, the 5-year overall survival of IBC is only 30% to 50% (25, 26). Due to the lack of patient samples for this rare disease, molecular studies have failed to identify specific molecular signatures that could predict treatment response, survival, or therapeutic targets (27-29). Nevertheless, despite the relatively small sample sizes available, a gene expression profile study of IBC patients in correlation with response to neoadjuvant chemotherapy was able to show that response to neoadjuvant chemotherapy in IBC was linked to immunity-related processes, providing evidence for a possible mechanism to predict pathological complete response (30). There has been an improvement in IBC diagnosis and staging due to significant advances in imaging, such as digital mammography, magnetic resonance imaging, and positron emission tomography-computed tomography, among others, increasing survival to approximately 40%, which is still a relatively low rate (31, 32). Continued investigation into significant molecular characteristics as well as effective therapeutic strategies remains a necessity.

1.4.1 Experimental therapeutic approaches for TNBC and IBC

Multiple experimental approaches are currently being explored for the treatment of these aggressive types of breast cancer, triple-negative and inflammatory. In IBC, molecular targets in vasculolymphatic processes (angiogenesis, lymphangiogenesis, and vasculogenesis) have demonstrated greater potential than in non-IBC (33, 34). Although loss of E-cadherin is a hallmark of epithelial-to-mesenchymal transition and may correlate with the promotion of metastasis, paradoxically, E-cadherin is overexpressed in IBC through an unknown mechanism

(35, 36). Others are currently investigating whether targeting EGFR and HER2 (which are overexpressed in about 60% of IBC tumors and associated with rapid tumor growth and metastasis via activation of the AKT and ERK/MEK oncogenic pathways), may aid in the development of effective targeted therapeutic strategies in IBC (37-39). In our research group, inhibition of histone deacetylases (HDACs) has additionally been explored for its effects on HER2/EGFR inhibitors as a therapeutic approach against HER2-overexpressing IBC (40).

In TNBC, new approaches involving the use of antiangiogenic agents as neoadjuvants to pre-operative chemotherapies have demonstrated improved patient prognosis and likelihood of pathological complete response (pCR), compared to patients with other breast cancer subtypes (41). Large biomarker programs are ongoing to identify TNBC subgroups that could have an increased benefit from such therapies (42). Targeted therapies involving inhibition of HDACs, mammalian target of rapamycin (mTOR), and growth factors such as fibroblast, epithelial and vascular endothelial growth factor receptors are currently being clinically tested in TNBC, showing insufficient improvement in patients' outcomes (43-46).

1.5 Limitations with current strategies and gaps in knowledge

To date, IBC and TNBC are challenges for both patients and biomedical professionals due to their poor prognoses and lack of significantly effective treatments or targeted therapy options, contributing to high mortality rates compared to other breast cancer subtypes. The main challenges with the current therapeutic strategies reside in the acquired resistance, recurrence, and high level of invasion/metastasis at time of diagnosis on IBC and TNBC patients (47). To address these issues, combination therapies, together with in-depth analysis of potential biomarkers associated with disease aggressiveness or treatment response in patients, have been

in development, but these still have not provided evidence of complete effectiveness against TNBC and IBC (29, 48). Therefore, it is essential to continue exploring potential combinational treatment strategies as well as molecular and physiological cellular mechanisms that are determinants of disease aggressiveness and response to treatments, potentially providing the identification of therapeutic strategies that are effective for the treatment of IBC and TNBC.

1.6 Goal of the project

In this project, our goal is to discover new physiological and molecular mechanisms contributing to TNBC and IBC aggressiveness and to identify novel combination therapy strategies with enhanced efficacy (**Figure 3**). Therefore, we hypothesized that combination

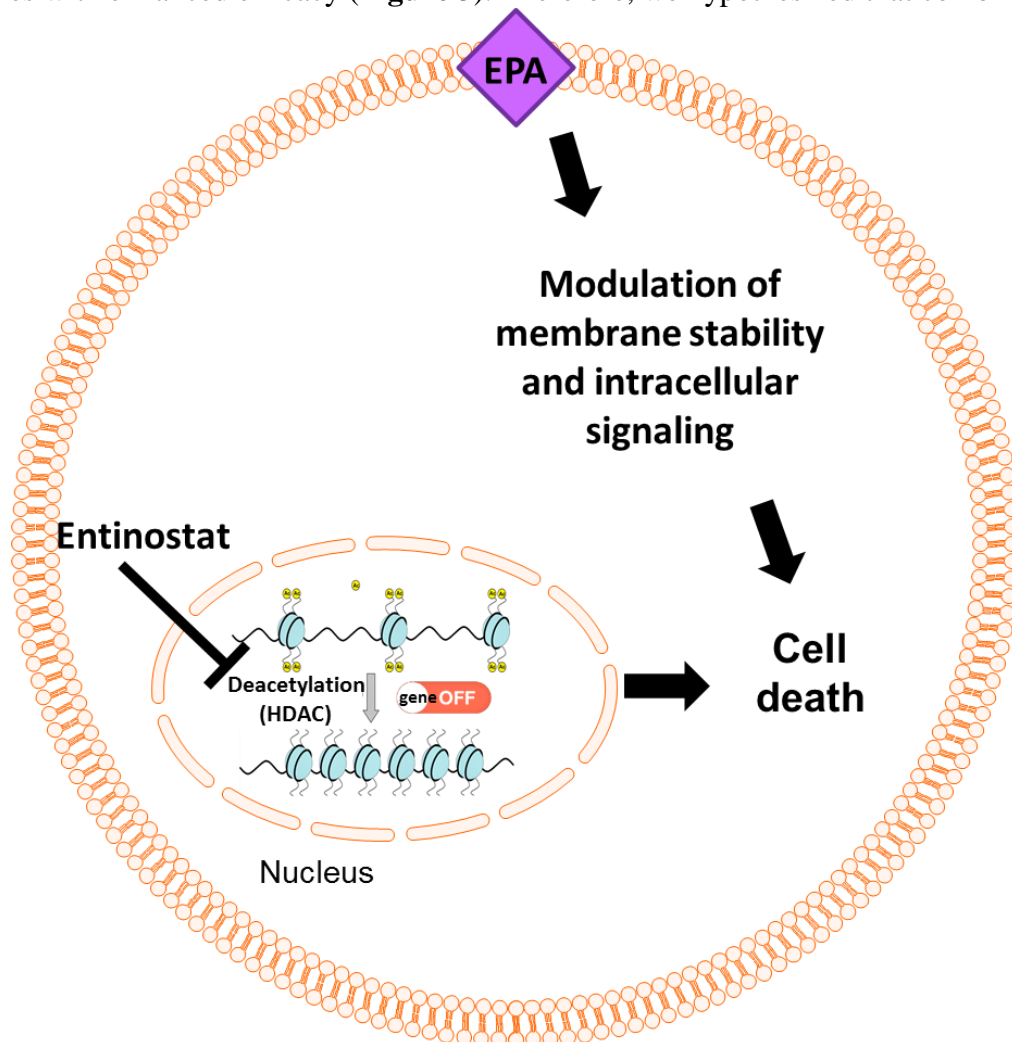


Figure 3. Illustrated diagram of major topics of interest to be evaluated in this study.

therapy strategies targeting tumor promoting factors would have enhanced efficacy against TNBC and IBC compared to monotherapies. First, we evaluated molecular mechanisms associated with the epigenetic modulation of Histone Deacetylases (HDACs), which are critical regulators of gene expression commonly disrupted in cancer cells, including IBC and TNBC, which are associated with cancer progression. We evaluated HDACs by use of an HDAC inhibitor, entinostat, in association with apoptosis induction in TNBC and IBC.

Additionally, we investigated the use of an anti-inflammatory omega-3 polyunsaturated fatty acid, eicosapentaenoic acid (EPA), as a potential strategy for the therapy of TNBC and IBC. Inflammation plays an important role in tumor development and progression, representing an important factor to target for effective cancer therapies. EPA has been linked to modifications in cell membrane physiology as well as destabilization of intracellular pathways associated with inflammation, which subsequently contributes to increased cytotoxic properties in cancer cells and decreased tumor proliferation.

My in-depth evaluation of the association of HDACs and inflammation contributions to IBC and TNBC cancer progression, as well as the efficacy of their targeting to apoptosis induction, provided new knowledge for TNBC and IBC development. Additionally, the evidence discovered through these studies served as a translational base supporting the development of clinical trials against the two most aggressive types of breast cancer.

CHAPTER 2: MATERIALS AND METHODS

2.1 Breast cancer patient tumor expression analysis

We analyzed the World IBC Consortium dataset that contains Affymetrix GeneChip (HG133 series) RNA hybridization profiles of 389 breast cancer patient samples, which include 137 IBC cases and 105 TNBC cases, as previously described (49). Briefly, the IBC cases included locally advanced (American Joint Committee on Cancer [AJCC] stage III) and metastatic (AJCC stage IV) cases. The non-IBC cases included both early-stage disease (AJCC stages I and II) and advanced-stage disease (locally advanced, AJCC stage III; and metastatic, AJCC stage IV). Information on data processing, normalization, and analyses has been previously reported (30). Regression models were used to delineate changes in *NOXA/PMAIP1* (204286_s_at) and *MCL1* (214056_at) gene expression. P-values, corrected for multiple comparisons, were considered significant only if the false discovery rate was smaller than 0.25.

We utilized the BreastMark algorithm to identify associations with disease progression and *EPHA2* expression. Developed by the Molecular Therapeutics for Cancer, Ireland (MTCI) at Dublin University (Glasnevin, Dublin) (50), this algorithm integrates mRNA gene expression and survival data for evaluation of genes that are significantly associated with disease-free survival (DFS) in breast cancer and its molecular subtypes. The algorithm contains gene expression data from 26 datasets on 12 different microarray platforms corresponding to approximately 17,000 genes in up to 4,738 samples, as well as detailed clinical data, allowing for correlation of subject outcome with gene expression, as previously described (50). We specifically evaluated the *EPHA2* mRNA expression in basal (TNBC) tumor subtypes as determined by the PAM50 molecular classifier (11).

2.2 Cell lines

Human breast cancer cell lines BT-549, SUM185PE, MDA-MB-157, MDA-MB-453, MDA-MB-231, HCC70, MDA-MB-468, MDA-MB-436, HCC1806, HCC1937, and Hs578T were purchased in 2011 from American Type Culture Collection (ATCC, Manassas, VA); SUM149PT, SUM159PT, and SUM190PT cells in 2011 from Asterand Bioscience, Inc. (Detroit, MI); and HCC3153 in 2013 from UT Southwestern Medical Center (Dallas, TX). KPL-4 cells were a kind gift in 2008 from Dr. Junichi Kurebayashi (Kawasaki Medical School, Kawasaki, Japan), IBC-3 cells from Dr. Wendy Woodward, and BCX010 cells were generously donated for this study by Dr. Funda Meric-Bernstam (The University of Texas MD Anderson Cancer Center, Houston, TX). HCC1806, MDA-MB-231, MDA-MB-468, MDA-MB-436, MDA-MB-157, MDA-MB-453, Hs578T, HCC70, and KPL-4 cells were maintained in Dulbecco's modified Eagle's medium/F12 medium (GIBCO) supplemented with fetal bovine serum (FBS; 10%) and penicillin-streptomycin (100 units/mL). SUM149PT, SUM190PT, SUM185PE, SUM159PT, BCX010 and IBC-3 cells were maintained in F12 medium (GIBCO) supplemented with FBS (5%), penicillin-streptomycin (100 units/mL), insulin (5 µg/mL), and hydrocortisone (1 µg/mL). BT-549, HCC1937, and HCC3153 cells were maintained in RPMI 1640 medium (GIBCO) supplemented with FBS (10%) and penicillin-streptomycin (100 units/mL). SUM190PT, SUM149PT, IBC-3, BCX010 and KPL-4 are IBC cell lines (51, 52). All cell lines were passaged for up to 20 times after thawing. Details about molecular receptor status and TNBC subtype classification can be found in **Table 1** (16). All used cell lines were authenticated by genotyping through MD Anderson Cancer Center's Characterized Cell Line Core Facility, and routinely tested for mycoplasma contamination using MycoAlert™ (Lonza, Allendale, NJ).

Cell line	Receptor status			TNBC subtype
	ER	PR	HER2	
HCC1806	-	-	-	BL
HCC1937	-	-	-	BL
HCC3153	-	-	-	BL
HCC70	-	-	-	BL
MDA-MB-468	-	-	-	BL
BCX010 *	-	-	-	BL
SUM149PT *	-	-	-	BL
MDA-MB-453	-	-	-	LAR
SUM185PT	-	-	-	LAR
BT-549	-	-	-	M
Hs578T	-	-	-	M
MDA-MB-157	-	-	-	M
MDA-MB-231	-	-	-	M
MDA-MB-436	-	-	-	M
SUM159PT	-	-	-	M
IBC-3 *	-	-	+	N/A
KPL-4 *	-	-	+	N/A
SUM190PT *	-	-	+	N/A

Table 1. Breast cancer cell lines' molecular receptor status and TNBC subtype classification. Sources for molecular receptor status, TNBC subtypes, and IBC classification: Asterand Bioscience, Inc. ER: estrogen receptor; PR: progesterone receptor; HER2: Human epidermal growth factor receptor 2; BL: basal-like; M: mesenchymal; LAR: luminal androgen receptor; +, positive status; -, negative status; *, IBC diagnosis; N/A, not applicable.

2.3 Reagents and antibodies

Entinostat (SNDX-275) was provided by Syndax Pharmaceuticals, Inc. Pimasertib (AS703026) was provided by EMD Serono, Inc. We obtained anti-NOXA (EMD Millipore, Billerica, MA), anti-MCL1 (R&D Systems, Minneapolis, MN, or Thermo Fisher Scientific, Waltham, MA), anti-PUMA, anti-BIM, anti-BAK, anti-BAX, anti-cleaved caspase 3, anti-cleaved caspase 9, and anti-Ki67 (Cell Signaling Technology, Beverly, MA), anti- α -tubulin (clone B-5-1-2; Sigma-Aldrich), and anti-horseradish peroxidase-conjugated antibodies (Thermo Scientific, Rockford, IL). The following small interfering RNAs (siRNAs) targeting NOXA were purchased from Sigma-Aldrich (St Louis, MO) and used for depletion of NOXA: SASI_Hs01_00136187, SASI_Hs01_00136188, SASI_Hs01_00136189, and SASI_Hs01_00136192. Knockdown efficacy of pooled siRNAs was tested by immunoblotting. Scrambled siRNA was purchased from Thermo Fisher Scientific (ON-TARGETplus non-targeting control pool, catalog number D-001810). The following expression vectors were purchased from GeneCopoeia (Rockville, MD): OmicsLink pReveiver-M77 expression clone NOXA (EX-I0491-M77), MCL1 (EX-G0192-M77), and Control (EX-EGFP-M77).

Eicosapentaenoic acid (EPA) and cholesterol powder bio-reagent suitable for cell culture were purchased from Sigma-Aldrich (St Louis, MO). Doxycycline was purchased from Research Products International (Mount Prospect, IL). Dasatinib was purchased from Selleck Chemicals (Houston, TX). Methyl- β -cyclodextrin (M β CD) was purchased from Santa Cruz Biotechnology (Santa Cruz, CA). All *in vitro* assays were performed after treatments for 24-48 hour with EPA (IC₂₀: 50 μ M), doxycycline (Dox, 1-3 μ g/mL), dasatinib (IC₂₀: 0.3 μ M), cholesterol (1 mM), Methyl- β -cyclodextrin (4 mM), or rosuvastatin (2.5 μ M).

We obtained anti-EPHA2, anti-phosphorylated EPHA2, anti-SRC, anti-phosphorylated SRC, anti-cleaved caspase 3, and anti-Ki67 (Cell Signaling Technology, Beverly, MA), anti-IgG-PE, anti-EPHA2-PE, anti-IgG-APC, anti-EPHA2-APC, anti-ABCA1 (Novus Biologicals, Littleton, CO), anti-SREBP2 (R&D Systems, Minneapolis, MN), anti-HMGCR (Thermo Fisher Scientific, Waltham, MA), anti-LDLR (Abcam, Cambridge, MA), anti- α -tubulin, anti- β -actin (Sigma-Aldrich), and anti-horseradish peroxidase-conjugated antibodies (Thermo Scientific, Rockford, IL). The following small interfering RNAs (siRNAs) targeting EPHA2 and ABCA1 were purchased from Sigma-Aldrich (St Louis, MO) and used for depletion of EPHA2: SASI_Hs01_00026514, SASI_Hs01_00026516, and SASI_Hs01_00026517; and ABCA1: SASI_Hs01_00129036, SASI_Hs01_00129036, and SASI_Hs01_00129038. Knockdown efficacy of pooled siRNAs was tested by immunoblotting. Scrambled siRNA control was purchased from Thermo Fisher Scientific (ON-TARGETplus non-targeting control pool, catalog number D-001810). The following expression vectors were purchased: Human EPHA2 and control (pLOC-GFP) (GE Healthcare Biosciences, Pittsburgh, PA), pCMV3-untagged expression clone ABCA1 (HG11924-UT), and control (pCMV3-GFP) (Sino Biologicals Inc., North Wales, PA). These were transfected into TN-IBC cells following manufacturer's instructions.

2.4 Western blot analysis

Total protein extracts were prepared using cold lysis buffer (50 mM Tris-HCl, pH 7.4, 1% NP-40, 150 mM NaCl, 10% glycerol, 1.5 mM MgCl₂, 1 mM EDTA, and phosphatase/protease inhibitors). Equal amounts of protein (15 to 20 μ g for each sample) were resolved by SDS-PAGE gel. Membranes were incubated with antibodies of interest overnight.

Signals were detected using an Odyssey IR imaging system (LI-COR Biosciences, Lincoln, NE) or chemiluminescent substrates (Thermo Scientific).

2.5 Quantitative real-time PCR

Total RNA was purified using the PureLink® RNA Mini Kit (Invitrogen), and real-time qRT-PCR was performed using the iScript™ One-Step RT-PCR Kit with SYBR® Green (Bio-Rad, Hercules, CA) according to the manufacturer's instructions, after treatment with entinostat (1 µM). Equal amounts of total RNA (15 ng for each sample) were mixed, and target genes were amplified with a specific primer set using the CFX96Touch™ Real-Time PCR Detection System (Bio-Rad). The following primers (Sigma-Aldrich) were used for detection of NOXA: 5'-CCAGCAGAGCTGGAAGTCGAGTG-3' (forward), and 5'-TGCAGTCAGGTTCTGAGCAGAAG-3' (reverse). 7SL scRNA (NR_002715.1) levels were used as an endogenous control; the following primers were used: 5'-ATCGGGTGTCCGCACTAAGTT-3' (forward), and 5'-CAGCACGGGAGTTTTGACCT-3' (reverse). The real-time PCR data were analyzed by comparative threshold cycle method using the iCycler CFX96 analyzer software (Bio-Rad).

2.6 Annexin V apoptosis assays

Apoptosis was measured with PE or APC Annexin V supplemented with 7AAD (BD Biosciences, San Jose, CA), or with Annexin V-green (Essen Bioscience, Ann Arbor, MI). Briefly, after treatment for 48 hours, apoptosis induction was quantified by flow cytometry analysis (after incubation with Annexin V-PE or -APC), or by IncuCyte® live cell analysis system (after incubation with Annexin V-green), according to the manufacturer's instructions.

2.7 *In vivo* xenograft animal models

Animal studies were approved by the IACUC and MD Anderson Animal Care and Use Committee. For the HDAC and MEK inhibitors studies, female athymic homozygous *nu/nu* mice, age 4-6 weeks old, were purchased from MD Anderson's Department of Experimental Radiation Oncology for the SUM190PT, SUM149PT, and MDA-MB-231 xenograft experiments. Mice were housed under pathogen-free conditions and treated in accordance with NIH guidelines. To establish breast cancer xenografts, SUM190PT (2×10^6 cells/100 μ L), SUM149PT (5×10^6 cells/100 μ L), or MDA-MB-231 (5×10^6 cells/100 μ L) cell suspensions were injected into one site in the abdominal mammary fat pad of each mouse. We observed 100% tumor incidence for all three cell lines. Drug treatments via daily oral gavage started when the tumors were approximately 100-150 mm³. We used 0.5% (w/v) methyl cellulose 400 solution (Wako Pure Chemical Industries, Ltd., Osaka, Japan) plus 0.25% Tween 20 as drugs vehicle. Tumor volume [$V = 0.5 \times (L \times W^2)$] and body weight were measured twice weekly. Drug treatment continued for 28 days (SUM190PT), 56 days (SUM149PT), or 42 days (MDA-MB-231), and then mice were euthanized. Tumor tissues were collected, sectioned and preserved both by flash freezing and paraffin block embedding for further analysis.

To study the antitumor efficacy of EPA therapy animal studies, female immunodeficient NOD SCID gamma (NSG) mice (NOD.*Cg-Prkdc^{scid} Il2rg^{tm1Wjl}/SzJ*, Jackson Laboratory, Bar Harbor, ME), aged 4-6 weeks, were purchased from MD Anderson's Department of Experimental Radiation Oncology for xenograft experiments. Mice were housed under pathogen-free conditions and treated in accordance with NIH guidelines. To establish breast cancer xenografts, SUM149PT (5×10^5 cells/100 μ L), or BCX010 (5×10^5 cells/100 μ L) cell suspensions were injected into one site in the fourth inguinal mammary fat pad of each mouse.

We observed 100% tumor incidence for all cell lines. Drug treatments started when the tumors were approximately 100-150 mm³; at this point mice were randomized among experimental treatment groups (N = 9 to 10 per group). EPA was administered *ad libitum* through customized AIN-76A mice diets (Research Diets Inc., New Brunswick, NJ) containing the FDA-approved Vascepa (purified EPA) at doses equivalent to the maximum (4 g) and half (2 g) human daily recommended doses; equivalent to 6 g and 3 g of Vascepa per kg of mice diet verified by chromatographic fatty acid analysis. These doses are equivalent to mice EPA daily intakes of 0.8 g/kg and 0.4 g/kg, considering an average daily food intake of 3.5 g, and average mice weight of 25 g. Doxycycline (2 mg/mL) water containing 2% sucrose was provided *ad libitum* to induce shRNA expression in pTRIPZ-transduced tumor cell lines implanted in mice. Dasatinib (2.5 mg/kg) treatment was provided via intraperitoneal injection six days a week. We used sterilized water solution plus 30% PEG 400 (Thermo Fisher Scientific), 1% Tween 80, and 4% dimethyl sulfoxide (Sigma-Aldrich) as drug vehicle. Tumor volume [$V = 0.5 \times (L \times W^2)$] and body weight were measured twice weekly. Mice tolerated all treatments with no significant adverse events or change in body weight noted. Drug treatments continued until primary tumor reached 1,500 mm³ or mice morbidity. Mice were then euthanized and tissues harvested for molecular analysis.

2.8 *In vitro* cell proliferation assay

For cell proliferation experiments *in vitro*, we utilized sulforhodamine B (SRB) (Sigma Aldrich), or CellTiter-Blue (Promega, Madison, WI) colorimetric protein staining assays were performed according to the manufacturer's instructions. The percentages of surviving cells from each group were estimated relative to the control culture, which was defined as 100% viability.

2.9 Soft agar assay

Cells (2×10^3 cells/well) were resuspended in 2 mL of 0.4% agarose solution in DMEM/F12 or F12 medium and overlaid onto the bottom agar layer (0.8%) in 6-well plates. The plates were incubated for 21 days with drugs, and colonies were stained with 200 μ L of MTT solution (1 mg/ml) for 2 hours. The stained colonies greater than 80 μ m in diameter were counted using the GelCount colony-counting system (Oxford Optronix, UK) according to the manufacturer's instructions. Means and standard deviations were calculated on the basis of the colony counts from triplicate wells

2.10 Co-immunoprecipitation

Cultured SUM190PT and SUM149PT cells were collected after described treatments, and were washed with pre-chilled PBS, followed by cell lysing with a cold non-denaturing lysis buffer (50 mM Tris-HCl, pH 7.4, 1% NP-40, 150 mM NaCl, 10% glycerol, 1.5 mM MgCl_2 , 1 mM EDTA, and phosphatase and protease inhibitors). To immunoprecipitate MCL1 proteins, lysate (500 μ g) was mixed with 5 μ g MCL1 antibody (R&D Systems) for 2 hours at 4°C with rotation. Protein G Sepharose 4 Fast Flow beads (GE Healthcare, Marlborough, MA) were added to the antigen–antibody complex and incubated for 1 hour at 4°C with rotation. Beads were recovered by low-speed centrifugation and washed with lysis buffer. LDS sample buffer and sample reducing agent (Novex Life Technologies, NuPAGE®) were added to each sample and incubated at 70°C for 10 minutes, centrifuged, and subjected to SDS-PAGE. After appropriate separation, gels were transferred and analyzed for co-immunoprecipitation using standard immunoblotting techniques as described previously

2.11 Immunohistochemistry (IHC)

Tumor tissues were fixed in neutral-buffered formalin and embedded in paraffin. Sections (5 μ m each) were prepared using a microtome, mounted on slides, deparaffinized in xylene, rehydrated in graded alcohols, and washed in distilled water. Antigens were retrieved by boiling the sections in 10 mM citric acid (pH 6.0) for 40 min. Endogenous peroxidases were quenched by incubation in 3% H₂O₂ for 10 min at room temperature. The slides were washed three times with phosphate-buffered saline (PBS) and blocked for 30 min with 10% normal goat serum in 1% bovine serum albumin/PBS. The slides were then exposed previously described antibodies. Immunostained slides were scanned with a high definition microscope, and the images were captured at a magnification of 50 \times and stored using ImageScope software according to the manufacturer's instructions. Immunostained slides were evaluated by densitometry using the ImageJ software.

2.12 TUNEL staining

DNA fragmentation in mouse tissue samples was measured by *in situ* terminal deoxynucleotidyl transferase-mediated dUTP nick end labeling (TUNEL) using the DeadEnd TUNEL kit (Promega, Madison, WI). The mouse tumor xenografts' TUNEL-positive cells were evaluated in 3 randomized fields at 20 \times magnification, and the average was expressed as the number of apoptotic cells for each sample.

2.13 Chromatin Immunoprecipitation

Acetylation levels of the *NOXA* gene promoter following entinostat treatment (1 μ M, 48 hours) were measured by chromatin immunoprecipitation (ChIP) assay using the Simple ChIP Enzymatic Chromatin IP Kit (magnetic beads) following manufacturer's protocol (Cell

Signaling Technology, Beverly, MA). Briefly, untreated and entinostat treated SUM149PT and SUM190PT cells (4×10^6 cells per sample) were nuclease digested and sonicated (3 cycles of 30 seconds) to shear DNA to approximately 150-900 bp in size. Sonicated chromatin samples were incubated with antibodies against acetylated-lysine, Histone H3 as positive control, or normal rabbit IgG as negative control (Cell Signaling Technology, Beverly, MA), overnight at 4°C with rotation. Two percent was used of total genomic DNA from nuclear extracts as input. Purified immunoprecipitation and input DNA were used as templates for RT-qPCR with the following primers to amplify the *NOXA* promoter region (Forward: 5'-AGTAATTTCTGGGGCCGAGC-3' and Reverse: 5'-GGCGTTATGGGAGCGGAC-3'). Quantification of DNA by RT-qPCR was done following manufacturer's protocol.

2.14 Synthetic-lethal siRNA screen

To identify a targetable candidate that would complement the antitumor effect of EPA, we performed a high-throughput, synthetic lethal siRNA screen using a kinome library containing 939 druggable genes in the TN-IBC cell line SUM149PT, in combination with EPA treatment. A reverse transfection method was performed in which 45 nM siRNA is initially allowed to complex in an assay plate with DharmaFECT-2 transfection reagent (0.07 μ L, GE Dharmacon, Lafayette, CO) for 30 minutes, followed by addition of 30 μ L of solution containing 750 cells/condition, after which the plates were incubated for 48 hours at 37°C in a 5% CO₂ atmosphere. After incubation, cells were treated with EPA (IC₅₀: 50 μ M) and incubated for an additional 72 hours at 37°C in a 5% CO₂ atmosphere. OTP3 and TOX were identified as optimal negative and positive siRNA transfection controls, respectively. After treatment, assay plates were imaged (IN-Cell Analyzer 6000, GE Healthcare Life Sciences) and cells were assessed for viability as determined after incubation with CellTiter-Blue® (Promega Corporation, Madison,

WI) and quantification of fluorescence intensity (PHERAstar FS Plate Reader, BMG Labtech Inc., Cary, NC). Data were normalized to the values for untreated controls, and statistical measures were applied to remove assay variability as previously described (53). The siRNA screen data have been deposited in Gene Expression Omnibus (GEO) with accession number: GSE102057.

2.15 Cell lines with doxycycline-inducible genes

We established doxycycline-inducible non-coding-shRNA or EPHA2-shRNA SUM149PT and BCX010 cell lines using the following inducible expression vectors: pTRIPZ non-targeting (RHS4743) and pTRIPZ-human-EPHA2 (V3THS_322576) inducible lentiviral shRNA vectors (GE Dharmacon), both containing a red fluorescent protein (RFP) tag. Briefly, lentivirus was produced using manufacturer's instructions, concentrated with PEG-it virus precipitation solution (System Biosciences, Palo Alto, CA) and applied to cultures of SUM149PT and BCX010 for 24 hours. Positive transductions were selected with puromycin (5 μ g/mL), followed by flow cytometry to isolate RFP-positive cells upon doxycycline treatment. EPHA2 knockdown was validated by western blot and flow cytometry following 24 hours doxycycline treatment.

2.16 Xenograft tumor cell sorting

Tumors containing RFP-positive cells following Dox treatment were mechanically homogenized prior to incubation in 3 mL collagenase A (1 mg/mL) for 10 minutes. The digested solution was neutralized with an equal volume of 5% FBS in phosphate-buffered saline solution (PBS), then filtered (40 μ m) and centrifuged at 400 x g for 5 minutes. Following centrifugation, the supernatant was discarded and the cell pellet was resuspended in 1 mL red

blood cell lysis buffer (StemCell Technologies, Cambridge, MA), and subjected to centrifugation again. After centrifugation, cells were resuspended in 2% FBS (500 μ L) in PBS, counted, and incubated with anti-IgG-APC or anti-EPHA2-APC antibody (5 μ L / 1×10^6 cells, Novus Biologicals) for 20 minutes, followed by centrifugation and two washings with 2% FBS (1 mL) in PBS wash. Cells were finally resuspended in 2% FBS (500 μ L) in PBS, and SYTOX[®] blue (1:500, Life Technologies, Carlsbad, CA) was added to stain dead cells before flow cytometry analysis. EPHA2 protein expression was quantified in the RFP-induced tumor cell population.

2.17 Membrane fluidity assay

Membrane fluidity was determined by using the lipophilic fluorescent probe Laurdan (6-dodecanoyl-2-dimethylaminonaphthalene, Thermo Fisher Scientific). Briefly, following treatment for 24 or 48 hours, the cell membranes were extracted by lysis with hypotonic buffer (0.2 mM EDTA, 1 mM NaHCO₃) containing protease/phosphatase inhibitors, and cells were allowed to swell for 30 minutes, followed by brief sonication. Remaining intact cells were removed by centrifugation at 800 x g for 10 minutes. The supernatant was collected and subjected to ultra-centrifugation at 100,000 x g for 45 minutes, yielding a crude total membrane pellet; this pellet was re-suspended in buffer (10 mM TRIS and anti-protease cocktail, in PBS) before addition of the Laurdan fluorescent probe and incubation for 1 hour at 37°C. After incubation, the fluorescence measurements were performed using a Quanta-Master model QM3-SS (Photon Technology International) cuvette-based fluorescence spectrometer. Using a Peltier TE temperature controller, the sample was held at a constant of 37°C and fluorescence measurements (excitation 350 nm; emission wavelengths, 440 and 490 nm) were performed.

Data were collected and analyzed using Felix 32 software. General polarization (GP, a measure of fluidity) of the membrane was determined by the following equation:

$$GP = \frac{(IF_{440nm} - IF_{490nm})}{(IF_{440nm} + IF_{490nm})}$$

Where IF_{440nm} and IF_{490nm} represent the fluorescence intensity detected at the 440 nm and 490 nm wavelengths, respectively. Higher GP values are indicative of increased polarization, or rigidity. Conversely, lower GP values represent a less rigid, more fluid state.

2.18 Membrane fluidity imaging

Following 24 to 48 hours of treatment, cells were washed with PBS and fixed with 4% formaldehyde for 20-30 minutes. Fixed cells were then incubated with 5 μ M C-laurdan for 20 minutes at room temperature. Following incubation, the cells were washed 3x with PBS, and mounted to a coverslip with Prolong Gold. Cells were imaged via confocal microscopy on a Nikon A1R with spectral imaging at 100x with an excitation of 405 nm. The emission was collected in two bands: 433-463 nm (IF_{440}) and 473-503 nm (IF_{490}). MatLab was used to calculate the 2D GP map, where the GP for each pixel was calculated from a ratio of the two fluorescence channels, as described (54). Briefly, each image was binned (2 x 2), background-subtracted, and threshold applied to keep only pixels with intensities greater than three standard deviations of the background value in both channels. The GP image was calculated for each pixel using the equation above.

2.19 Fatty acid analysis

Total lipids from mouse diet pellets, tumor tissues and serum samples were extracted by the method of Folch *et al.* (55, 56). Total phospholipids were separated by thin-layer

chromatography on silica gel 60 plates using chloroform/methanol/acetic acid/water (90:8:1:0.8, v/v) as the developing solvent. Isolated lipid fractions were methylated, and the resultant fatty acid methyl esters were analyzed by gas chromatography/mass spectrometry as described elsewhere (57).

2.20 Mass spectrometry EPA analysis

Phospholipids were extracted from membranes of treated cells for quantifications of lipid profiles. Briefly, to extract membrane phospholipids, cell pellets were resuspended in chilled PBS (50 μ L), and cold 100% methanol (100 μ L) was added into 20 μ L aliquots of the cell homogenates. After mixing by vortex, samples were subjected to centrifugation at 3,000 rpm for 5 minutes at 4°C. Each supernatant was transferred into a new tube, and analyzed by liquid chromatography-mass spectrometry (LC-MS; 1290 LC System and 6460 Triple Quadruple MS, Agilent, Santa Clara, CA). For the LC instrument, a C18 high-performance liquid chromatography (HPLC) column (Phenomenex Kinetex, Torrance, CA) was utilized using 0.1% formic acid in water as mobile phase A and 0.1% formic acid in acetonitrile as mobile phase B. The MS instrument was utilized in positive-ion electrospray mode, and ion scan mode was set at MS2=184 (phosphatidylcholine) and MS2=264 (ceramide). Output data were processed using the MassHunter WorkStation Software (Agilent).

2.21 Cholesterol quantification

Total cellular membrane fractions were extracted from treated cells using the Subcellular Protein Fractionation assay (Thermo Scientific) according to the manufacturer's instructions. After the cell membrane fraction was extracted, cholesterol concentration was quantified by Amplex[®] Red Cholesterol Assay (Thermo Fisher Scientific) according to manufacturer's

instructions. Briefly, extracted membrane fraction (20 µg) was diluted in reaction buffer (50 µL; 0.1 M potassium phosphate, pH 7.4, 0.05 M NaCl, 5 mM cholic acid, 0.1% Triton[®] X-100 in deionized water), Amplex Red working solution (50 µL; 2 U/mL horseradish peroxidase, 2 U/mL cholesterol oxidase, 0.2 U/mL cholesterol esterase, 0.75 µL Amplex Red reagent solution, 0.5 µL HRP solution, 0.5 µL cholesterol oxidase solution, and 0.05 µL cholesterol esterase solution in reaction buffer) was added and the tubes were incubated at 37°C for 30 minutes. After incubation, fluorescence was measured in a fluorescence plate reader using excitation at 570 nm and emission detection at 590 nm.

2.22 Statistical analysis

For experimental outcomes, descriptive statistics (mean and standard error of the mean) were summarized for each group. An analysis of variance (ANOVA) model was used to compare the mean outcome values among the tested groups. The log-rank test was used to compare survival curves. Statistical analyses were performed using an unpaired *t*-test with Prism version 5 (GraphPad Software, La Jolla, CA). *P* values of < 0.05 were considered statistically significant. Synthetic-lethal siRNA screen data analysis was carried out using t-test followed by Beta-Uniform mixture model to adjust p-values in statistical computing software R (version 3.0.1) (58).

CHAPTER 3: IDENTIFICATION OF AN HDAC AND MEK INHIBITORS

COMBINATION STRATEGY AGAINST TNBC AND IBC

This chapter is based upon the manuscript by: A. M. Torres-Adorno, J. Lee, T. Kogawa, P. Ordentlich, D. Tripathy, B. Lim, N. T. Ueno, Histone deacetylase inhibitor enhances the efficacy of MEK inhibitor through NOXA-mediated MCL1 degradation in triple-negative and inflammatory breast cancer. *Clin Cancer Res*, (2017) (59). According to the American Association for Cancer Research, no permission is necessary for use of materials from this publication by authors on doctoral dissertation work.

3.1 Introduction

3.1.1 Epigenetic modulation in cancer

Epigenetic modulation in malignancies often silences genes that regulate proliferation and metastasis, thereby contributing to tumor aggressiveness. Histone deacetylases (HDACs) are critical regulators of gene expression; they do so through enzymatic removal of acetyl groups from histones that prevents DNA access to the transcriptional machinery that promotes gene expression (**Figure 4**). Aberrant expression of HDACs, leading to tumorigenesis, is observed in multiple types of human cancers.

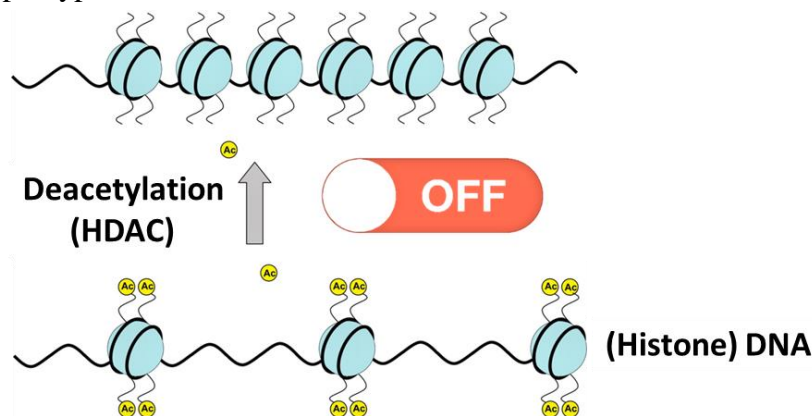


Figure 4. Diagram of histone deacetylases activity in the removal of acetyl groups from histones and silencing of gene expression.

3.1.2 Histone deacetylase inhibitors

In the last decade, multiple HDAC inhibitors have been developed as anti-cancer drugs and have shown anti-tumor action (60). Entinostat (formerly MS-275, Syndax Pharmaceuticals, Inc., Waltham, MA), a selective class I HDAC inhibitor with low toxicity to normal cells, is a synthetic benzamide derivative that can reduce the proliferation of cancer cells and tumors xenografts in a variety of human cancers (61). Entinostat also displayed preliminary therapeutic efficacy in a randomized phase II clinical trials for ER-positive breast cancer patients (62).

Although it is not known from available clinical trials whether entinostat can induce the expression of pro-apoptotic proteins in IBC and TNBC tumors, recent preclinical evidence demonstrated entinostat-induced expression of the pro-apoptotic BIM protein in IBC and TNBC (40), suggesting the induction of apoptosis as a major mechanism of tumor suppression.

3.1.3 The BCL-2 family of proteins and apoptosis regulation

The Bcl-2 family of proteins are critical modulators of apoptosis, acting immediately upstream of irreversible cellular damage, where anti-apoptotic and pro-apoptotic family members control the release of apoptogenic factors from mitochondria (63). NOXA, a Bcl-2 homology domain 3 (BH3)-only pro-apoptotic protein, is epigenetically silenced by histone acetylation in cancer (64, 65). Independently, NOXA displays weak pro-apoptotic activity, however it is a crucial modulator of cell death through its ability to interact with the pro-survival Bcl-2 molecule MCL1 (induced myeloid leukemia cell differentiation protein 1). MCL1 is commonly amplified in TNBC and has been shown to be an adverse prognostic factor for survival (66). Degradation of MCL1 during cell death is uniquely associated with the formation of an MCL1/NOXA complex, while stabilization of MCL1 is associated with its ability to bind

other BH3-only members (i.e. PUMA or BIM) (67-69). Alternatively, MCL1 protein can be stabilized through the activation of the mitogen-activated protein kinase/extracellular signal-regulated kinase (ERK) signaling pathway, which promotes survival and drug resistance in cancer cells (70-72). Since MCL1 is crucial to cancer cell survival, drugs that target the ERK pathway may have therapeutic value through their ability to reduce MCL1 expression.

3.1.4 Oncogenic MEK/ERK pathway and TNBC

ERK is an important therapeutic target in TNBC; high ERK expression correlates with shorter patient overall survival (73). While ERK inhibitors have not been effective in clinical testing, compounds that inhibit MEK (an upstream activator of ERK) including selumetinib (formerly AZD6244) (74, 75), and the more potent compound pimasertib (formerly AS703026, EMD Serono, Inc., Rockland, MA) (76, 77) have displayed clinical activity in phase II trials for melanoma and ovarian cancer (78, 79).

3.1.5 Gap in knowledge

While the effectiveness of these HDAC and MEK inhibiting compounds remains to be clinically established in breast cancer, it have been previously shown their potential for preventing metastasis in preclinical xenograft models of TNBC (80). As such, there is a need to identify the efficacy of a combination therapy utilizing ERK and HDAC inhibitors, potentially due to their parallel inhibitory effects on MCL1 protein levels in TNBC and IBC.

3.2 Results

3.2.1 NOXA and MCL1 expression are molecularly and clinically relevant to entinostat and pimasertib treatment in IBC and TNBC.

Previous studies reported entinostat-induced expression of the pro-apoptotic protein BIM in TNBC and IBC cell lines, suggesting the induction of apoptosis as a major mechanism of tumor suppression (40). To identify apoptosis-related molecular changes induced by entinostat in TNBC and IBC cells following treatment, we performed a quantitative PCR array with 28 apoptosis-related probes on two established cell lines: SUM190PT (IBC), and SUM149PT (IBC-TNBC), chosen because of their IBC and TNBC status. We found that *NOXA/PMAIP1* (also called phorbol-12-myristate-13-acetate-induced protein 1, or PMAIP1) was among the top upregulated apoptosis-related mRNAs after 48 hours of entinostat treatment on both cell lines (**Table 2**), consistent with previous observations in acute myeloid leukemia (81). Because NOXA promotes intrinsic apoptosis through proteasomal degradation of the anti-apoptotic protein MCL1, while the ERK pathway is known to support MCL1's stabilization, we next analyzed the effect of entinostat on the phosphorylation/activation of ERK (p-ERK) in IBC (IBC3, KPL-4, SUM149PT, and SUM190PT) and non-IBC (BT-474, MDA-MD-231, MDA-MB-468, and SKBR3) cell lines. After 48 hours of treatment, entinostat induced p-ERK expression in IBC (3 out of 4) and TNBC (MDA-MB-468) while no inducing effect was observed on another major cancer-related pathway, AKT, among the tested cell lines (**Figure 5**). These results suggest p-ERK could act as a stabilizer for MCL1 in IBC and TNBC, representing a potential target that could enhance apoptosis in combination with entinostat treatment.

Based on this observation, we pursued further studies addressing how NOXA/MCL1 expression may contribute to the therapeutic efficacy of combining entinostat and an ERK

pathway inhibitor in IBC and TNBC. We first determined the clinical relevance of NOXA and MCL1 expression levels to breast cancer patient outcome. We analyzed a previously published cDNA microarray dataset of breast cancer patient samples, which contains IBC (35%) and non-IBC (65%; 27% TNBC) cases (49). Kaplan-Meier survival analysis revealed that low MCL1 mRNA expression levels within patient tumors significantly correlated with longer patient overall survival (OS) and distant metastasis-free survival (DMFS) than high MCL1 mRNA levels ($P = 0.017$ and 0.0041 , respectively) (**Figure 6A, D**). Conversely, high NOXA expression was associated with longer OS (a nearly significant difference, $P = 0.052$), but not DMFS (nonsignificant, $P = 0.64$) in this cohort (**Figure 6B, E**). When stratified by both MCL1 and NOXA tumor expression, significantly longer OS and DMFS were seen in patients with low MCL1/high NOXA expression than in patients with high MCL1/low NOXA expression ($P = 0.0008$ and 0.02 , respectively) (**Figure 6C, F**).

Next, we investigated NOXA and MCL1 *in vitro*. Using quantitative real-time PCR analysis, and chromatin immunoprecipitation (ChIP), we confirmed increased NOXA mRNA expression associated with NOXA gene promoter acetylation levels following entinostat treatment ($1 \mu\text{M}$) in SUM190PT and, to a lesser degree, SUM149PT cells, compared to the untreated control (**Figure 7**). To further confirm this finding, we screened other IBC (KPL-4 and IBC-3) and TNBC (SUM159PT, BT-549, SUM185PE, MDA-MB-157, MDA-MB-453, MDA-MB-231, HCC70, MDA-MB-468, MDA-MB-436, HCC1806, HCC1937, HCC3153, and Hs578T) cell lines (**Figure 8**). Compared to untreated cell lines, NOXA mRNA was induced by entinostat treatment in 65% (11 of 17) of the IBC and TNBC cell lines tested. Immunoblotting analysis was performed on all cell lines to identify relationships between protein expression levels of NOXA and MCL1 after entinostat treatment (data shown for 12 cell lines, **Figure 9**).

Gene symbol	Description	SUM149PT	SUM190PT
		Fold-change (log2)	Fold-change (log2)
BCL2A1	BCL2-related protein A1	4.63	0.41
TNFRSF10B	tumor necrosis factor receptor superfamily, member 10b	0.98	1.68
TNFRSF9	tumor necrosis factor receptor superfamily, member 9	3.28	1.30
BIRC3	baculoviral IAP repeat-containing 3	2.95	3.80
BCL2L2	BCL2-like 2	-0.78	-1.22
CASP4	caspase 4, apoptosis-related cysteine peptidase	1.41	0.91
PMAIP1	phorbol-12-myristate-13-acetate-induced protein 1	1.73	4.26
BRAF	v-raf murine sarcoma viral oncogene homolog B1	0.90	0.59
SP1	Sp1 transcription factor	-0.75	-0.49
NOL3	nucleolar protein 3 (apoptosis repressor with CARD domain)	-1.55	-1.74
CFLAR	CASP8 and FADD-like apoptosis regulator	-0.63	-0.67
TP53BP2	tumor protein p53 binding protein, 2	0.82	1.00
TNFRSF10A	tumor necrosis factor receptor superfamily, member 10a	-0.81	-0.25
BCL10	B-cell CLL/lymphoma 10	0.77	0.40
TP53	tumor protein p53	-2.33	-0.67
RIPK2	receptor-interacting serine-threonine kinase 2	0.84	0.52
XIAP	X-linked inhibitor of apoptosis	-0.53	-0.31
LTBR	lymphotoxin beta receptor (TNFR superfamily, member 3)	-0.52	-0.86
TNFSF10	tumor necrosis factor (ligand) superfamily, member 10	0.83	-1.21
HDAC1	histone deacetylase 1	0.26	1.86
MAPK1	mitogen-activated protein kinase 1	0.17	0.29
BCL2L11	BCL2-like 11 (apoptosis facilitator)	0.67	1.08
CASP3	caspase 3, apoptosis-related cysteine peptidase	-0.74	0.68
AKT1	v-akt murine thymoma viral oncogene homolog 1	-0.74	-1.30
IGF1R	insulin-like growth factor 1 receptor	0.44	-0.33
BID	BH3 interacting domain death agonist	-0.74	-0.70
MCL1	myeloid cell leukemia sequence 1 (BCL2-related)	0.44	0.39
BAG1	BCL2-associated athanogene	-0.70	-0.66

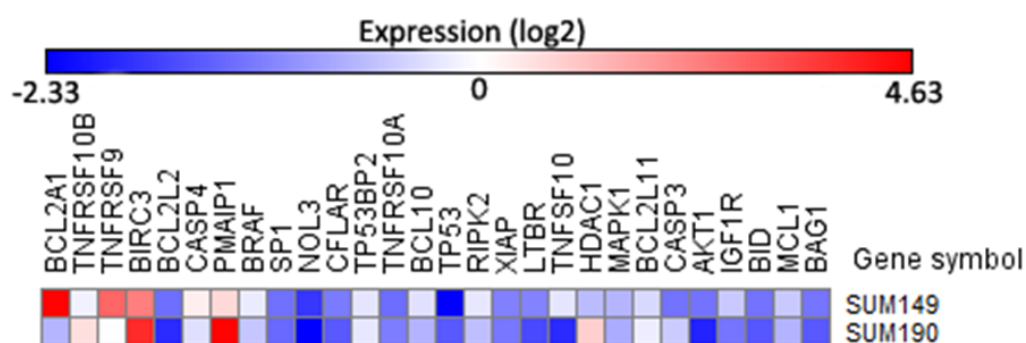


Table 2. Effect of entinostat on the expression of apoptosis-related gene pathways. The expression profile of apoptosis-related genes for SUM149PT and SUM190PT cell lines after entinostat treatment for 48 hours. Results are represented as the fold-change of the log2 values of entinostat treated cells in comparison to the values observed in non-treated cells. GENE-E software (The Broad Institute, Cambridge, MA) was utilized for heat map visualization of gene expression data.

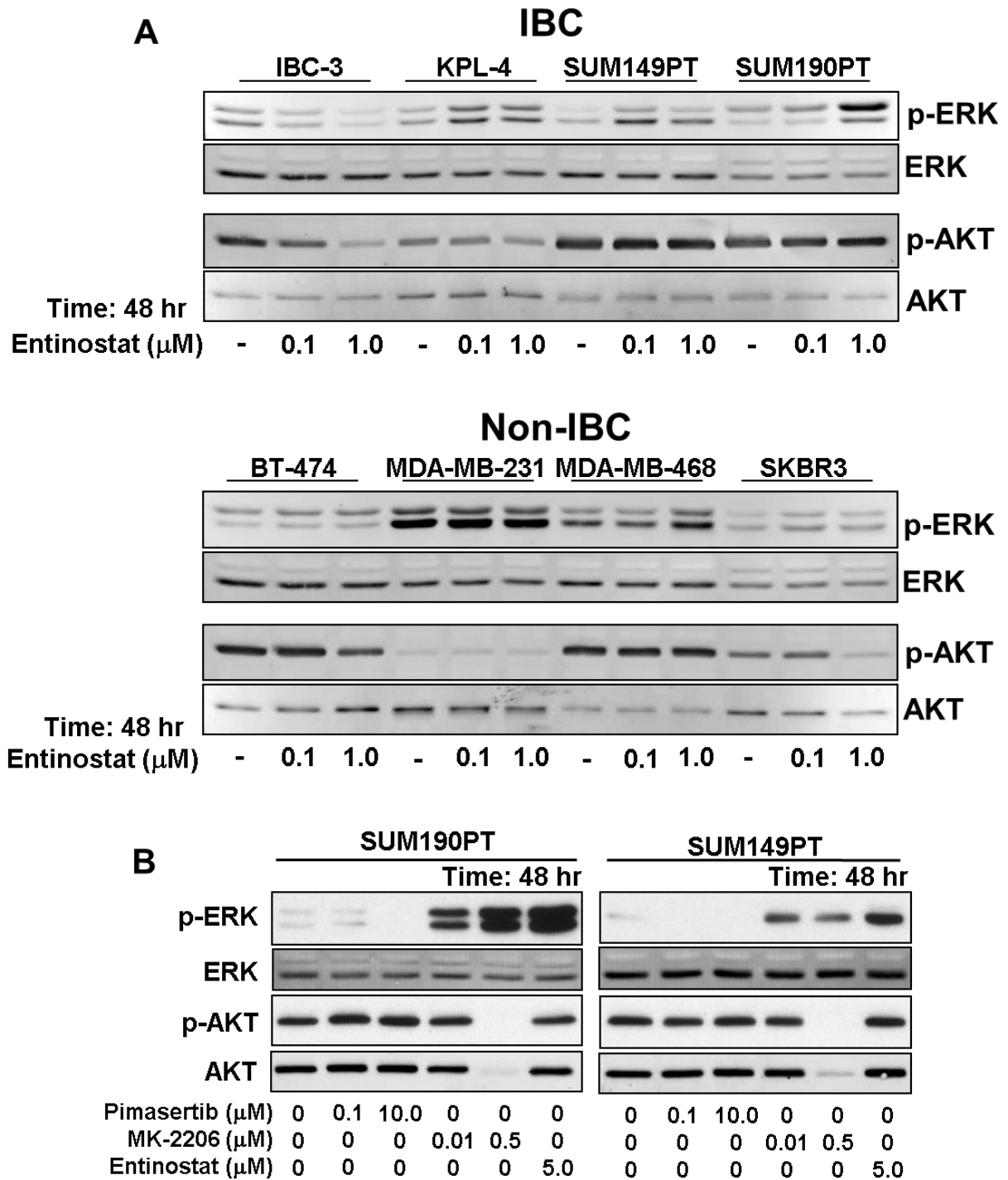


Figure 5. Entinostat induces increased phosphorylation/activation of the pro-survival ERK pathway in IBC cell lines. A, IBC and non-IBC cell lines were treated with various concentrations of entinostat, and ERK, p-ERK, AKT, and p-AKT protein expression was determined by immunoblotting analysis. B, SUM190PT and SUM149PT cells were treated with the ERK pathway inhibitor pimasertib or the AKT pathway inhibitor MK-2206 to confirm increased activation of p-ERK after entinostat treatment. Total AKT and ERK expression was used as a protein loading control.

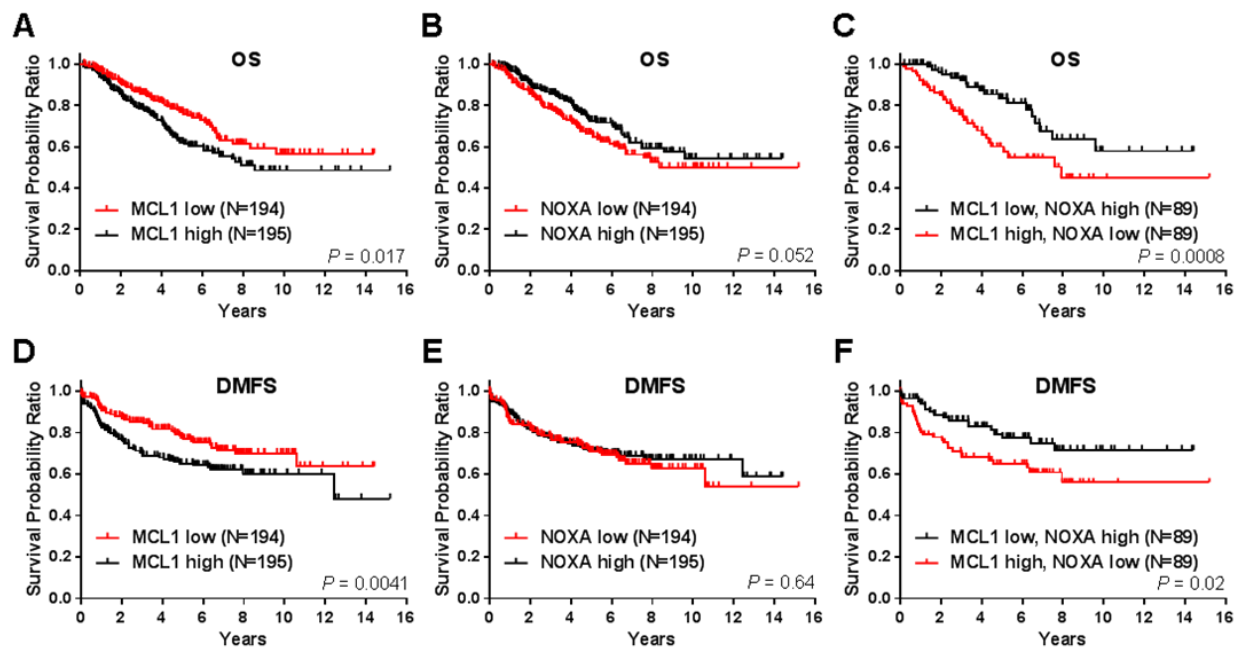


Figure 6. High MCL1/low NOXA co-expression is associated with poor outcome in breast cancer patients. Kaplan-Meier survival curves for overall survival (OS) and distant metastasis-free survival (DMFS) of breast cancer patients from the IBC World Consortium dataset, correlated to *NOXA* and *MCL1* tumor mRNA levels. The log-rank test was used to compare survival curves for high and low MCL1 (A, D), high and low NOXA (B, E), and high or low MCL1 in correlation with low or high NOXA (C, F). The initial numbers of patients at risk in each group are indicated in the key.

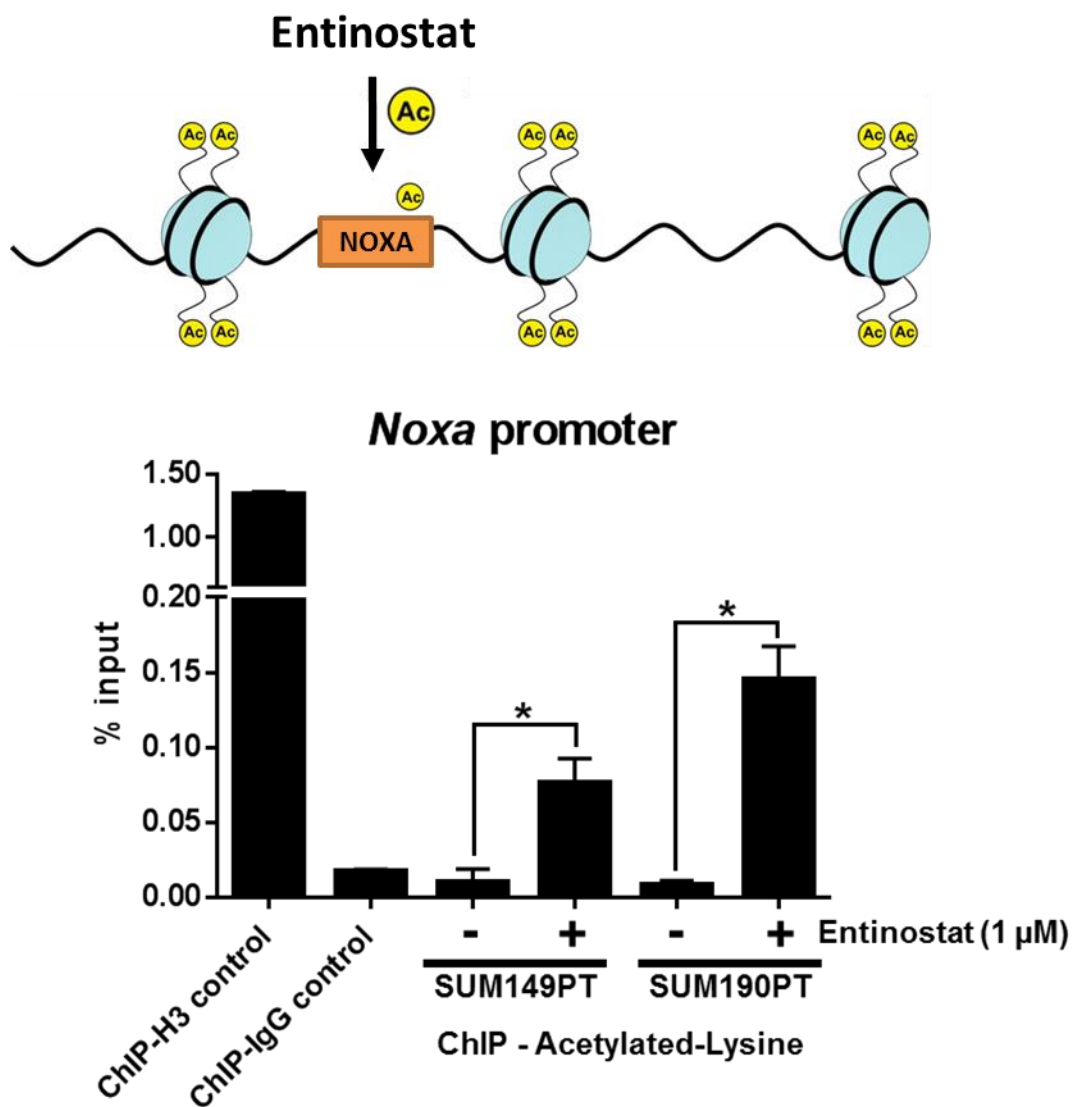


Figure 7. Increased *NOXA* gene promoter acetylation levels following entinostat treatment. SUM149PT and SUM190PT cell lines were treated with entinostat (1 μ M) for 48 hours, and *NOXA* gene promoter acetylation was assessed by ChIP assay with an acetylated-lysine antibody. H3 and IgG antibodies were used as positive and negative ChIP controls, respectively. *NOXA* promoter DNA expression was determined by RT-qPCR; Percent of *NOXA*-promoter DNA from input samples is presented. *, P < 0.05.

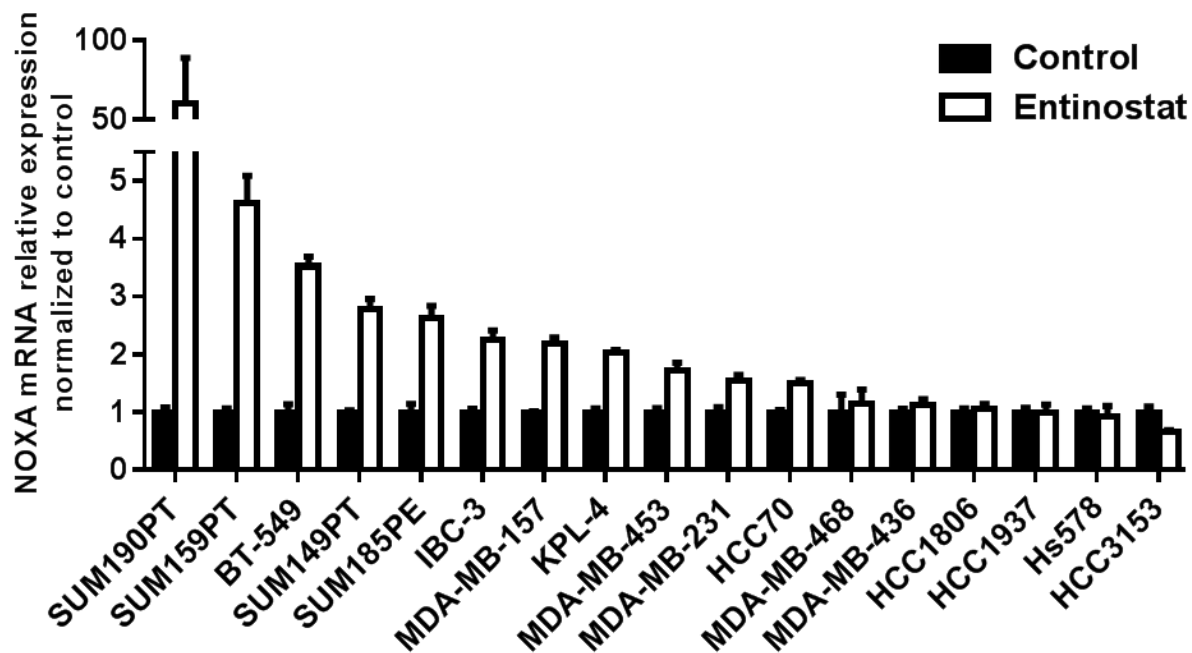


Figure 8. Entinostat treatment selectively increases expression of *NOXA* mRNA in TNBC and IBC cell lines. *NOXA* mRNA levels were analyzed in multiple TNBC and IBC cell lines using quantitative real-time PCR after 48 hours of treatment with entinostat (1 μ M), compared to the untreated control. Data were pooled from three independent experiments.

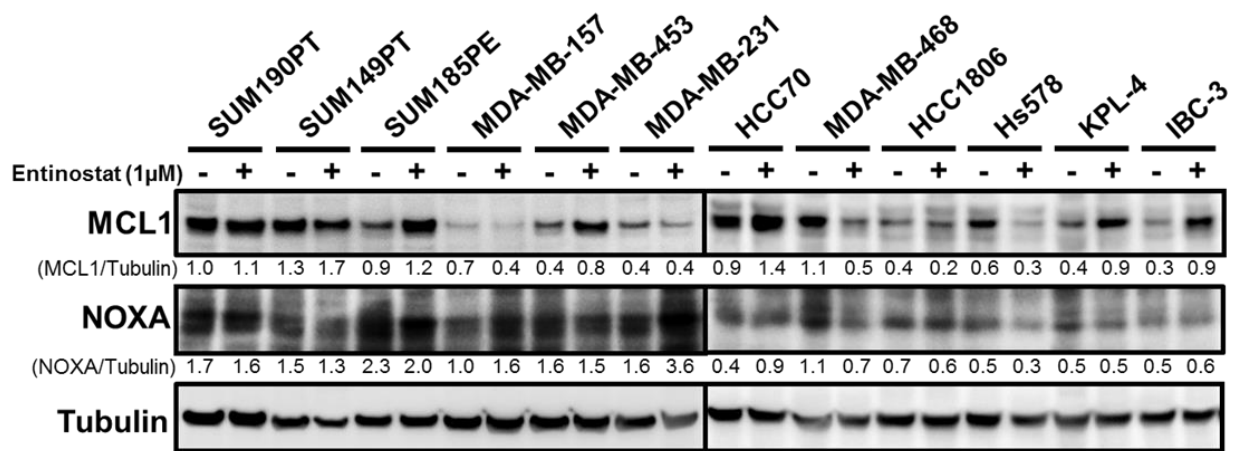


Figure 9. Basal MCL1 protein expression is present in most TNBC and IBC cell lines. NOXA and MCL1 protein expression levels were determined in multiple TNBC and IBC cell lines by immunoblotting analysis after 48 hours of treatment with entinostat (1 μM). Pixel density of proteins was quantified for each condition, and ratios of protein/tubulin are shown above the blots. Detectable-MCL1-expressing cell lines were defined as those with pixel density of MCL1/tubulin ≥ 0.4 , the average density of MCL1 among all tested cell lines. Tubulin expression was used as a protein loading control.

NOXA protein expression did not positively correlate with increased *NOXA* mRNA expression levels, possibly due to the short protein half-life of NOXA through proteasome-dependent degradation (82). We also identified detectable levels of MCL1 protein expression in 80% of cell lines, as defined by MCL1/tubulin pixel density ≥ 0.4 (the average MCL1 pixel density among all cell lines), and observed induction of MCL1 protein expression in multiple cell lines following entinostat treatment. Together with our preliminary data demonstrating that entinostat mediated p-ERK expression (**Figure 5**), the changes in protein levels of MCL1 suggest the stabilization of MCL1 through p-ERK pathway activation in TNBC and IBC cells.

3.2.2 Entinostat and pimasertib combination therapy synergize to inhibit the growth of aggressive breast cancer cells that overexpress NOXA after entinostat treatment.

As a monotherapy for TNBC and IBC, the efficacy of entinostat may be hindered due to the induction of MCL1 through p-ERK activation. Thus, we hypothesized that addition of the MEK inhibitor pimasertib may potentiate cellular cytotoxicity of entinostat by simultaneously blocking ERK activation. Synergistic killing by the combination therapy was observed in 12 of 17 IBC and TNBC cell lines tested (representative data shown for three cell lines, **Figure 10A**), with response predominantly correlated to each cell line's level of *NOXA* mRNA induction after entinostat treatment (representative data for combination index (CI) shown for eight cell lines, **Figure 11**). Sixty percent of cell lines responding to combination therapy had high basal MCL1 protein levels (MCL1/tubulin pixel density \geq average, 0.4), while the other 40% of responding cell lines displayed synergistic cell killing despite low MCL1 expression, which may be associated with the induced levels of NOXA, as observed in previously. Therefore, the effectiveness of combination treatment was correlated to *NOXA*-mRNA-inducible cell lines,

potentially inducing apoptosis by enhanced targeting of MCL1, providing a mechanism that could circumvent the problems associated with monotherapy.

To determine cell death induction levels after treatment, we next analyzed the effect of entinostat and pimasertib on apoptosis after dose response experiments of clinically achievable ($\leq 1 \mu\text{mol/L}$) doses. The SUM190PT and SUM149PT cell lines were selected for further analysis based on their TNBC and/or IBC status, as well as their significant induction of NOXA-mRNA following entinostat treatment. The HCC1806 TNBC cell line was selected as a negative control based on its lack of entinostat-mediated NOXA-mRNA induction and apparent resistance to treatment. As shown in **Figure 10B**, single entinostat or pimasertib treatment induced apoptosis by 10% and 9%, respectively, in SUM190PT cells and by 16% and 6% in SUM149PT cells, compared with the control (untreated cells). However, combination treatment significantly increased the proportion of apoptotic cells by 30% in SUM190PT and SUM149PT cells compared with the control. The TNBC cell line HCC1806 did not respond to single or combination treatment, which correlates to its inability to express NOXA following entinostat treatment. Collectively, these data suggest that the combination of entinostat and pimasertib is most effective in TNBC and IBC cell lines in which NOXA can be induced.

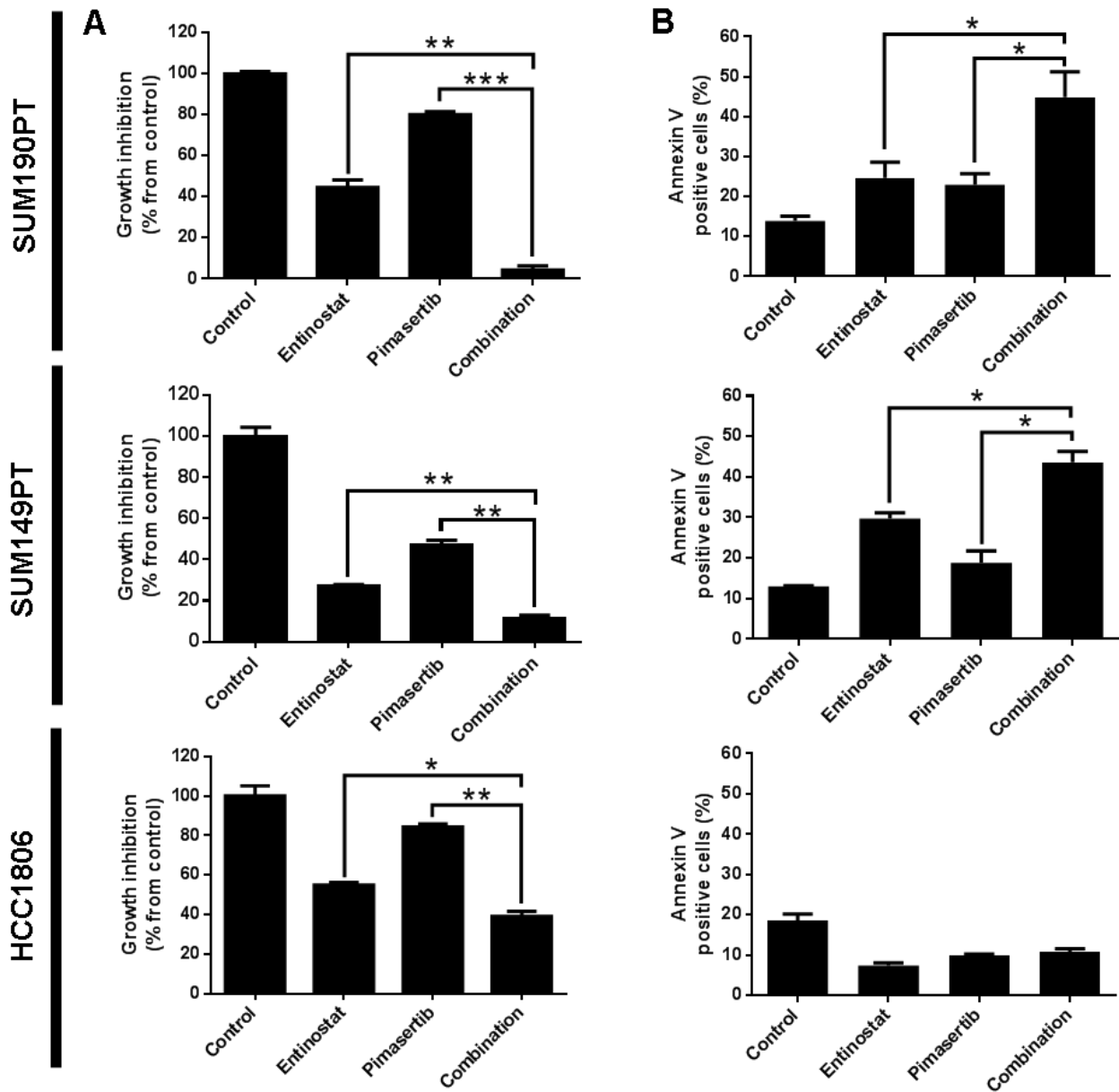


Figure 10. Entinostat and pimasertib combination treatment enhanced cell death in IBC and TNBC cell lines that overexpressed NOXA after entinostat treatment. SUM190PT, SUM149PT, and HCC1806 cells were treated with clinically achievable ($\leq 1 \mu\text{mol/L}$) doses, representative data shown for entinostat ($1 \mu\text{M}$) and pimasertib ($1 \mu\text{M}$) for 48-72 hours. The IC_{50} values of entinostat were determined for SUM190PT, SUM149PT, and HCC1806 cell lines to be $0.6 \mu\text{M}$, $0.3 \mu\text{M}$, and $0.9 \mu\text{M}$, respectively; the IC_{50} values of pimasertib were $1.9 \mu\text{M}$, $0.6 \mu\text{M}$, and $2.5 \mu\text{M}$, respectively. Cell proliferation and apoptosis were measured by SRB staining (A) and Annexin V-PE staining (B), respectively. Data were pooled from three independent experiments and presented as mean \pm SEM. *, $P < 0.05$; **, $P < 0.001$; ***, $P < 0.0001$.

	SUM190PT	SUM159PT	BT549	SUM149PT	SUM185PE	HCC70	MDA-MB-468	HCC1806
1:1	Combination	Combination	Combination	Combination	Combination	Combination	Combination	Combination
μM	Fa CI	Fa CI	Fa CI	Fa CI	Fa CI	Fa CI	Fa CI	Fa CI
1	0.99 0.089	0.75 0.89	0.695 0.20	0.99 0.20	0.93 0.17	0.93 0.19	0.58 1.34	0.746 1.44

Figure 11. TNBC and IBC cell lines overexpressing NOXA after entinostat treatment exhibit synergy of combination treatment with pimasertib. The entinostat and pimasertib dose–effect for combination treatment (1 μM , 1:1 ratio) synergism was calculated using CalcuSyn software (Biosoft, Cambridge, UK). A fractional index (Fa), or the fraction of cells affected by the dose, of 1.0 indicates 100% growth inhibition. Combination index (CI) is a quantitative measure of the degree of drug interaction: <0.9 = synergy, $0.9 - 1.1$ = additive effect, > 1.1 = no synergy.

As the efficacy of the combination therapy correlated with the induction of pro-apoptotic NOXA, we next assessed the broader spectrum of proteins involved during apoptosis. We initially assessed the effect of single and combination therapy on the expression of downstream pathway members BIM, BAK, BAX, PUMA and caspase-9 (**Figure 12**). After 48 hours of treatment, we found that the anti-apoptotic MCL1 protein was reduced, while the NOXA-regulated, pro-apoptotic BCL-2 proteins BIM, BAX and BAK were elevated in two IBC cell lines. As expected, we detected increased levels of cleaved caspase-9, which indicates the induction of apoptosis in these cell lines. As a negative control, we did not observe alterations in MCL1, NOXA or cleaved caspase-9 in the therapeutically insensitive HCC1806 cells (**Figure 13**), consistent with this cell line's observed lack of apoptosis induction following combination treatment (**Figure 10B**). PUMA expression was not consistently altered after single or combination treatments, suggesting that it may not play a main role in MCL1 degradation. These data suggest that NOXA-based regulation of apoptosis may be responsible for therapeutic efficacy in TNBC and IBC.

Because NOXA can bind to and enhance the degradation of MCL1 protein (69), and we had observed induction of NOXA expression and increased apoptosis in cell lines sensitive to combination therapy, we hypothesized that NOXA-MCL1 binding may contribute to cell death with our therapy. To confirm whether NOXA bound MCL1 in our system, we performed an MCL1 immunoprecipitation assay on cell lines following treatment. Following MCL1 precipitation, we were able to detect elevated NOXA protein by immunoblotting analysis in two cell lines treated with both entinostat and pimasertib (**Figure 14**). These results suggest that our combination therapy leads to enhanced apoptosis in TNBC and IBC cells by reducing MCL1 expression potentially through NOXA-mediated degradation of MCL1.

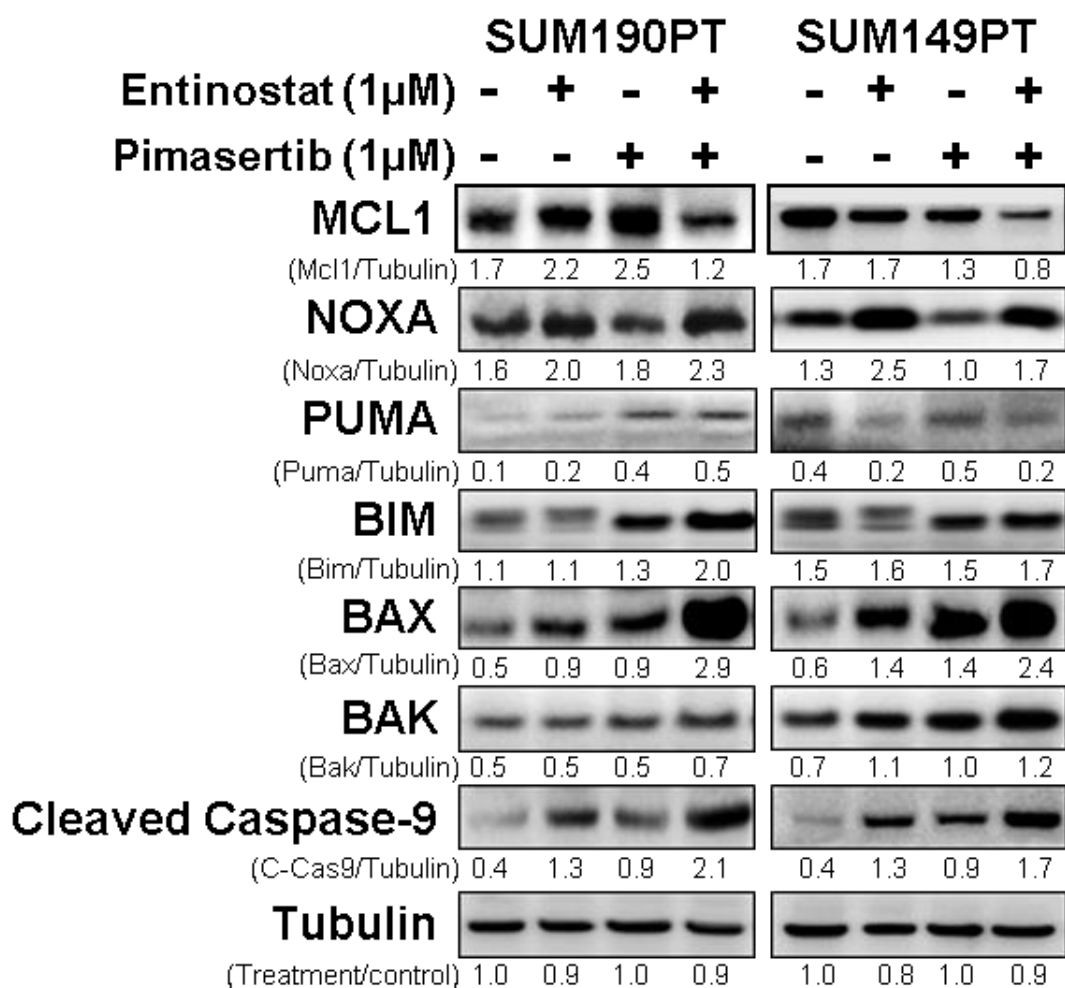


Figure 12. Mitochondrial apoptosis activated following combination therapy. MCL1, NOXA, PUMA, and mitochondrial apoptosis-related proteins BIM, BAX, BAK, and cleaved caspase-9 were examined through immunoblotting analysis. Pixel density of proteins was quantified for each condition, and the ratios of protein/tubulin or treatment/control are shown next to the blots; tubulin expression was used as a protein loading control.

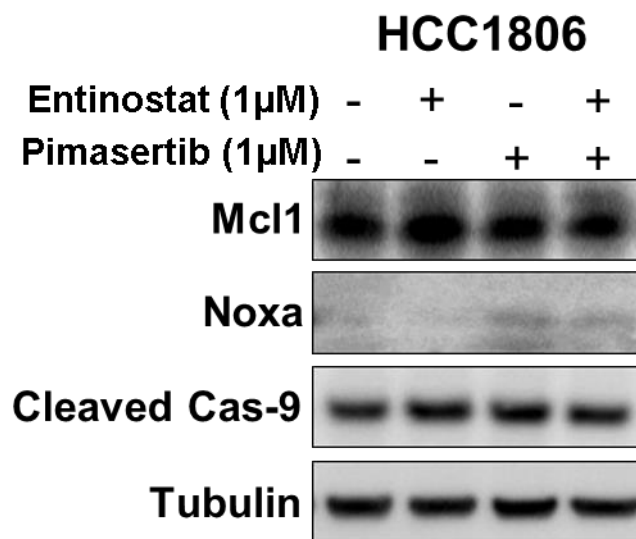


Figure 13. Low-NOXA-inducible HCC1806 cell line did activated mitochondrial apoptosis after entinostat and pimasertib single or combination treatments. Expression levels of NOXA, MCL1, and apoptosis-related protein cleaved caspase-9 were determined through immunoblotting analysis in the low-NOXA-inducible HCC1806 cell line after 48 hours of treatment with entinostat (1 μ M) and pimasertib (1 μ M). Tubulin expression was used as a protein loading control.

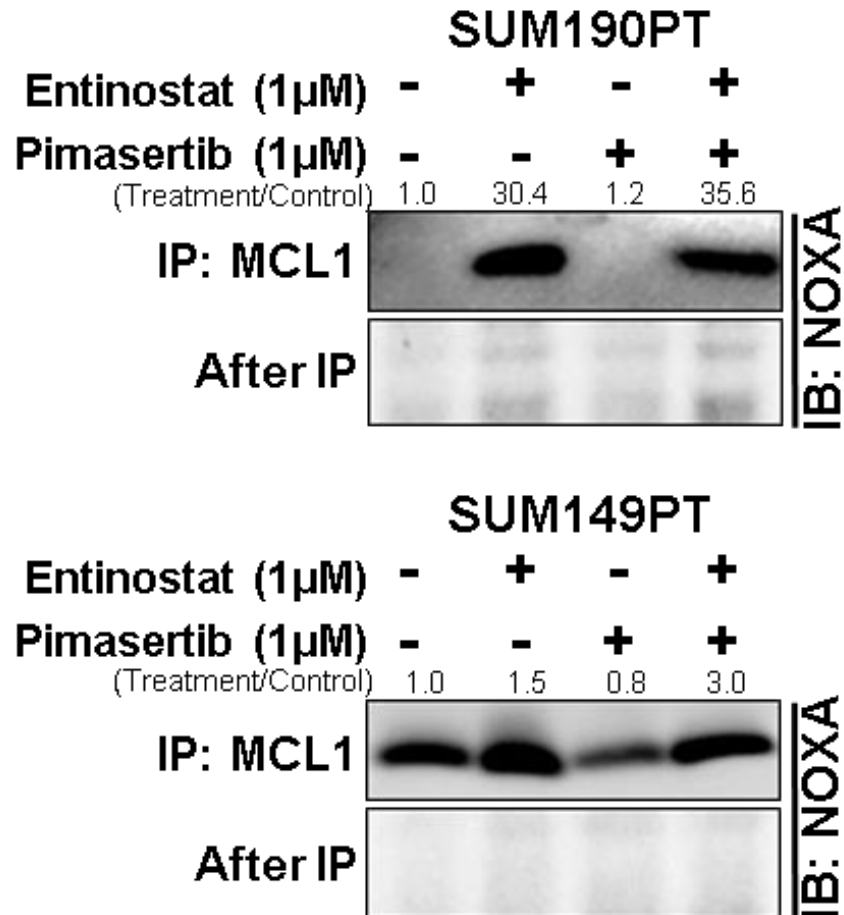


Figure 14. NOXA binds to MCL1 following combination entinostat and pimasertib treatment. NOXA/MCL1 binding on SUM190PT and SUM149PT cells was determined after entinostat (1 μM) and pimasertib (1 μM) individual and combination treatment by immunoprecipitation (IP) using anti-MCL1 antibody and immunoblotting with anti-NOXA antibody. After-IP samples were also blotted with NOXA antibody as an IP control. Pixel density of proteins was quantified for each condition, and the ratios of protein/tubulin or treatment/control are shown next to the blots; tubulin expression was used as a protein loading control.

3.2.3 NOXA and MCL1 play important roles in regulation of sensitization of IBC and TNBC cells to entinostat and pimasertib treatment.

To determine whether NOXA is a critical component in defining the therapeutic efficacy of entinostat and pimasertib, we functionally silenced *NOXA* mRNA expression and assessed the response of SUM190PT and SUM149PT cells to treatment (**Figure 15A**). When treated with entinostat, NOXA-silenced SUM190PT and SUM149PT cells did not display altered activation of caspase-3, however the loss of NOXA expression hindered the cytotoxic effects of entinostat compared to scrambled siRNA control ($P < 0.05$, and $P < 0.005$, respectively) (**Figure 15A-B**). The unaltered induction of cleaved caspase-3 upon siNOXA inhibition is probably due to the high levels of *NOXA* mRNA that are still induced after entinostat treatment of siNOXA-transfected SUM190PT and SUM149PT cells (5- and 3-fold increase, **Figure 15A**), permitting apoptosis. These results suggest a role for NOXA in enabling cytotoxicity after entinostat treatment.

In a reverse-complementary approach, we assessed whether transient over-expression of NOXA could modulate cells' response in combination with pimasertib in the treatment-sensitive SUM190PT and SUM149PT cells, or the treatment-resistant HCC1806 cells, which lack entinostat-mediated NOXA mRNA induction (**Figure 15C**). Following overexpression of NOXA and pimasertib treatment, SUM190PT and SUM149PT cells had significant inhibition of cell proliferation compared to untreated cells ($P < 0.0001$, and $P < 0.005$, respectively) (**Figure 15D**), further supporting the significance of NOXA mediating MCL1 degradation and enhancing pimasertib treatment. In contrast, HCC1806 cells had increased resistance to pimasertib treatment after NOXA overexpression. These findings suggest that the HCC1806 resistant cell line could have an alternative mechanism by which it is able to override NOXA

activity, possibly due to expression of other anti-apoptotic proteins, or activation of cell survival pathways, avoiding NOXA-mediated apoptosis.

As we have demonstrated that NOXA can affect overall protein levels of MCL1 leading to altered drug sensitivity in IBC and TNBC cells, we next assessed whether alteration of MCL1 could similarly modulate the therapeutic action of our rationalized combination treatment. Following transient MCL1 expression, entinostat and pimasertib single and combination treatments were tested in SUM190PT and SUM149PT cells (**Figure 16A, B**). Overexpression of MCL1 significantly reversed the sensitivity of SUM190PT and SUM149PT cells to entinostat single ($P < 0.05$) and combination treatments ($P < 0.0001$). Conversely, when we treated SUM190PT and SUM149PT cells with a highly selective MCL1 inhibitor, UMI-77, in combination with pimasertib, we observed synergistic growth inhibition (CI values < 0.6 and 0.9 , respectively; data not shown), accompanied by a significant induction of apoptosis compared to untreated control cells ($P < 0.05$) (**Figure 16C, D**). These data indicate that MCL1 is critical for the resistance of IBC and TNBC cells to treatment, and suggests a synergistic anti-proliferative combination of pimasertib with inhibitors of MCL1 expression, such as through entinostat-mediated NOXA degradation of MCL1.

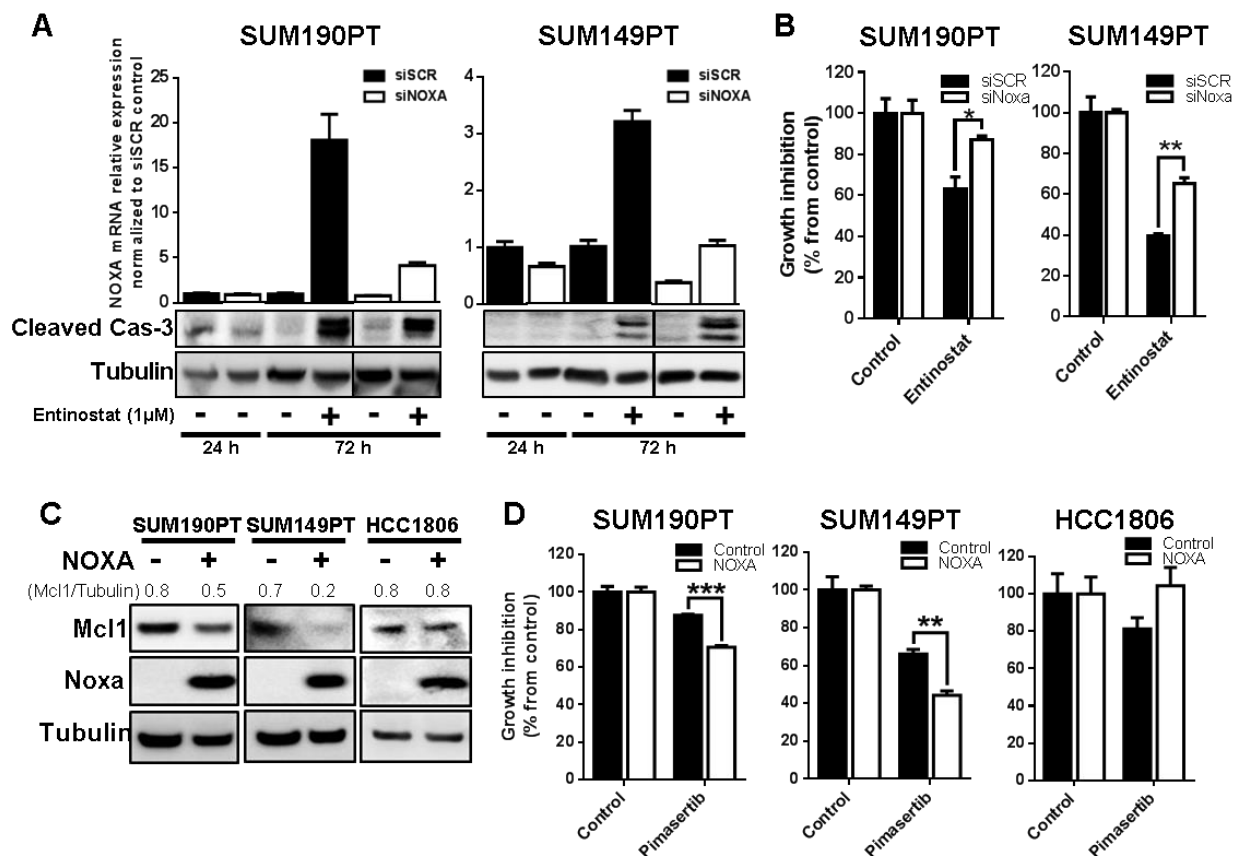


Figure 15. NOXA expression plays an important role in the regulation of sensitization of TNBC and IBC cells to treatment. SUM190PT and SUM149PT cells were transfected with NOXA (siNOXA) or Scrambled (siSCR) siRNA through electroporation. Knockdown of NOXA mRNA and induction of apoptosis as measured by cleaved caspase-3 after siRNA inhibition were confirmed by quantitative RT-PCR and immunoblotting analysis (A), respectively, after entinostat treatment for 24 and 72 hours. Cell proliferation after siRNA and entinostat treatment was measured by SRB staining after 72 hours (B). SUM190PT, SUM149PT, and HCC1806 cells were transfected with either a NOXA-expressing vector or empty control vector by electroporation. Expression of NOXA, as well as MCL1, was analyzed by immunoblotting analysis 72 hours after transfection (C). Pixel density of MCL1 was quantified for each condition, and the ratios of MCL1/tubulin are shown above the blots; tubulin expression was used as a protein loading control. Proliferation of cells with NOXA overexpression in response to treatment with pimasertib (2.5 μM) was determined by SRB staining after 72 hours (D). Data were pooled from three independent experiments and presented as mean ± SEM. *, $P < 0.05$; **, $P < 0.005$; ***, $P < 0.0001$.

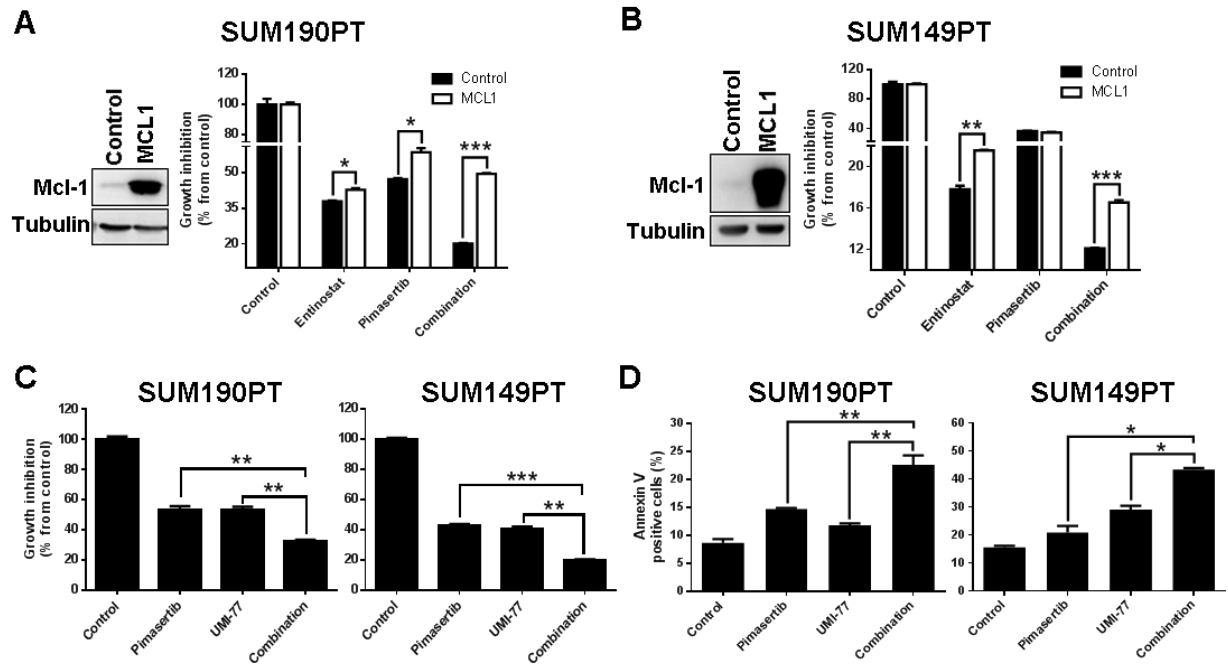


Figure 16. MCL1 protein expression and activity have a significant role in the sensitivity of TNBC and IBC cells to pimasertib and entinostat combination treatment. SUM190PT and SUM149PT cells were transfected with either MCL1-expressing or empty control vectors by electroporation (A, B). Induced expression of MCL1 protein was confirmed by immunoblotting analysis. The ability of MCL1 overexpression to induce cell proliferation after entinostat (5 μ M) and pimasertib (5 μ M) single and combination treatments was measured by SRB staining after 72 hours. Cell proliferation (C) and apoptosis (D) were determined by SRB staining and Annexin V-PE staining, respectively, in SUM190PT and SUM149PT cells after inhibition of MCL1 by the small molecule inhibitor UMI-77 (0.3 μ M and 5 μ M, respectively) in combination with pimasertib (1 μ M). Data were pooled from three independent experiments and presented as mean \pm SEM. Tubulin expression was used as a protein loading control. *, $P < 0.05$; **, $P < 0.001$; ***, $P < 0.0001$.

3.2.4 Entinostat and pimasertib combination treatment suppresses tumorigenic potential *in vitro* and *in vivo* tumor growth in xenograft models of aggressive breast cancer.

Prior to the *in vivo* drug testing, we first assessed whether the combination of entinostat and pimasertib could affect the ability of TNBC and IBC cells to form anchorage-independent tumor spheroids *in vitro*. Preliminary studies indicated that the IC₅₀ doses for both drugs were too toxic in this experimental setting to allow any colony growth (data not shown). Therefore, we selected lower doses than the IC₅₀ for both entinostat and pimasertib. Combination treatment significantly reduced the number of colonies formed by SUM190PT and SUM149PT cells compared to single-drug treatments ($P < 0.05$), whereas in the treatment-resistant HCC1806 cells entinostat did not affect tumorigenicity, and pimasertib and combination treatment only mildly inhibited colony formation (**Figure 17**).

After confirming reduced cell proliferation and anchorage-independent growth following entinostat and pimasertib combination treatment *in vitro*, we next determined whether these two drugs could inhibit tumor growth in preclinical xenograft animal models of TNBC and IBC. Mice ($n = 10$ to 12 per group) were treated with optimized doses of entinostat (20 mg/kg/day for SUM190PT, 5 mg/kg/day for SUM149PT), pimasertib (30 mg/kg/day for SUM190PT, 0.5 mg/kg/day for SUM149PT), or a combination of both drugs. When compared to mice treated with vehicle control, combination-treatment mice displayed a significant reduction in tumor growth rate by 79% ($P < 0.0001$) and 65% ($P < 0.001$) in SUM190PT and SUM149PT cells, respectively (**Figure 18**). Of importance, while high dose single treatment of entinostat (20mg/kg) or pimasertib (30mg/kg) significantly inhibited tumor growth (**Figure 18** and **Figure 19A**), at lower doses the combination treatment outperformed single treatment in SUM149PT (**Figure 18**) and MDA-MB-231 xenografts (**Figure 19B**). Mice tolerated all treatments with no

significant change in body weight noted (**Figure 20**). Immunostaining for markers of proliferation and cell death in SUM190PT, SUM149PT, and MDA-MB-231 primary tumors identified, as expected, a reduction of Ki67-positivity and an increase in TUNEL or cleaved caspase-3 staining in tumors receiving combination treatment (**Figure 21** and **Figure 19B**). Lastly, after entinostat and pimasertib combination treatment protein lysate expression of tumor samples from SUM190PT and SUM149PT xenograft models revealed higher protein expression of NOXA and its downstream marker of mitochondrial cell death, cleaved caspase-9, together with decreased expression of MCL1 (average protein expression quantified relative to tubulin loading control, n = 5 tumors per treatment group, **Figure 22 A, B**). Together, these results suggest increased apoptosis consistent with TUNEL staining following entinostat and pimasertib combination treatment through mediation of NOXA expression and subsequent degradation of MCL1 enhanced by pimasertib in TNBC and IBC.

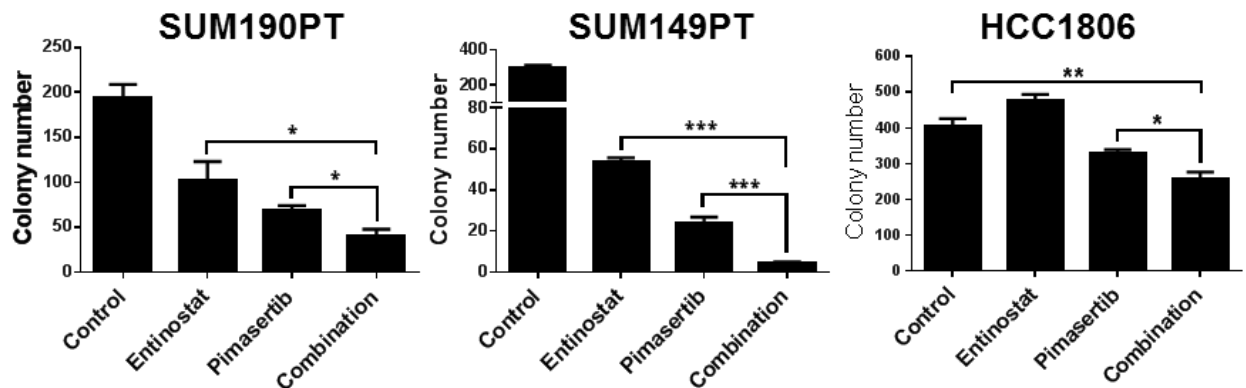


Figure 17. Entinostat and pimasertib combination treatment inhibits colony formation *in vitro*. SUM190PT, SUM149PT and HCC1806 cell lines were treated with entinostat (0.01 and 0.05 μ M, respectively) and/or pimasertib (0.01 and 0.05 μ M, respectively) and allowed to grow in an anchorage-independent environment for 2-3 weeks; clonal growth was measured at the treatment endpoint by colony formation (A). Data were pooled from three independent experiments and presented as mean \pm SEM. *, $P < 0.05$; **, $P < 0.001$; ***, $P < 0.0001$.

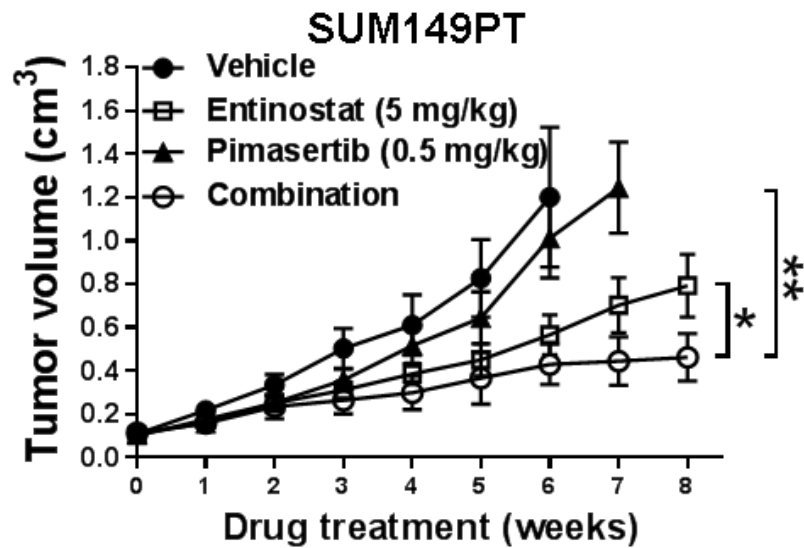
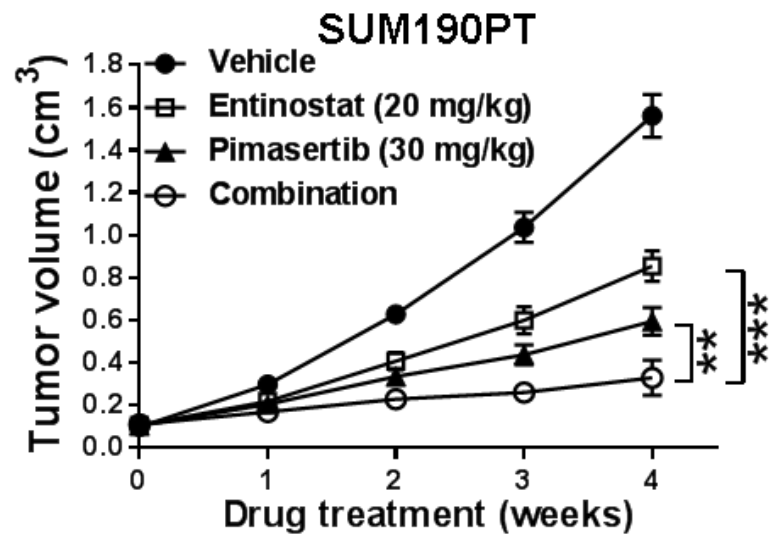


Figure 18. Entinostat and pimasertib combination treatment inhibits tumor growth *in vivo*. Tumor volume measurements for SUM190PT and SUM149PT tumor xenograft-bearing mice (n=12/group and 10/group, respectively) treated via oral gavage daily for up to 2 months with vehicle, entinostat (20 or 5 mg/kg), and/or pimasertib (30 or 0.5 mg/kg). *, P < 0.05; **, P < 0.001; ***, P < 0.0001.

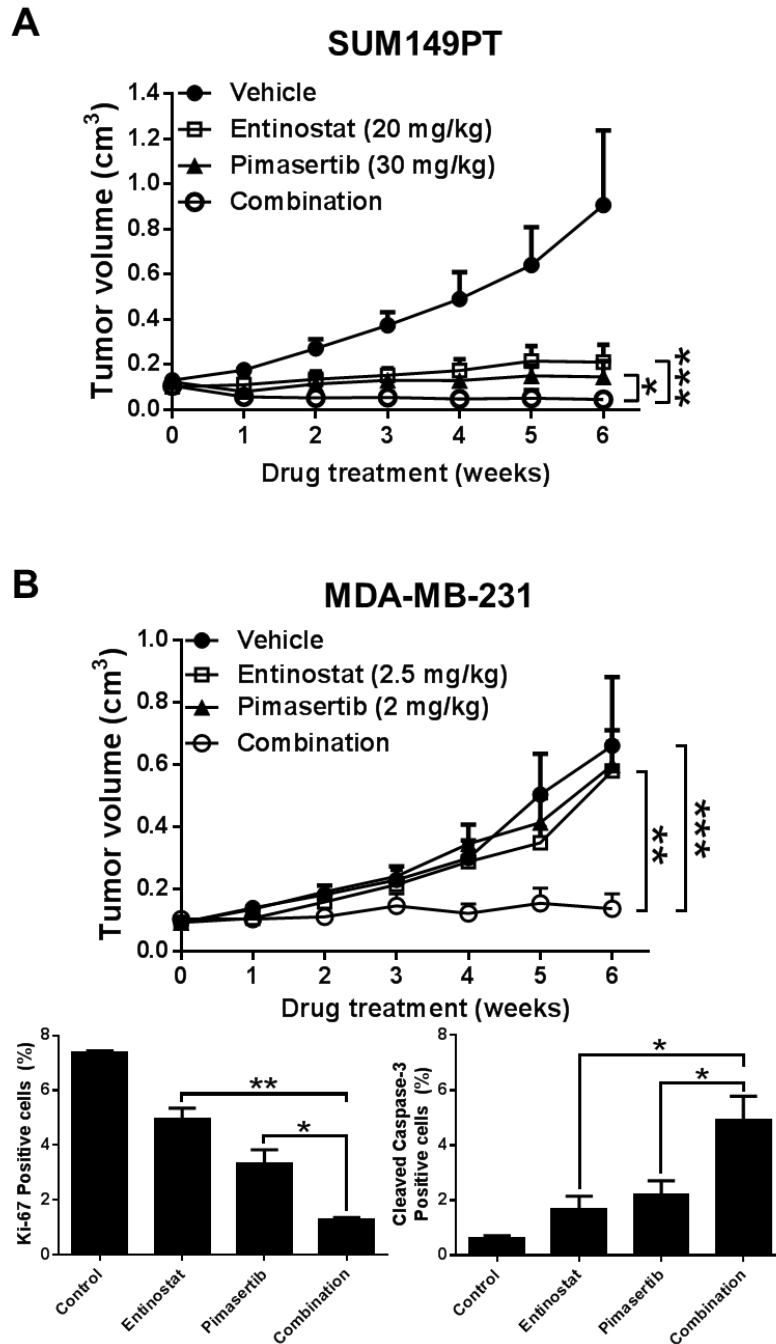


Figure 19. Higher and lower doses of entinostat and pimasertib combination treatment induce tumor regression in IBC and TNBC xenograft models. A, SUM149PT tumor-bearing mice (n=12/group) were treated with high doses of entinostat (20 mg/kg/day) and/or pimasertib (30 mg/kg/day), similarly to the experiments in SUM190PT xenografts (Figure 6C), via oral gavage daily for 6 weeks. B, Low doses of entinostat (2.5 mg/kg/day) and pimasertib (2 mg/kg/day) were tested on a third TNBC xenograft model, MDA-MB-231 (n=9/group) via oral gavage daily for 6 weeks. Paraformaldehyde-fixed paraffin tumor sections from MDA-MB-231 tumor-bearing mice from each treatment group were immunostained with anti-Ki-67 or anti-cleaved caspase-3 antibodies (bottom bar graphs). Images from IHC staining were converted by ImageJ software to accomplish quantification of Ki-67 and cleaved caspase-3 expression. Quantification of IHC staining is represented as mean \pm SEM. *, P<0.05; **, P<0.001; ***, P<0.0001.

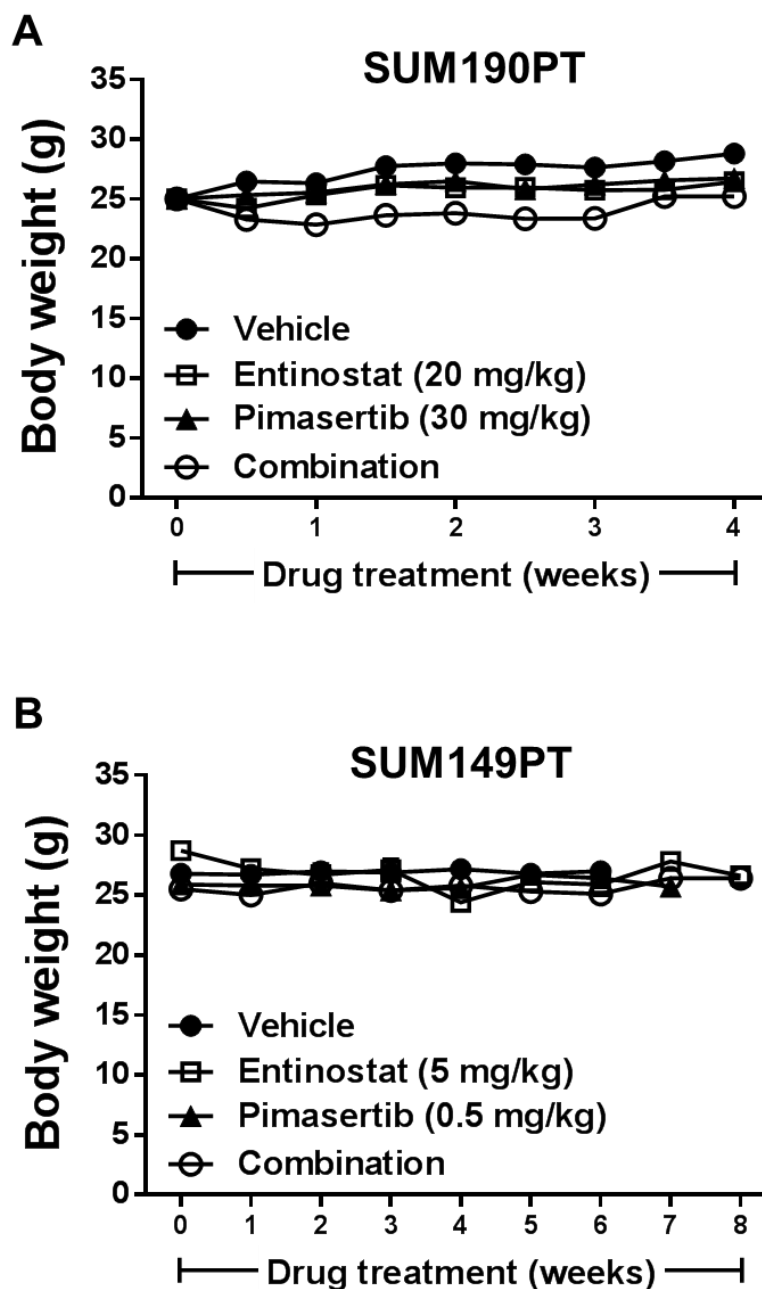


Figure 20. No toxicity was observed after entinostat and pimasertib single and combination treatments *in vivo*. Evaluation of average mice body weights during animal experiments. Measurements were taken twice a week for each treatment group in SUM190PT (A) and SUM149PT (B) tumor-bearing mice.

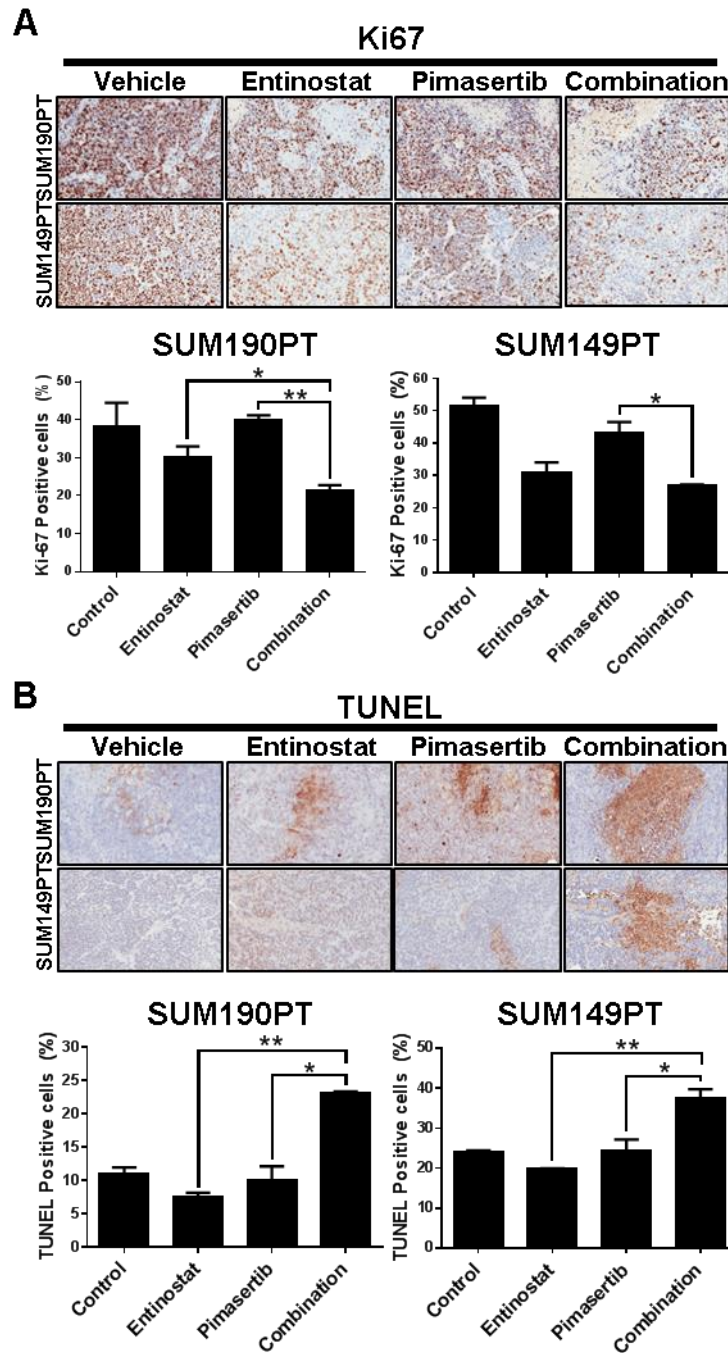


Figure 21. Combination entinostat and pimasertib therapy inhibits proliferation, and promotes apoptosis, *in vivo*. Immunohistochemistry (IHC) staining from SUM190PT and SUM149PT tumor xenografts treated with vehicle or the indicated drugs. Paraformaldehyde-fixed paraffin sections were incubated with (A) anti-Ki-67 antibody, and (B) TUNEL staining was performed. Representative images of 5 IHC staining experiments are illustrated. Magnification, 20x. The images were converted by ImageJ software to accomplish quantification of Ki-67 and TUNEL expression. Quantification of IHC staining is represented as mean \pm SEM. *, $P < 0.05$; **, $P < 0.001$; ***, $P < 0.0001$.

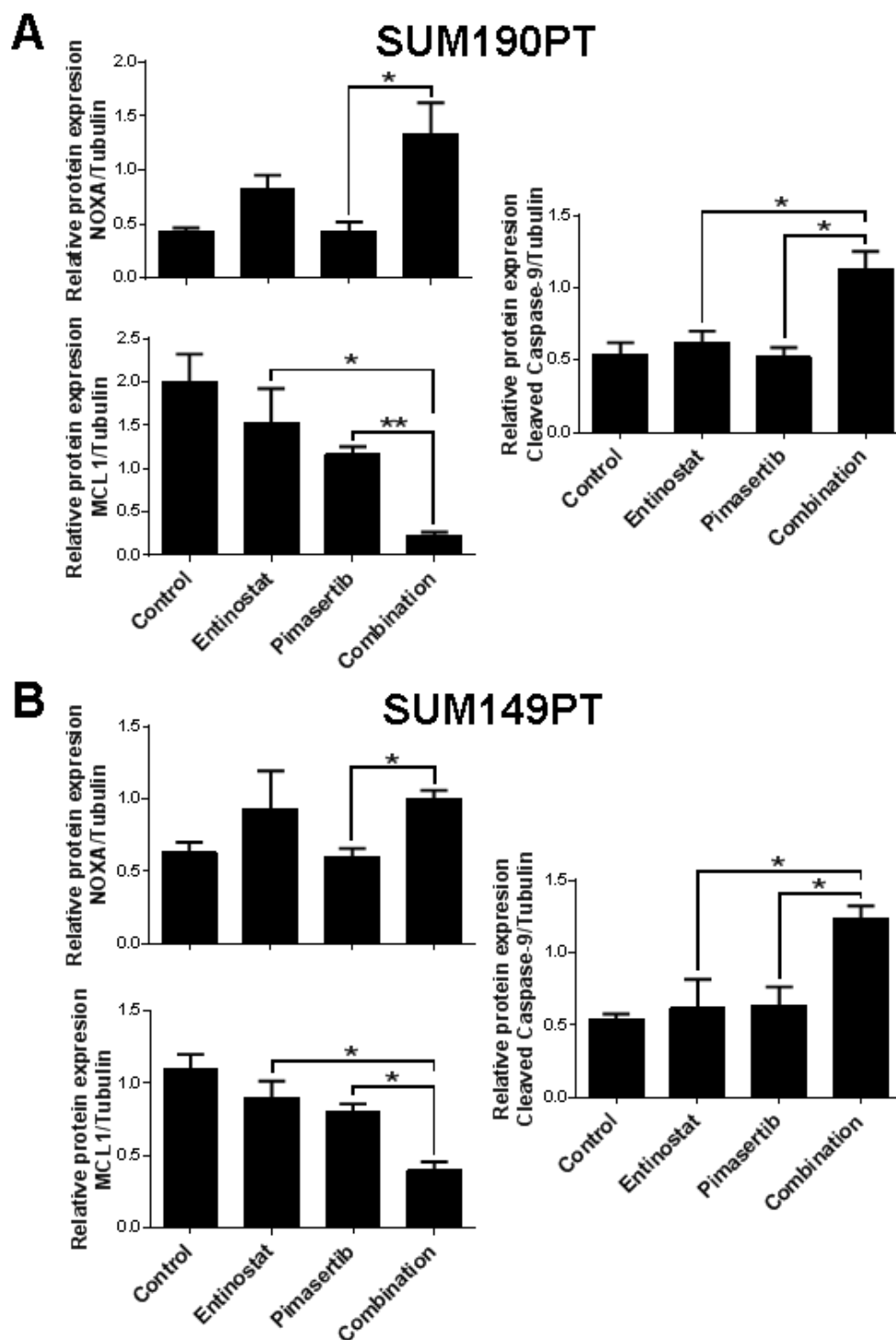


Figure 22. Entinostat and pimasertib combination treatment promotes NOXA-mediated apoptosis and decreased expression of MCL1. Protein expression (represented as mean \pm SEM) relative to loading control after immunoblotting analysis of NOXA, MCL1, and cleaved caspase-9 expression in protein lysates of five representative tumor samples from each treatment group of mice bearing SUM190PT or SUM149PT tumors. Tubulin expression was used as a protein loading control. Pixel density of protein bands was quantified for each condition using ImageJ software. *, $P < 0.05$; **, $P < 0.001$; ***, $P < 0.0001$.

3.3 Discussion

Our study has revealed that combination of entinostat and pimasertib synergistically act to reduce tumorigenic potential, proliferation, and *in vivo* growth of tumor using preclinical models of TNBC and IBC. The effectiveness of this treatment was significantly associated to the ability of tumors to induce mRNA expression of *NOXA*, a member of the Bcl-2 family of apoptosis-regulating proteins, in 65% of TNBC and IBC cell lines following entinostat treatment, leading to enhanced degradation of the anti-apoptotic protein MCL1 in IBC and TNBC. Further, in our retrospective genomic analyses on an extensive clinical cohort of breast cancer patients, we were able to associate high-MCL1/low-*NOXA* tumor expression in breast tumors with worse OS and DMFS outcomes when compared with low-MCL1/high-*NOXA*-expressing tumors, which supports the translational potential for targeting these molecules in the clinical setting.

Several studies have demonstrated that entinostat induces apoptosis by expression of death receptor tumor necrosis factor (TNF)-related apoptosis-inducing ligand (TRAIL) and transcriptional upregulation of pro-apoptotic Bcl-2 proteins BIM and *NOXA* in acute myeloid leukemia (81) and in HER2-overexpressing breast cancers (40), supporting chemosensitization (83). Here, we identified selective induction of *NOXA* mRNA expression after entinostat treatment in a subset of IBC and TNBC cell lines, which often correlated with increased protein expression of MCL1 as well as p-ERK, a known stabilizer of MCL1. Thus, our data suggest that besides the induction of *NOXA* after single entinostat treatment, additional p-ERK induction could play a role in the stabilization of anti-apoptotic MCL1, supporting our strategy of testing an ERK pathway inhibitor, pimasertib, as a synergistic partner.

The interaction between MCL1 and NOXA contributing to apoptosis has been previously demonstrated, whereby MCL1 is recruited from the cytosol into the mitochondria by NOXA promoting BIM release from MCL1 sequestration, which initiates MCL1 phosphorylation and subsequent ubiquitination triggering proteasome-mediated degradation (68, 84). Here, we demonstrate that NOXA bound to MCL1 leading to its degradation following entinostat and pimasertib treatment. This was associated with activation of mitochondrial/proteasome-mediated apoptosis in SUM190PT and SUM149PT cell lines as measured through BIM, BAX, BAK, and caspase-3 and -9 cleavages *in vitro* and *in vivo*, whereas single or combination treatments failed to reduce tumorigenic potential and induce apoptosis in the treatment-resistant HCC1806 cells, which lack entinostat-mediated NOXA mRNA induction. We suggest that the minimal treatment effects inducing apoptosis on HCC1806 cells may be attributed to entinostat ability to inhibit cell proliferation by inducing p21-mediated G1 cell cycle arrest following low doses of entinostat treatment, as reported by others (85). Therefore, the clinically relevant entinostat doses tested in our study may not be effective at inducing apoptosis in the HCC1806 cell line. Further investigation is necessary to fully understand the potential mechanisms of inducing treatment resistance.

We recognize that there are slightly different treatment sensitivity levels observed between the SUM190PT and SUM149PT cell lines, which may be due to diverse NOXA/MCL1 binding abilities, NOXA mRNA induction levels, or SUM190PT HER2-positivity possibly affecting NOXA expression via TP53. There is evidence that HER2 signaling negatively regulates the function of TP53, a known positive regulator of NOXA expression, making it possible for HER2 to have an indirect inhibitory role on NOXA via TP53 (86). Additionally, we have previously identified that entinostat can sensitize trastuzumab/lapatinib-resistant HER2-

positive cells to treatment by induction of apoptosis via FOXO3-mediated Bim1 expression (40). Therefore, future studies into the potential role of HER2 positivity in relation to NOXA, as well as a potential rationale for an entinostat-trastuzumab-pimasertib triple-combination therapy for instance, needs to be further explored as a possible therapeutic approach in HER2-positive breast cancer.

Inhibition of pro-apoptotic NOXA through siRNA, as well as vector-induced expression of anti-apoptotic MCL1, significantly induced resistance of SUM190PT and SUM149PT cells to entinostat and pimasertib separately, as well as to combination treatment, when compared to control transfections. Our findings confirmed the important role NOXA plays in sensitivity of TNBC and IBC cell lines to combination treatment, in that transient transfection of a NOXA-expressing vector reduced MCL1 protein levels, as well as sensitized the cells in combination with pimasertib. Further experiments should be done to provide more evidence supporting the direct role of NOXA and MCL1 driving combination treatment sensitivity, such as by developing NOXA and MCL1 protein inducible expression/suppression models, as well as constructs with mutated functional domains to determine their individual roles affecting combination treatment synergy.

IBC and TNBC remain diseases without an effective targeted therapy that can significantly affect patients' morbidity and/or survival. Our study provides preclinical evidence for the translational potential of a combined entinostat and pimasertib therapy for patients with the most aggressive molecular and clinical diagnoses of breast cancer, TNBC and IBC, especially for those with tumors expressing high levels of MCL1 and p-ERK, or increased levels following initial entinostat treatment. Although p-ERK has been reported to be a biomarker of

poor prognosis in breast cancer (87), a potential challenge for the clinical application of our therapeutic strategy is that there are no treatment-predictive biomarkers established for the selection of patients who could benefit from MCL1-inhibition treatment. With the goal of discovering such a biomarker, a chemical genomic study identified that tumors with low expression of BCL-xL, an anti-apoptotic BCL2 family member, were associated with sensitivity of breast and non-small cell lung cancer tumors *in vivo* to compounds that inhibit MCL1, representing a potential strategy that may be established in the clinic for the selection of patients who could benefit from MCL1-inhibition treatments (88). More importantly, the genomic and proteomic analyses performed in our current study are translatable to the clinical trial setting, allowing the study of baseline and treatment-induced MCL1 and NOXA expression levels in patient tumors. As supported by the results of our *in vivo* studies, the inclusion of MCL1 and NOXA expression measurement could provide robust predictive biomarkers of treatment response to entinostat and pimasertib combination therapy.

CHAPTER 4: IDENTIFICATION OF A COMBINATIONAL THERAPY STRATEGY OF EICOSAPENTAENOIC ACID AND EPHA2-TARGETING AGAINST TN-IBC

4.1 Introduction

4.1.1 Inflammation in cancer

Inflammation is a biological process designed to fight infections and heal wounds. Inadvertently, inflammation can support tumor formation, growth and angiogenesis by supplying bioactive molecules that facilitate progression and metastasis in multiple types of cancer, including that of the breast (89-91). Large-scale studies of genetic variations of inflammation across cancer sites has indeed revealed an association with increased risk of cancer development, suggesting inflammation as an initiator or promoter of cancer (92). There are two distinct types of inflammation associated to tumor formation: tumor-extrinsic, and tumor-intrinsic. Tumor-extrinsic inflammation can involve multiple factors, such as obesity, autoimmune diseases, bacterial/viral infections, tobacco exposure, and alcohol consumption, which can increase the risk of cancer occurrence and promote its progression (93). Cancer-intrinsic inflammation on the other hand, is triggered by the aberrant expression of cancer-associated genes within a cell, contributing to tumor progression by recruiting and activating inflammatory cells to its microenvironment (93). Both the extrinsic and the intrinsic types of inflammations can subsequently result in immunosuppression of the surrounding of a malignant cell providing an ideal microenvironment for the development of a tumor.

4.1.2 Inflammation in TN-IBC

Pathological assessment of triple-negative IBC (TN-IBC) has identified increased expression of molecular mediators of inflammation, such as COX2 (prostaglandin G/H synthase

2), and prostaglandin E2 (PGE₂), representing potential therapeutic targets (94). Therefore, this suggests the potential to investigate compounds that can target these inflammatory molecules for the treatment of TN-IBC.

4.1.3 Anti-inflammatory compounds against TN-IBC

The majority of cells involved in cancer –associated inflammation are genetically stable and not subject to the emergence of drug resistance, therefore targeting inflammation represents a viable strategy for cancer therapy. In clinical trials, the consumption of non-steroidal anti-inflammatory drugs, such as aspirins, naproxen and ibuprofen, has been associated to a reduced cancer risk, and long-term reduction in the incidence and mortality for several cancer types including breast cancer (95). Therefore, those findings suggests the use of anti-inflammatory compounds and specific inhibitors of inflammatory pathways for the treatment and prevention of cancer.

Recent findings from our laboratory have demonstrated that inhibition of inflammatory pathways such as through the use of celecoxib, a COX2 inhibitor, or lovaza which contains omega-3 fatty acids with anti-inflammatory properties, can inhibit the growth of TN-IBC cells *in vitro* and of tumors xenografts *in vivo*.

4.1.3.1 Eicosapentaenoic acid (EPA)

Eicosapentaenoic acid (EPA), a polyunsaturated omega-3 fatty acid which has been approved for the treatment of hypertriglyceridemia, is additionally known to inhibit inflammatory pathways, and has been observed to inhibit tumor initiation, progression, and growth *in vivo* by exerting anti-inflammatory effects in cancer cells (96, 97). Evaluation of an

U.S. Food and Drug Administration (FDA)-approved EPA-purified form, Vascepa, has been observed to have a safer toxicological profile than other available omega-3 fatty acids, such as docosahexaenoic acid (DHA), providing an ideal anti-inflammatory compound to be investigated as a therapeutic agent against TN-IBC (98, 99). Omega-3 fatty acids such as EPA can also modulate cancer cells motility by incorporating into the plasma membrane in where they modify lipid rafts increasing membrane compaction, modification of intracellular signaling, and inhibition of invasiveness of cancer cells (**Figure 23**) (100-102).

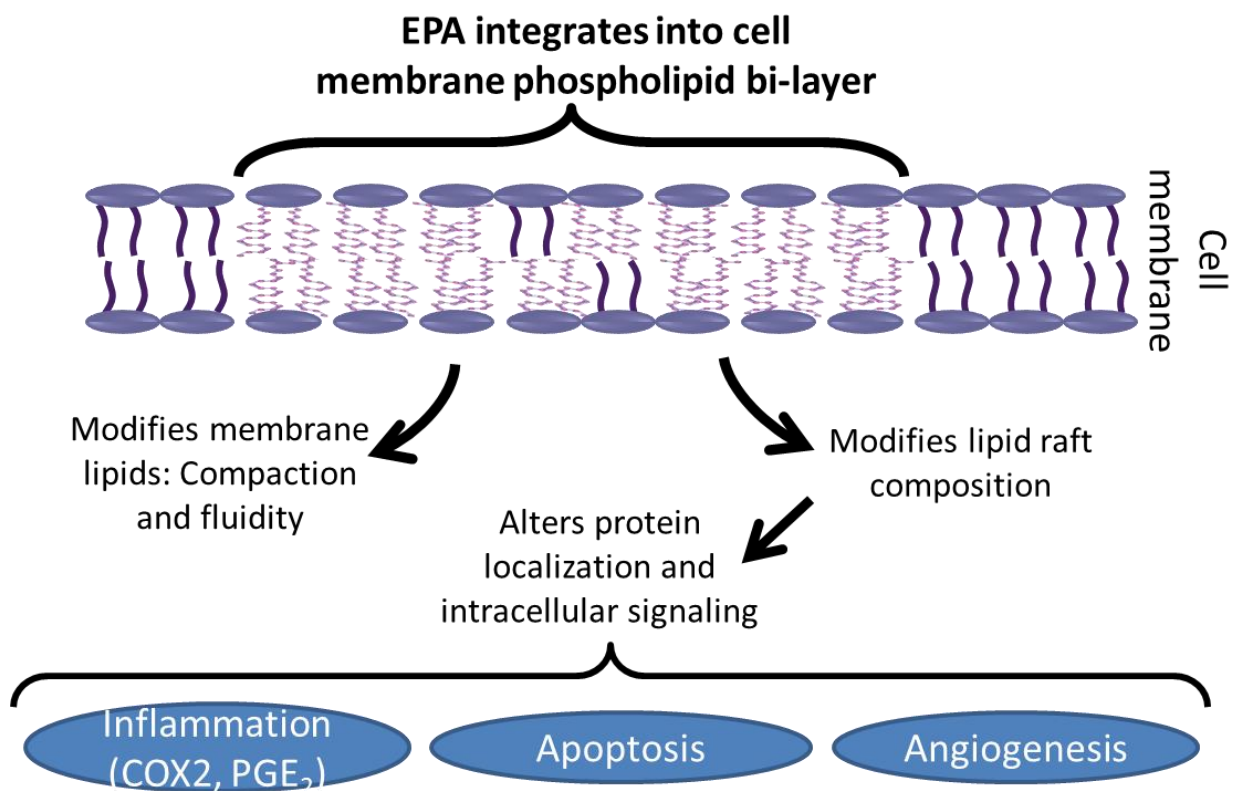


Figure 23. Diagram of EPA activity in cell membrane and intracellular pathways.

4.1.4 Ephrin family of receptor tyrosine kinases

The Ephrin molecules comprise the largest family of receptor tyrosine kinases in the mammalian genome, and are expressed at variant levels in most cell types (*103*). Ephrins are known to be associated to inflammatory diseases, as well as increasingly recognized as important players in carcinogenesis (*104*). Ephrin receptors (EPHs) and their receptor interacting proteins (Ephrin) ligands, can be classified based on their sequence homology, receptor-ligand binding preferences, and ephrin membrane anchorage (*105*). An important signature of EPHs/ephrins are their bidirectional signaling by which they control multiple biological functions associated to cellular homeostasis (*106*). Alteration in EPHs/ephrins signaling in humans, and particularly EPH receptor ligand-independent functions, have been associated to aberrant cell functions and oncogenic features (*107*).

4.1.4.1 Ephrin type-A receptor 2 (EPHA2)

Among EPHs, emerging evidence on the ligand independent functions of the EPH receptor EPHA2, continue to accumulate in association to cancer progression. EPHA2, a cell-surface receptor tyrosine kinase associated to proto-oncogene tyrosine-protein kinase Src (SRC) signaling, is aberrantly expressed in multiple cancer types in where it plays an important ligand-independent role in tumor growth and metastasis (*108-110*). As a cell surface receptor, EPHA2 localization has been implicated in the modulation of gap junctions and cell plasma membrane fluidity attributing to increased cell motility in tumor invasion (*111-113*). Therefore, EPHA2 is an emerging molecule of interest for therapeutic targeting in cancer.

4.1.5 Gap in Knowledge

Even though the efficacy of anti-inflammatory compounds have been demonstrated to improve cancer patients outcome, the translation of anti-inflammatories as a monotherapy, including omega-3 fatty acids, has been largely ineffective in solid tumors (*114, 115*).

Additionally, the regulation of EPA in cancer cell plasma membrane fluidity status have been implicated to the modulation of invasive and metastatic potential (*116-118*). However, there has not been evidence of increased membrane rigidity as a mechanism of apoptosis induction following combination therapy against TN-IBC. Therefore, the ability of EPA to kill cancer cells at concentrations well tolerated in humans, as well as its anti-inflammatory and membrane fluidity regulatory properties, support development of a novel EPA-based combinational treatment that enhances its efficacy for the treatment of TN-IBC patients.

4.2 Results

4.2.1 Eicosapentaenoic acid reduces tumor growth in a TN-IBC xenograft model

Polyunsaturated omega-3 fatty acids (PUFAs), such as EPA, have been observed to inhibit tumor initiation, progression and growth *in vivo* by exerting anti-inflammatory effects in cancer cells (96, 97). In particular, compared to other PUFAs supplements, EPA has additional health benefits making it the safest option (98). To assess EPA effects inhibiting tumor growth and prolonging survival in a pre-clinical xenograft model of TN-IBC, SUM149PT, we evaluated the mice treated with EPA at the dose equivalent to the human FDA-approved (0.8 g/kg), as well as half-dose (0.4 g/kg) (**Figure 24**). After treatment with EPA-diets (n = 10 per group) tumor and blood serum samples were collected when mice reached study endpoint (morbidity, or tumor burden of 1,500 mm³) for further analysis, including EPA lipid content. We validated the incorporation of EPA in serum total lipids (**Figure 25A**), as well as within the tumor phospholipid fraction (**Figure 25B**), in a dose-dependent manner. Moreover, we observed a significant inhibition of tumor growth (**Figure 25C**), and prolonged survival to endpoint (**Figure 25D**), on mice receiving 0.8 g/kg EPA when compared to half dose and control ($P < 0.05$). These data validates a potential role for EPA inhibiting TN-IBC tumor growth, and prolonging survival, but also provides evidence for the potential lack of efficacy for EPA as a monotherapy for cancer. Therefore, there is a need to identify a potential combination strategy that could enhance the therapeutic efficacy of EPA in treating TN-IBC.

4.2.2 Identification of EPHA2 as a clinically relevant target that can enhance EPA therapy against TN-IBC

To identify a potential candidate that enhances the sensitivity of TN-IBC cells to EPA, we performed a functional genomic, synthetic-lethal siRNA screen in SUM149PT cells.

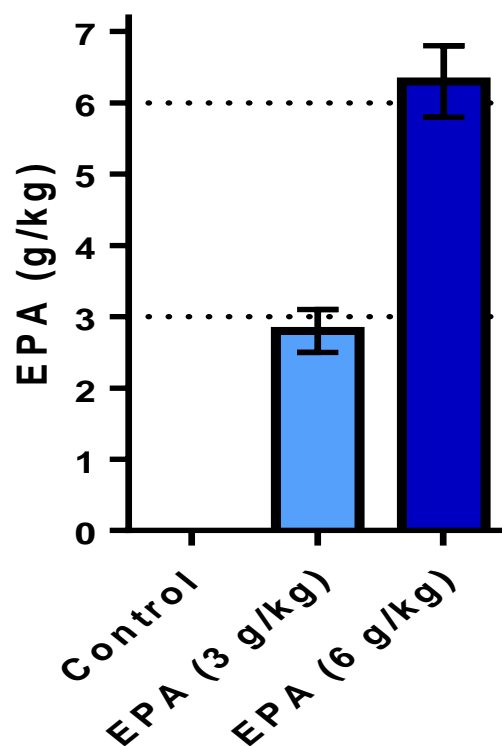


Figure 24. EPA (Vascepa) formulated diet equivalent to daily human dose. Customized AIN-76A mice diets containing the FDA-approved EPA purified form, Vascepa, were validated by chromatographic fatty acid analysis to contain doses equivalent to the human full (4 g) and half (2 g) daily doses: 6 and 3 g of Vascepa per kg of mice diet. These diets EPA concentrations are equivalent to mice EPA daily intakes of 0.8 and 0.4 g/kg, respectively, considering an average daily food intake of 3.5 g, and average mice weight of 25 g.

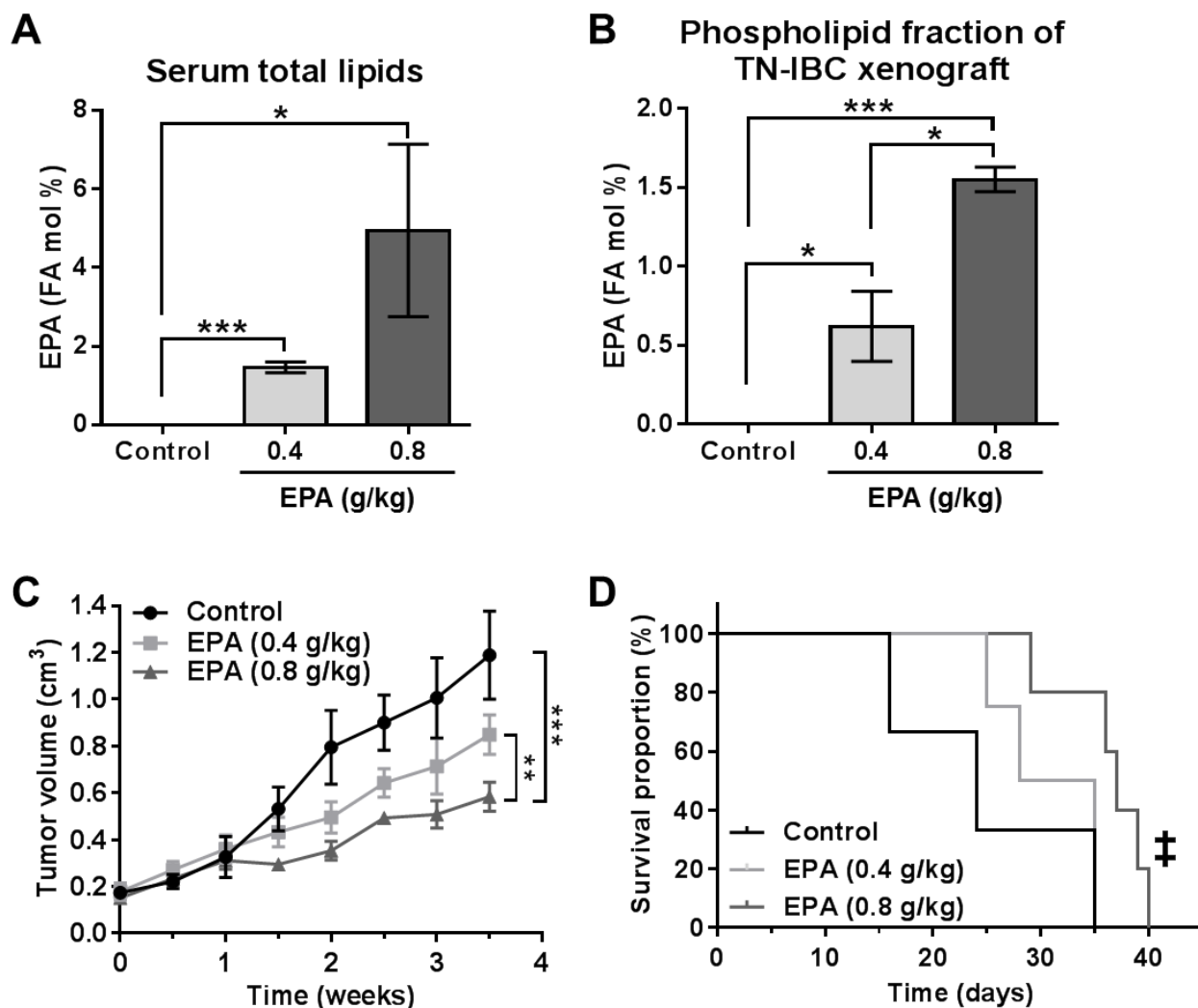


Figure 25. Eicosapentaenoic acid reduced tumor growth in a preclinical model of TN-IBC. EPA dose dependently inhibited tumor growth, and prolonged mice survival. Following EPA treatments (0.4 and 0.8 g/kg), the mol percentage of EPA in serum total fatty acids (FA) was analyzed by gas chromatography/mass spectrometry (**A**), and the tumor phospholipid fraction (**B**). (**C**) Tumor growth (volume), and (**D**) survival (endpoint = 1,500 mm³ tumor) were measured for SUM149PT tumor-bearing mice treated with EPA. Unpaired T-test: *, $P < 0.05$; **, $P < 0.001$; ***, $P < 0.0001$. Log-rank: ‡, $P < 0.05$ compared to EPA 0.4 g/kg and control.

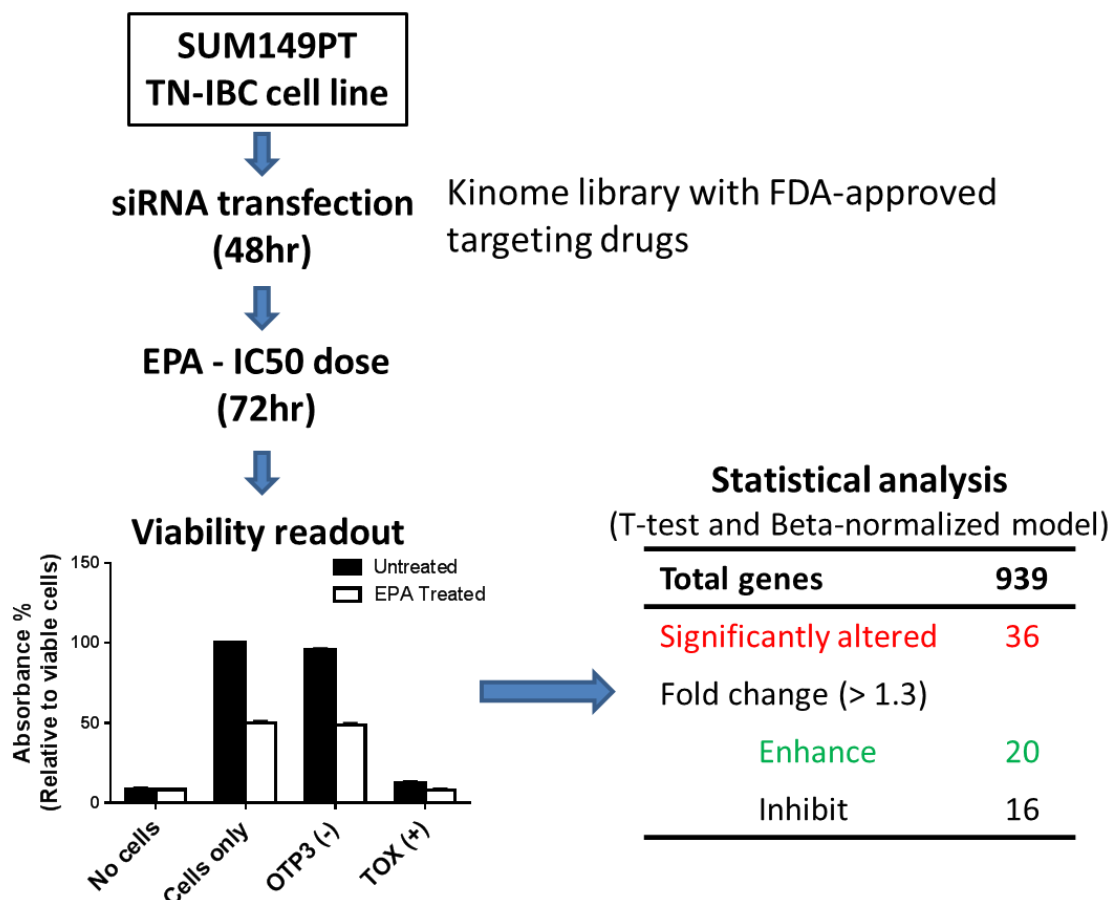


Figure 26. Diagram of functional high-throughput siRNA screen identifies candidate genes sensitizing TN-IBC cells to EPA therapy.

We employed a siRNA library directed against kinase genes for which FDA-approved drugs are currently available (**Figure 26**). To identify top candidates, we applied two selection criteria, namely: 1) absence of toxicity when the target is inhibited without EPA treatment, and 2) significantly enhancing the efficacy of EPA upon combination treatment. Using these criteria, we identified a total of 20 genes sensitizing SUM149PT cells to EPA, with EPHA2, DUSP4 and EDG2 among the top three candidates (**Table 3** and **Figure 27A**). Secondary validation using the specific inhibition of EPHA2, DUSP4 and EDG2 by multiple individual siRNAs, provided evidence for the candidates' potential enhancing the sensitivity of SUM149PT cells to EPA treatment (**Figure 27B**). Among top three candidates, we decided to focus on EPHA2, a cell surface receptor tyrosine kinase, because of the known association of its increased expression

with cancer progression (119). These results identify EPHA2 as a lead target for an EPA-based combination therapy in TN-IBC.

We pursued further studies to determine the clinical significance of EPHA2 expression among breast cancer patients. To achieve this, we analyzed the relevance of EPHA2 expression in breast cancer cell lines among published mRNA expression datasets (120), as well as in-house protein assessment. TNBC cell lines were significantly associated to higher EPHA2 protein (**Figure 28A-B**), and mRNA (**Figure 29**), expression when compared to cell lines from the other breast cancer subtypes HER2 positive, or hormone receptor (HR) positive. We further investigated EPHA2 expression in association with disease-free survival (DFS) using the BreastMark web-based mRNA dataset of breast cancer patient samples (50). Consistent with our findings in breast cancer cell lines, Kaplan-Meier survival curves revealed high EPHA2 expression to be specifically correlated with poor TNBC (basal-like) patient DFS, while not to HER2- or HR-positive patients (**Figure 30**). Together, these results strongly suggest the clinical significance of EPHA2 targeting, with specific clinical implications for the treatment of TN-IBC.

4.2.3 EPHA2 therapy in combination with EPHA2 inhibition synergistically kills cells through induction of apoptosis

To define the role of EPHA2 enhancing an EPA-based combination therapy in TN-IBC, we utilized functional gene silencing and drug-based inhibition studies. We genetically-engineered two TN-IBC cell lines, SUM149PT and BCX010, to express a doxycycline (dox)-inducible EPHA2-shRNA cassette using the pTRIPZ lentiviral system (**Figure 31**). We established two TN-IBC cell lines, SUM149PT and BCX010, transduced with doxycycline

Enhance cytotoxicity			Inhibit cytotoxicity		
Gene Symbol	Fold increase cytotoxicity	<i>P</i> -value	Gene Symbol	Fold increase cytotoxicity	<i>P</i> -value
PFKL	2.9	< 0.0001	ADRA2B	-1.5	< 0.0001
EPHA2	2.7	< 0.0001	CSNK1E	-1.6	< 0.0001
DUSP4	2.6	< 0.0001	GNAT1	-1.8	< 0.0001
EDG2	2.6	< 0.0001	HSMDPKIN	-1.8	< 0.0001
FZD8	2.5	< 0.0001	GNAS	-1.8	< 0.0001
CDC42BPB	2.5	0.001	STK31	-1.9	< 0.0001
MOS	2.4	< 0.0001	PIP5KL1	-1.9	< 0.0001
CSNK1G3	2.3	< 0.0001	EPHB1	-1.9	< 0.0001
DAPK2	2.0	< 0.0001	ADORA2A	-1.9	< 0.0001
ADCYAP1R1	1.9	< 0.0001	BMPR1A	-2.1	< 0.0001
LMTK2	1.9	0.003	NAGK	-2.2	< 0.0001
SRC	1.7	0.003	CX3CR1	-2.2	< 0.0001
CELSR1	1.7	< 0.0001	TAF1L	-2.3	< 0.0001
GNAI1	1.7	0.001	RET	-2.4	< 0.0001
TGFBR2	1.7	0.002	MAPK1	-2.5	0.001
MVK	1.6	0.003	AXL	-2.5	< 0.0001
GUCY2C	1.5	0.001			
ABL2	1.5	0.003			
FZD4	1.5	0.001			
GSK3B	1.4	0.001			

Table 3. Candidate genes significantly affecting SUM149 TN-IBC cells sensitivity to EPA.

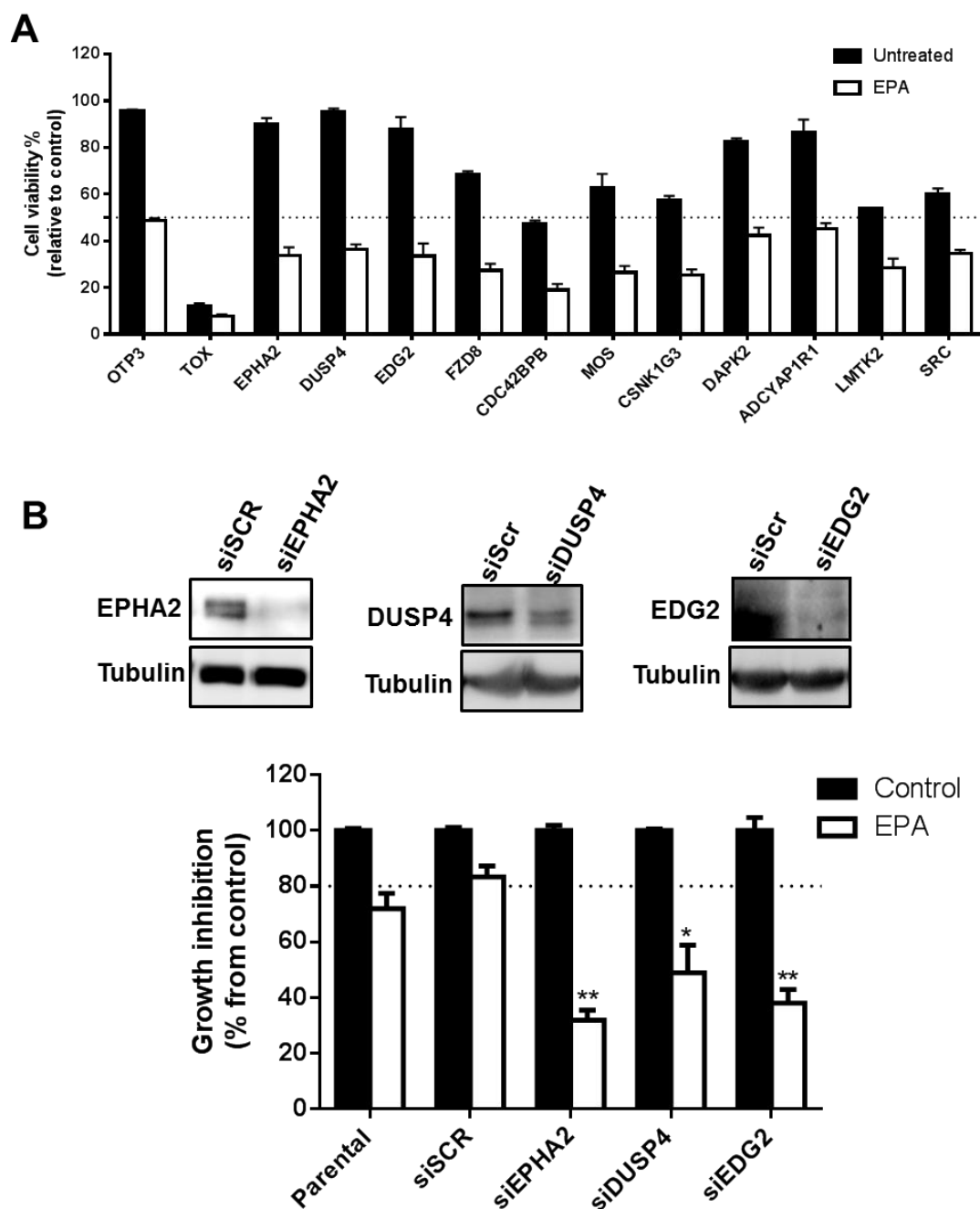


Figure 27. Top significant targeting candidates enhance TN-IBC cells sensitivity to EPA. EPHA2, DUSP4 and EDG2 were validated as a top candidates sensitizing TN-IBC cells to EPA therapy. (A) Viability readout of the top 12 significant gene siRNAs from high-throughput siRNA synthetic-lethal functional screening sensitizing SUM149PT cells to EPA. TOX and OTP3 were used as positive and negative transfection controls, respectively. (B) EPHA2, DUSP4 and EDG2 inhibition was validated by immunoblotting analysis with anti-EPHA2, -DUSP4, and -EDG2 antibodies (top), and viability assays (bottom), after transfection with EPHA2, DUSP4, and EDG2-siRNAs in combination with EPA treatment, compared to untreated, parental and scrambled control (siSCR) transfections. Data were pooled from three independent experiments and presented as mean \pm SD. Unpaired T-test: *, $P < 0.05$; **, $P < 0.0001$.

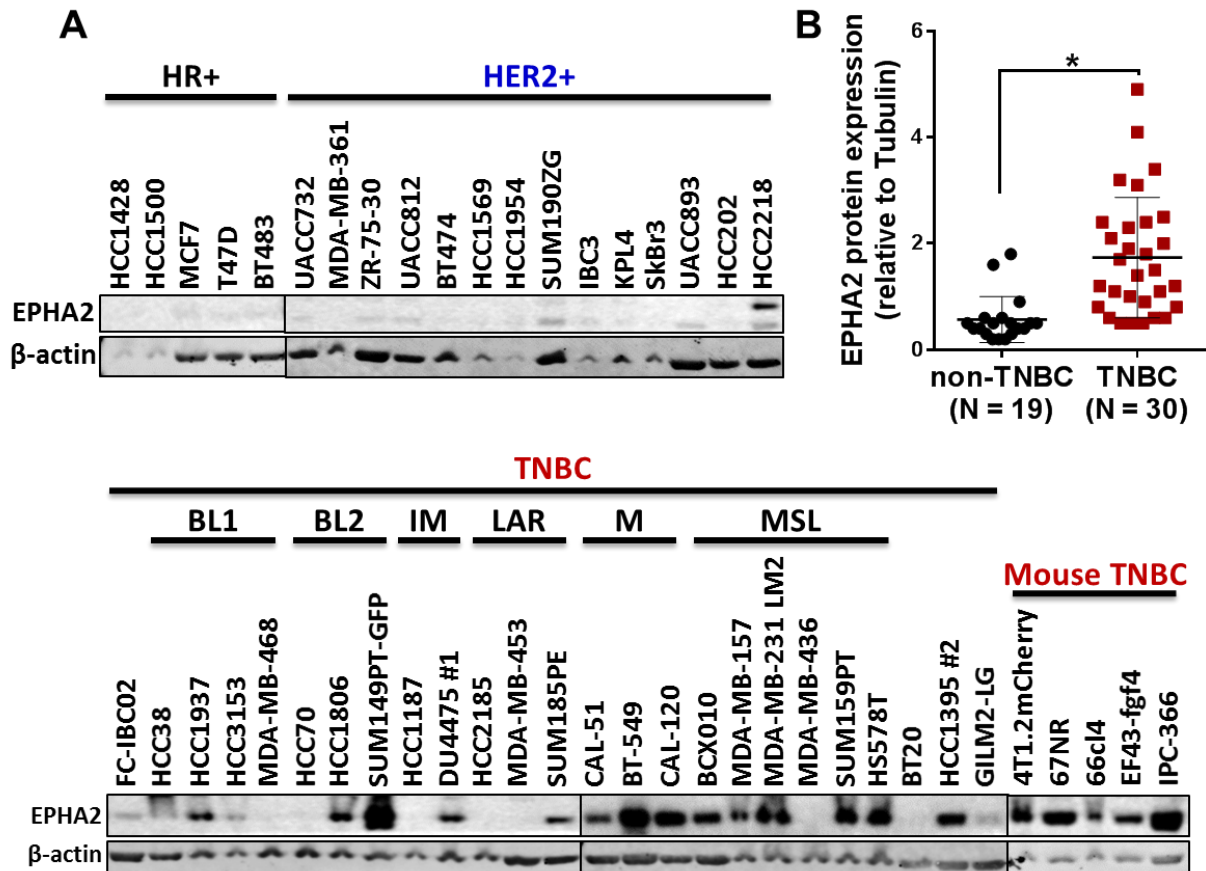


Figure 28. Basal EPHA2 protein expression is present in most TN and TN-IBC cell lines. (A) EPHA2 protein expression levels were determined in multiple human and mouse breast cancer cell lines by immunoblotting analysis. Breast cancer cell lines are grouped by hormone receptor positive (HR+), HER-2 positive (HER2+), or triple-receptor negative (TNBC) status. (B) The pixel density ratios of EPHA2/actin for each cell line was used to generate the graph; β-actin expression was used as a protein loading control. Unpaired T-test: *, $P < 0.0001$.

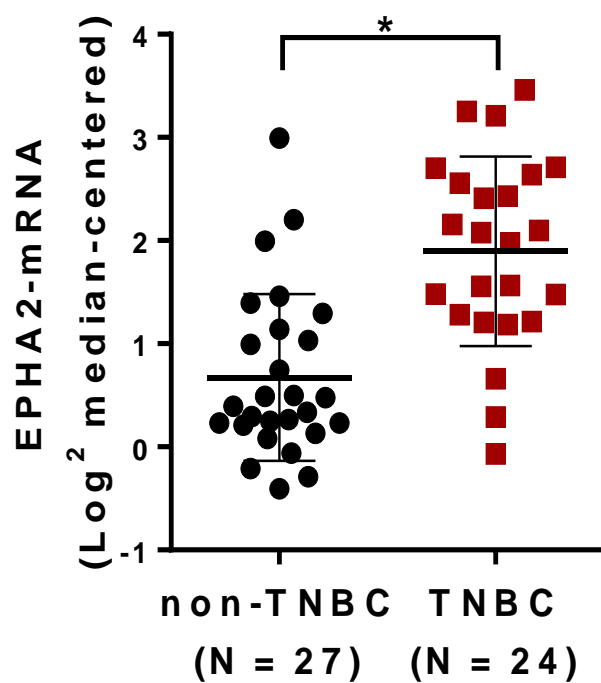


Figure 29. EPHA2 mRNA expression is predominantly higher in TNBC cell lines. EPHA2 mRNA expression levels were determined between TNBC and non-TNBC cell lines using a previously published dataset of breast cancer cell lines. Unpaired T-test: *, $P < 0.0001$.

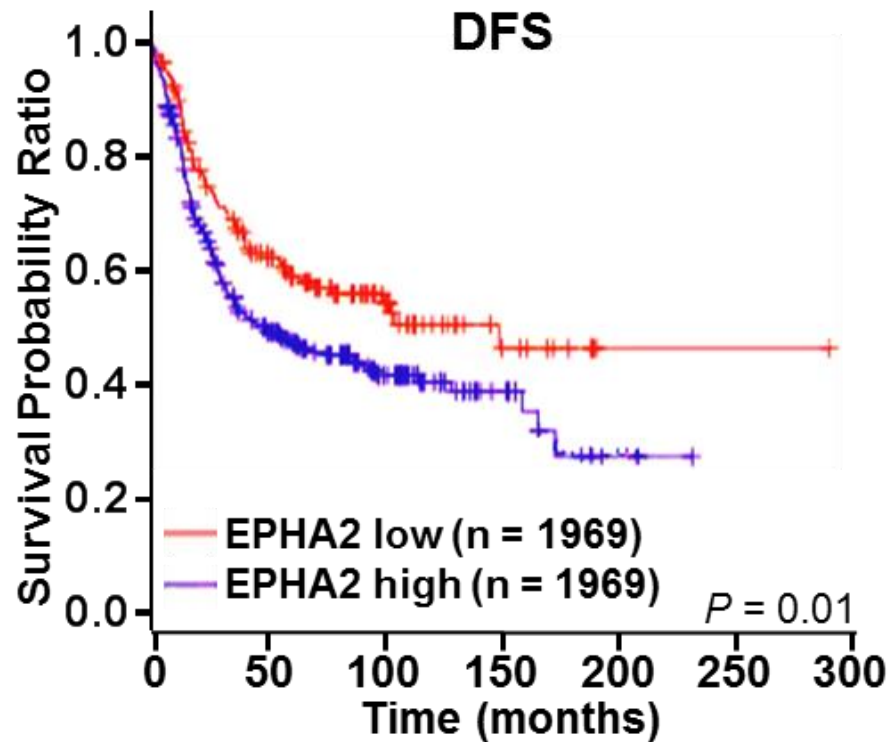


Figure 30. EPHA2 is a clinically significant target that enhances TN-IBC cells sensitivity to EPA. Kaplan-Meier survival curve for disease-free survival (DFS) of TNBC/basal-like breast cancer patients using the BreastMark mRNA dataset was used to determine correlation to *EPHA2* tumor mRNA levels. The log-rank test was used to compare survival curves for high versus low EPHA2. The initial numbers of patients at risk in each group are indicated in the key.

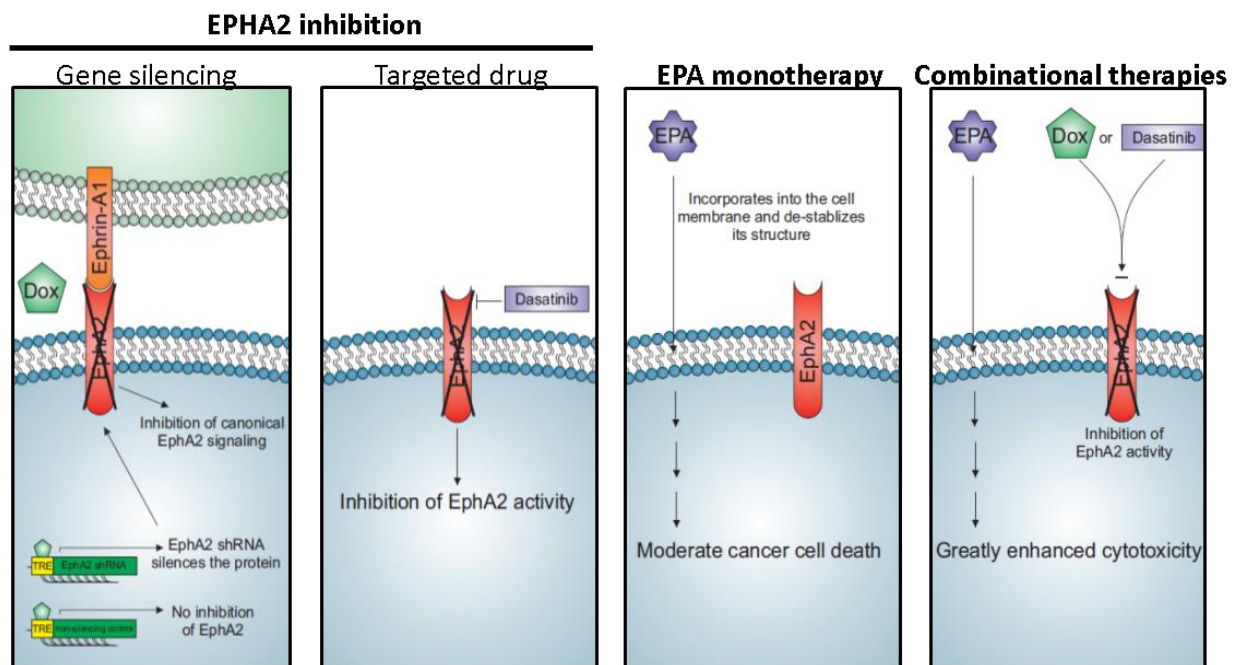


Figure 31. Diagram of gene-silencing, and drug targeted, inhibition of EPHA2 strategies to be tested in combination with EPA treatment.

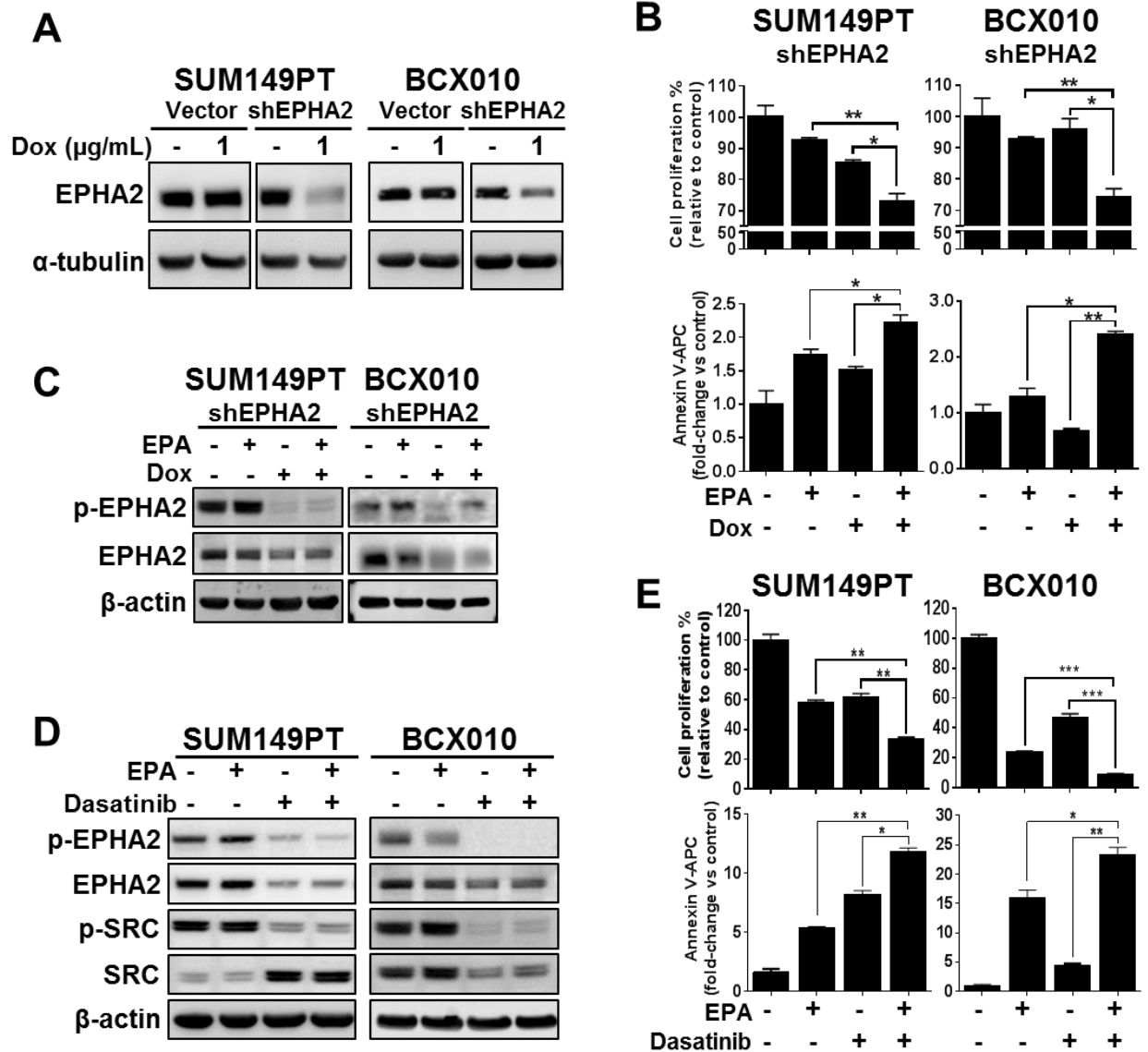


Figure 32. Gene silencing and targeted EPHA2 inhibition acts synergistically with EPA against TN-IBC in vitro. EPHA2 inhibition decreased proliferation and enhanced apoptosis induction following combination treatments with EPA. (A), EPHA2 gene silencing in SUM149PT and BCX010 doxycycline-inducible shRNA cell lines confirmed by immunoblotting analysis of EPHA2 protein expression. (B), Proliferation (top), and apoptosis (bottom), levels were determined EPHA2 knockdown TN-IBC cell lines using cell proliferation and Annexin V staining, respectively, following doxycycline (Dox) induction in combination with EPA. (C), Inhibition of EPHA2 activity was confirmed following EPA and dox-inducible shEPHA2 treatments by immunoblotting analysis. (D) Effects of dasatinib treatment on EPHA2 and SRC was assessed by immunoblotting. Expression of α -tubulin and β -actin were used as a protein loading control. (E), Proliferation (top), and apoptosis (bottom), levels were similarly assessed in SUM149 and BCX010 cell lines following dasatinib in combination with EPA. Data were pooled from three independent experiments and presented as mean \pm SD. Unpaired T-test: *, $P < 0.05$; **, $P < 0.001$; ***, $P < 0.0001$.

(dox)-inducible EPHA2-shRNA (**Figure 32A**). Treating with doxycycline in combination with EPA, we observed synergistic cell growth inhibition and induction of apoptosis ($P < 0.05$) (**Figure 32B**). Silencing of EPHA2 protein activity following treatments was confirmed by immunoblotting analysis (**Figure 32C**). In a second complimentary approach, we assessed the efficacy of IC_{50} concentrations of dasatinib (**Table 4**), a small molecule inhibitor that targets EPHA2 and SRC, to successfully target EPHA2 and SRC protein activity (**Figure 32D**). Upon dasatinib treatment in combination with EPA, we observed a significant inhibition of cell growth ($P < 0.001$), as well as induction of apoptosis ($P < 0.05$), in SUM149PT and BCX010 cell lines when compared to monotherapy and untreated controls (**Figure 32E**). These data supports the efficacy of EPHA2-targeting as a partner that enhances the cytotoxicity of EPA against TN-IBC.

Cell line	EPA		Dasatinib		Combination	
	μM	Fa	μM	Fa	Fa	CI
SUM149	50	0.52	0.31	0.634	0.95	0.19
BCX010	55	0.76	0.63	0.53	0.91	0.57
BT549	55	0.41	0.63	0.44	0.59	0.79
SUM159	100	0.56	5	0.45	0.80	0.28

Table 4. IC_{50} values of breast cancer cell lines following EPA and dasatinib single and combination treatments.

4.2.4 Combination treatment of EPA and EPHA2 inhibition modifies the cell membrane rigidity status and lipid structure of TN-IBC cell lines.

Highly lipophilic EPA is known to incorporate in the plasma membrane of cells in where it can alter membrane structure and protein localization (101). In order to determine the incorporation of EPA in TN-IBC cells membrane, we evaluated EPA content on SUM149PT cell plasma membrane fraction by mass spectrometry following *in vitro* supplementation with EPA (**Figure 33A**). After confirming the incorporation of EPA in cell membranes, we proceeded to determine if EPA plays a direct role modulating EPHA2 protein expression and cell surface localization. Using immunoblotting and flow cytometry analysis, we were able to determine that even though EPA treatment does not significantly affect whole cell EPHA2 expression, it does plays a role inducing the internalization of EPHA2 receptor from the cell surface (**Figure 33B**). These results suggest that while EPA may not affect EPHA2 protein expression, it could be directly affecting EPHA2 signaling by inducing its internalization from TN-IBC cells surface.

To explore the role of EPA treatment in combination with EPHA2 inhibition in TN-IBC cells plasma membrane, we evaluated the general polarization status following combination treatments. After treatments, we identified an increase in cell membrane general rigidity following combination therapy in SUM149PT and BCX010 cells ($P < 0.001$ and 0.05 , respectively), when compared to monotherapy and untreated control (**Figure 34A-B**). These results indicate that specific inhibition of EPHA2 in combination with EPA treatment significantly increase cell membrane rigidity.

Following our findings on the increased cell membrane rigidity status after EPA and EPHA2-inhibition combination treatments, we proceeded to confirm this phenomenon by evaluating the lipid profile of a main membrane phospholipid group, the phosphatidylcholine (PC) family, by mass spectrometry (**Figure 35**). Following single and combination EPA and EPHA2-shRNA doxycycline-inducible inhibition in SUM149PT cells, we observed a trend towards higher abundance of longer carbon structure PC family members in cell membrane following EPA monotherapy, and even more so when combined with EPHA2-shRNA inhibition (**Figure 36A**). This is also evidenced by abundance of each carbon and unsaturation number subfamilies, which also significantly trend towards higher carbon and unsaturation number structures (**Figure 36B**). These data suggest that upon combination of EPA and EPHA2 inhibition, the PC lipid family is slightly modified in the direction of longer-carbon family members, which is consistent with increased membrane rigidity, or polarization, status.

Because cholesterol is a main regulator of membrane rigidity in cells, we evaluated cell plasma membrane cholesterol content in association to increased membrane rigidity after EPA and EPHA2-inhibition combination therapy. After EPA treatment in combination with EPHA2 inhibition, we identified a significant accumulation of cholesterol incorporated in the plasma membrane of SUM149 and BCX010 cells after combination treatments, when compared to monotherapies ($P < 0.05$) and untreated control ($P < 0.001$) (**Figure 37**). Collectively, these results suggest that combination EPA and EPHA-inhibition treatment significantly increase cell membrane rigidity by increasing cholesterol accumulation in the plasma membrane of TN-IBC cells.

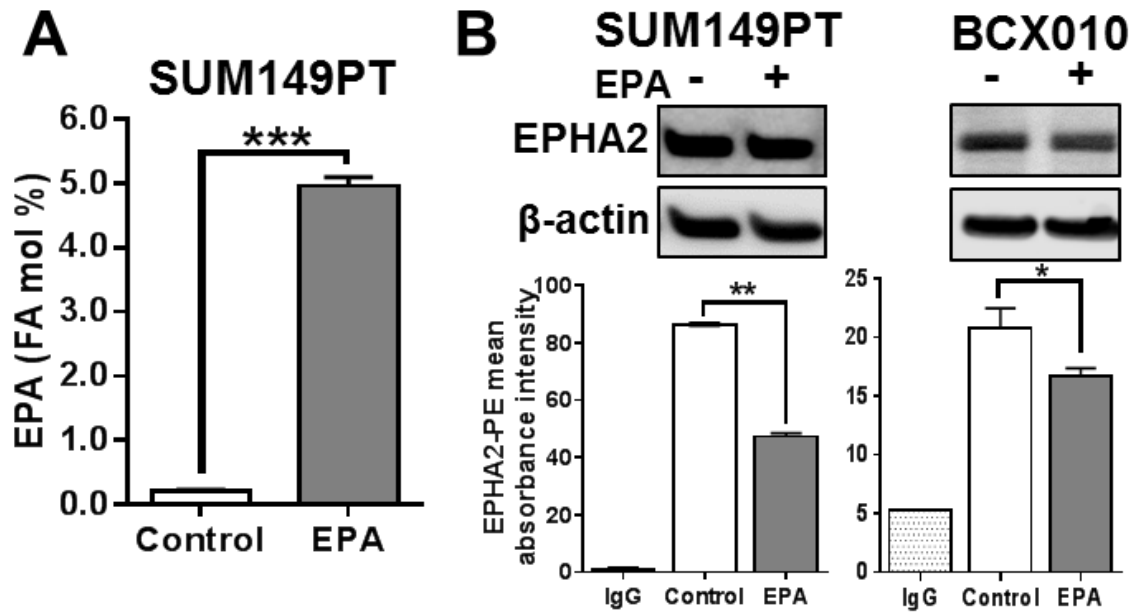


Figure 33. EPA in combination incorporates in the plasma membrane, and induces the internalization of EPHA2. (A), Detection of EPA within TN-IBC cells membrane following treatment. (B), Total (top), and cell surface (bottom), EPHA2 protein expression after EPA treatment in TN-IBC cell lines, as determined by immunoblotting and flow cytometry, respectively. Actin was used as a protein loading control; IgG was used as a negative control for flow cytometric analysis. *, $P < 0.05$; **, $P < 0.001$; *** $P < 0.0001$

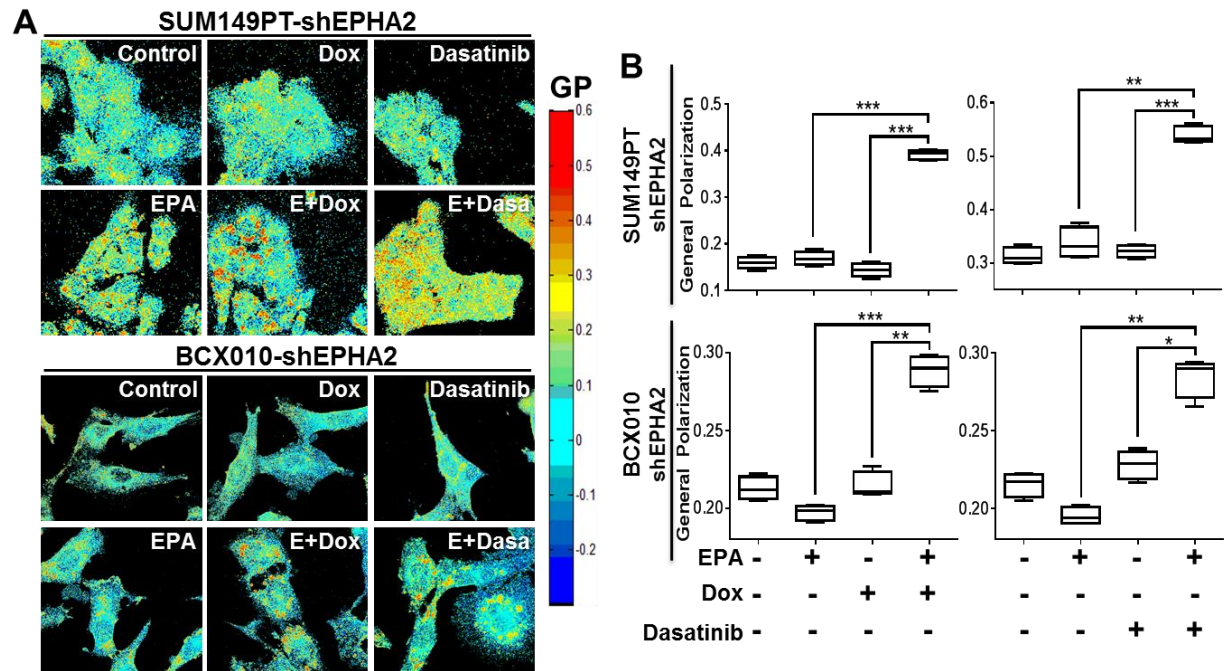


Figure 34. Combination treatment of EPA and EPHA2-inhibition increases plasma cell membrane rigidity on TN-IBC cell lines. Imaging (A) and quantification (B) of cell membrane general polarization (GP, rigidity) after treatments with EPA in combination with doxycycline inducible EPHA2-shRNA (Dox), or dasatinib, in SUM149PT and BCX010 cells. Higher GP values indicate increased cell membrane compaction/rigidity. Data were pooled from three independent experiments and presented as mean \pm SD. T-test: *, $P < 0.05$; **, $P < 0.001$; *** $P < 0.0001$.

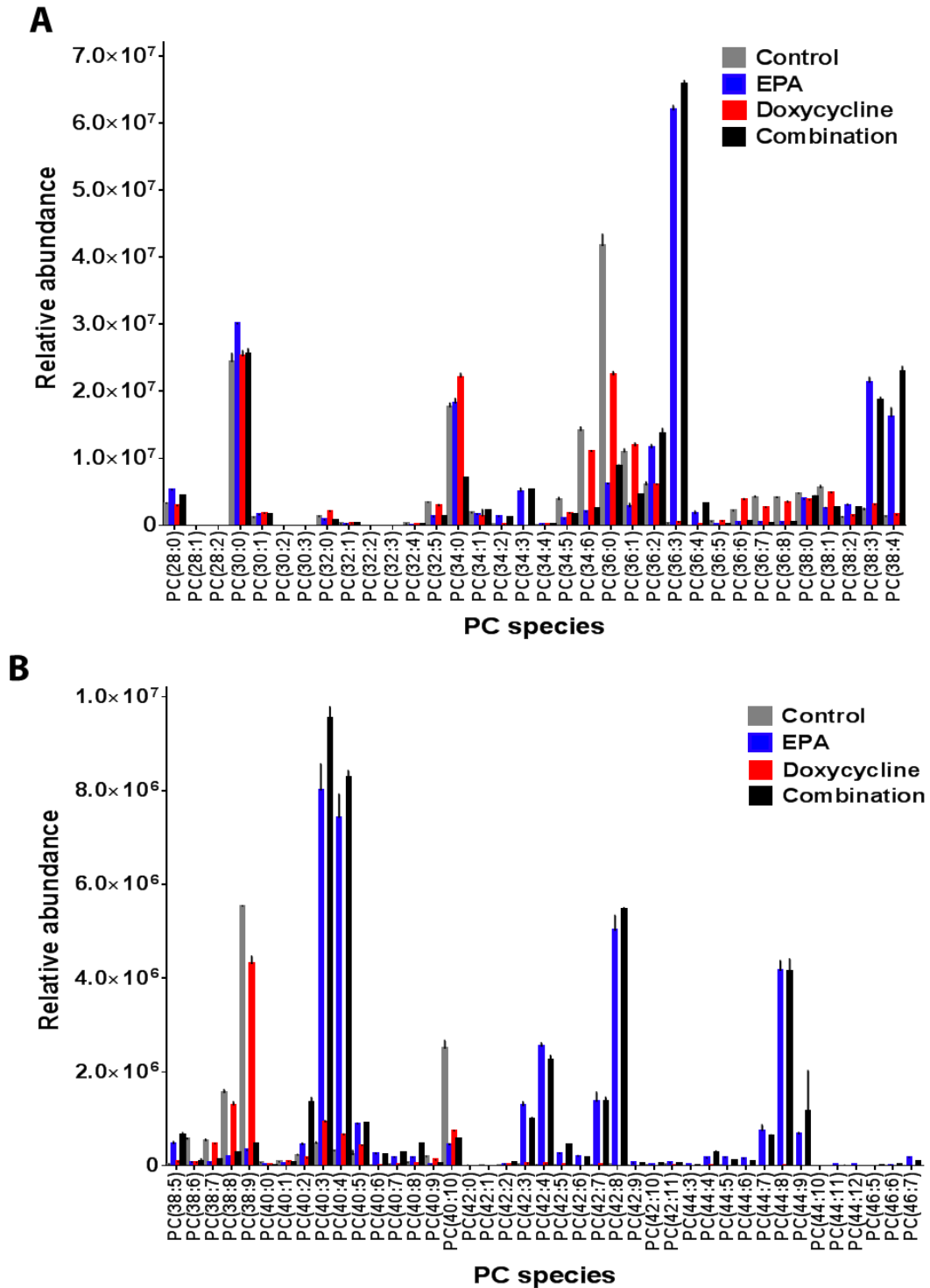


Figure 35. Phosphatidylcholine plasma membrane lipid profiling of SUM149PT cells after EPA and EPHA2-targeting treatments. Complete Phosphatidylcholine (PC) lipid species relative abundance profile quantified by mass spectrometry analysis. PC species are grouped by smaller (**A**), and larger (**B**), carbon structure in the membrane of SUM149PT-shEPHA2 inducible cells after treatments with EPA (55 μ M) in combination with EPHA2-shRNA (Doxycycline, 1 μ g/mL). Data were pooled from at three independent experiments and presented as mean \pm SD.

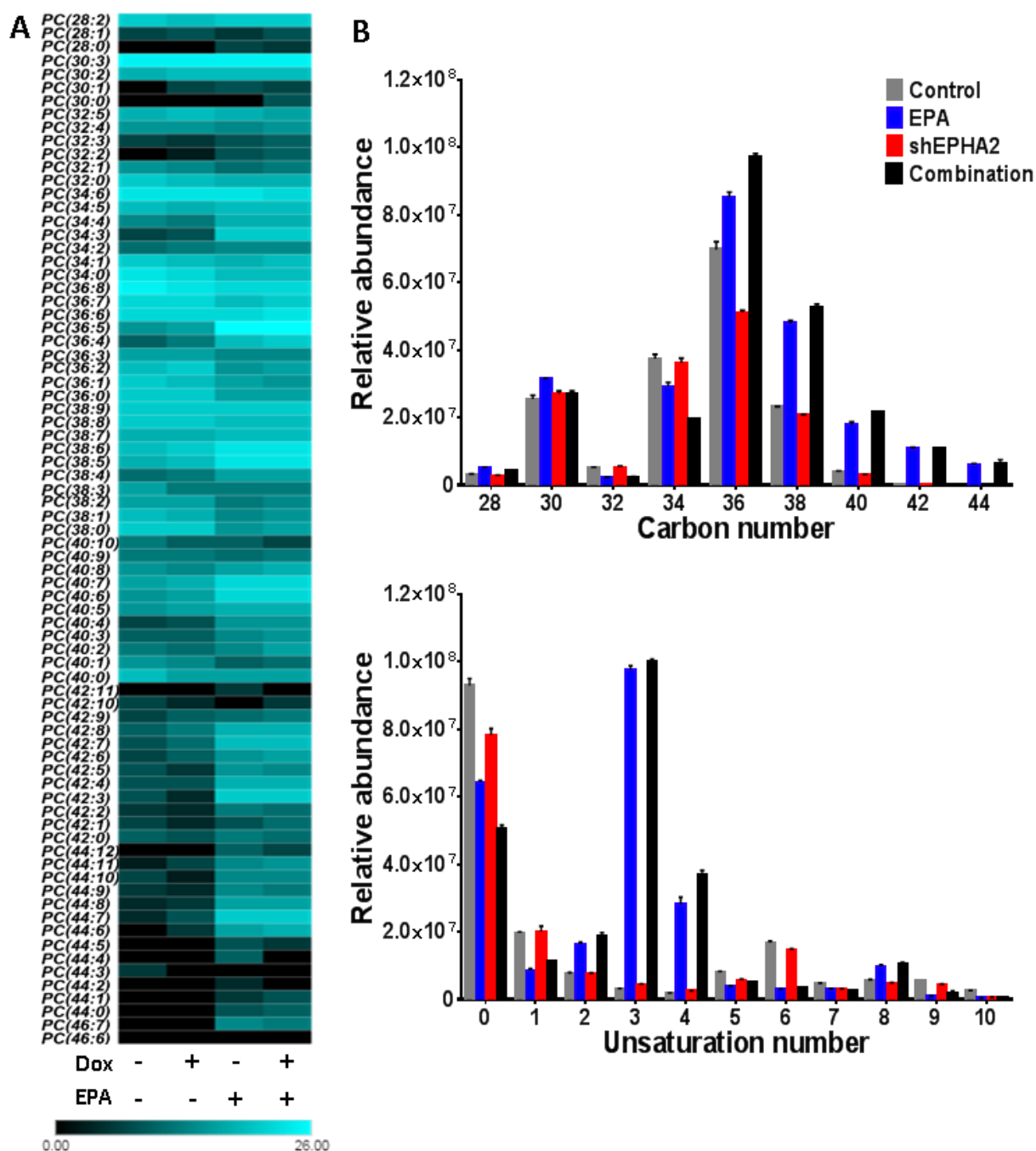


Figure 36. Combination treatment of EPA and EPHA2-inhibition modifies plasma cell membrane lipid composition of TN-IBC cell lines. (A), Heat map for the relative abundance profile of Phosphatidylcholine (PC) phospholipid family members quantified by mass spectrometry analysis after EPA and EPHA2-shRNA (Dox, 1 $\mu\text{g}/\text{mL}$) in doxycycline inducible SUM149PT cells, sorted from lower to higher family member carbon and unsaturation (carbon:unsaturation) number. (B), Summary of PC lipid profile grouped by carbon (top) and unsaturation (bottom) number. Data were pooled from three independent experiments and presented as mean \pm SD.

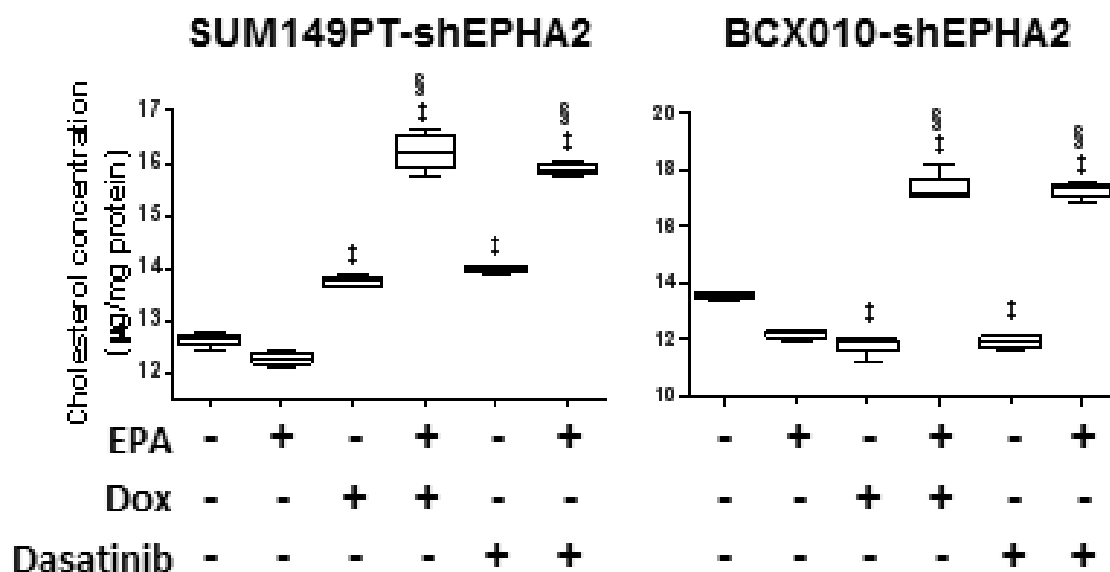


Figure 37. Cholesterol accumulates in plasma membrane fraction following EPA and EPHA2-inhibition treatment. Quantification of cholesterol concentration in the membrane fraction of SUM149PT and BCX010 cells after treatments with EPA in combination with EPHA2-shRNA (Dox), or dasatinib. Data were pooled from three independent experiments and presented as mean \pm SD. Unpaired T-test: *, $P < 0.05$; **, $P < 0.001$; *** $P < 0.0001$; ‡, $P < 0.05$ compared to EPA; §, $P < 0.0001$, compared to dasatinib or doxycycline.

4.2.5 The cholesterol exporter protein, ABCA1, is a critical mediator of apoptosis in TN-IBC cells response to EPA and EPHA2-inhibition therapy.

Our findings on the increased membrane rigidity by the accumulation of cholesterol in the plasma membrane prompted us to investigate a role of cholesterol directly regulating TN-IBC cell membrane fluidity and treatment sensitivity. We first assessed the effect of cholesterol in cell membrane rigidity following EPA-based treatments in TN-IBC cells. Following treatments in addition to cholesterol supplementation, or starvation of cholesterol using methyl- β -cyclodextrin (M β CD) (**Figure 38 and Figure 39**), we observed enhancement ($P < 0.05$) and reversal ($P < 0.0001$), respectively, of cell membrane rigidity compared to combination EPA and EPHA2 inhibition treatments (**Figure 40A**). We further determined the role of cholesterol modulation and cell membrane fluidity affecting TN-IBC cells apoptosis. We identified a direct correlation between increased membrane rigidity following combination treatment in addition to cholesterol supplementation and apoptosis induction, when compared to combination treatments alone, and in combination to rosuvastatin, a cholesterol biosynthesis inhibitor, significantly reversing cell death induction (**Figure 40B**). These data suggests that cholesterol may be responsible for enhancing membrane rigidity and apoptosis induction, potentially suggesting that cholesterol regulation pathways may be subsequently leading to induction of apoptosis in TN-IBC.

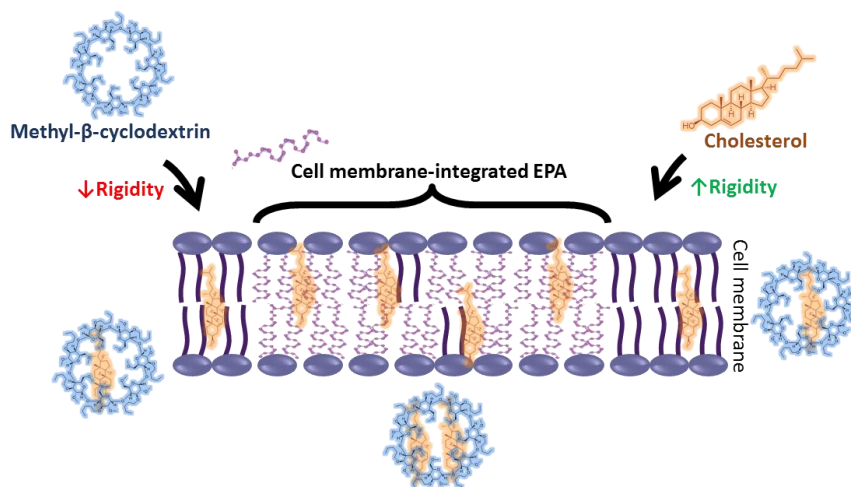


Figure 38. Diagram for cholesterol modulation techniques used to modify cell membrane fluidity.

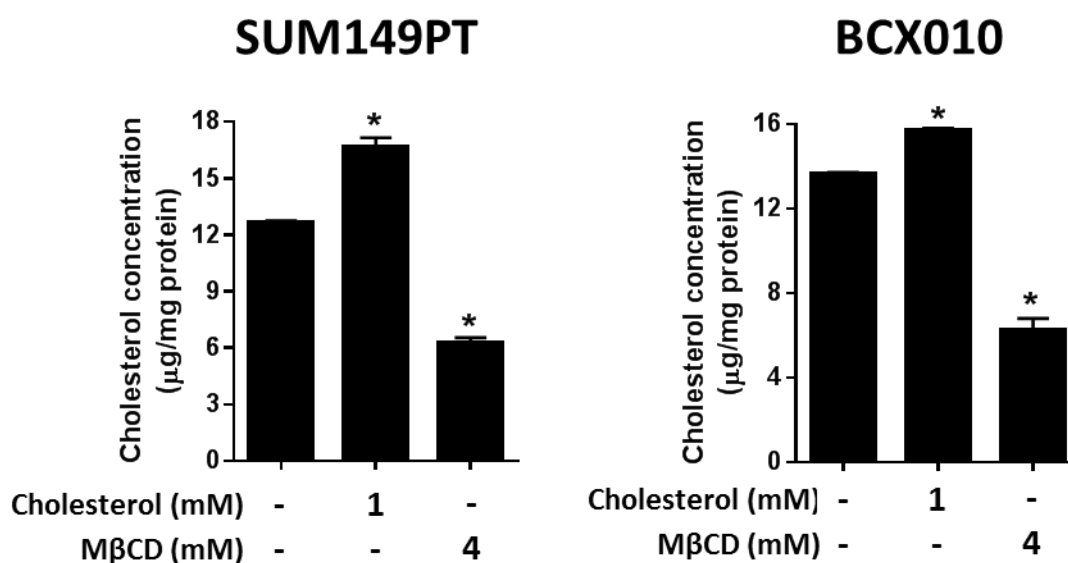


Figure 39. Modulation of cholesterol concentration in the membrane fraction of TN-IBC cells. Cholesterol concentration in the membrane fraction of SUM149PT and BCX010 cells was determined using Amplex Red Cholesterol assay after cholesterol removal using Methyl- β -cyclodextrin (M β CD: 4 mM), or supplementation (Cholesterol: 1 mM). Data were pooled from five independent experiments, and represented as mean \pm SD. Unpaired T-test: *, $P < 0.001$.

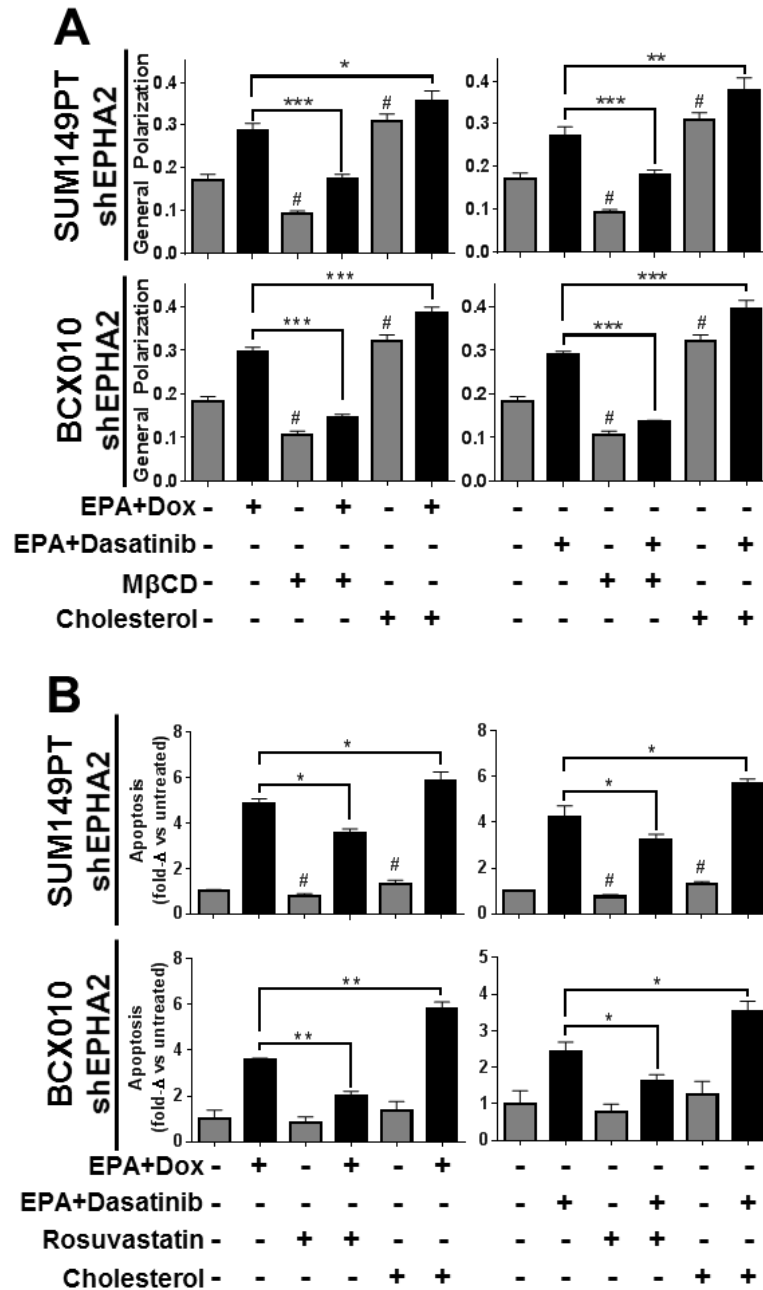


Figure 40. Accumulation of intracellular cholesterol plays a role in the induction of apoptosis following combination EPA and EPHA2-targeting therapy in TN-IBC cells. ABCA1 plays an important role in the regulation of membrane rigidity by accumulation of intracellular cholesterol in TN-IBC cells after combination EPA and EPHA2-inhibition treatment. Quantification of cell membrane general polarization (rigidity) (A), or fold-induction of apoptosis relative to untreated control (B), after cellular cholesterol removal (Methyl- β -cyclodextrin, M β CD; or rosuvastatin), or supplementation (Cholesterol), in TN-IBC cells treated with EPA in combination with Doxycycline-inducible EPHA2-shRNA (Dox), or dasatinib. Higher GP values indicate increased cell membrane compaction/rigidity. Data were pooled from at least three independent experiments and presented as mean of fold-change compared to untreated control \pm SD. Unpaired T-test: *, $P < 0.05$; **, $P < 0.001$; *** $P < 0.0001$; #, $P < 0.05$ compared to untreated control.

Cholesterol homeostasis is a key determinant of cell viability (121, 122). To evaluate potential cholesterol modulating mechanisms associated to combination treatment, we determined the expression of main cholesterol exporting (ATP-binding cassette sub-family A member 1, ABCA1), importing (low-density lipoprotein receptor, LDLR), and biosynthesis inducer (sterol regulatory element-binding protein2, SREBP-2; and 3-hydroxy-3-methylglutaryl-coenzyme A reductase, HMGCR) proteins (**Figure 41**). Following combination treatments, we identified significant inhibition of ABCA1 and SREBP-2 when compared to single treatment and untreated controls (**Figure 42**). The inhibition of ABCA1 would suggest that cholesterol may accumulate within cells preventing the molecular activation of the SREBP-2 matured form, and leading to an increase in cell membrane rigidity, and subsequently cell death. To determine whether ABCA1 is a critical component of cell membrane rigidity, we

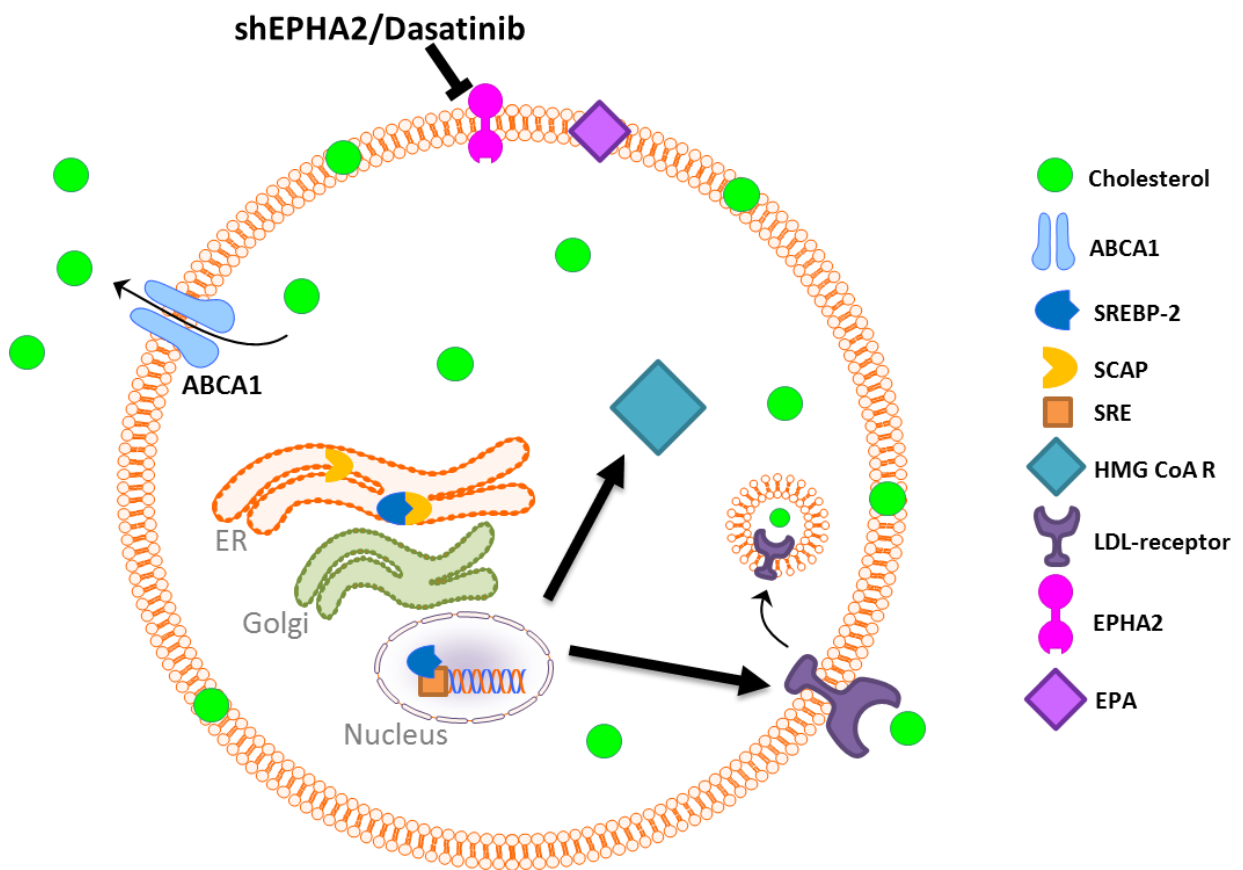


Figure 41. Diagram of main regulators of cellular cholesterol homeostasis.

performed gain/loss-of-expression studies to assess the response of SUM149PT and BCX010 cells to combination treatment (**Figure 43A-B**). Over-expression of ABCA1 reversed cell membrane rigidity following EPA therapy, as well as cell death induction, when compared to controls (**Figure 43C-D**). In a reverse-complimentary approach, *ABCA1*-silenced TN-IBC cells displayed increased cell membrane rigidity, and cell death, when compared to controls (**Figure 43C-D**). These results provide direct evidence for the requirement of ABCA1 inhibition for effective EPA combination therapy synergism in TN-IBC by increased membrane rigidity and apoptosis induction. Lastly, we evaluated whether we could further confirm the relevance of cholesterol accumulation as a crucial factor that promotes TN-IBC cells cytotoxicity following *ABCA1* mRNA silencing. After inhibition of cholesterol biosynthesis by rosuvastatin, we observed a significant inhibition of apoptosis induction in *ABCA1*-silenced SUM149PT and BCX010 cells compared to single rosuvastatin or *ABCA1*-siRNA conditions (**Figure 44**). Altogether, this data confirms a role for ABCA1 inhibition and cholesterol accumulation as important factors that regulate treatment synergism of combination EPA and EPHA2 inhibition against TN-IBC.

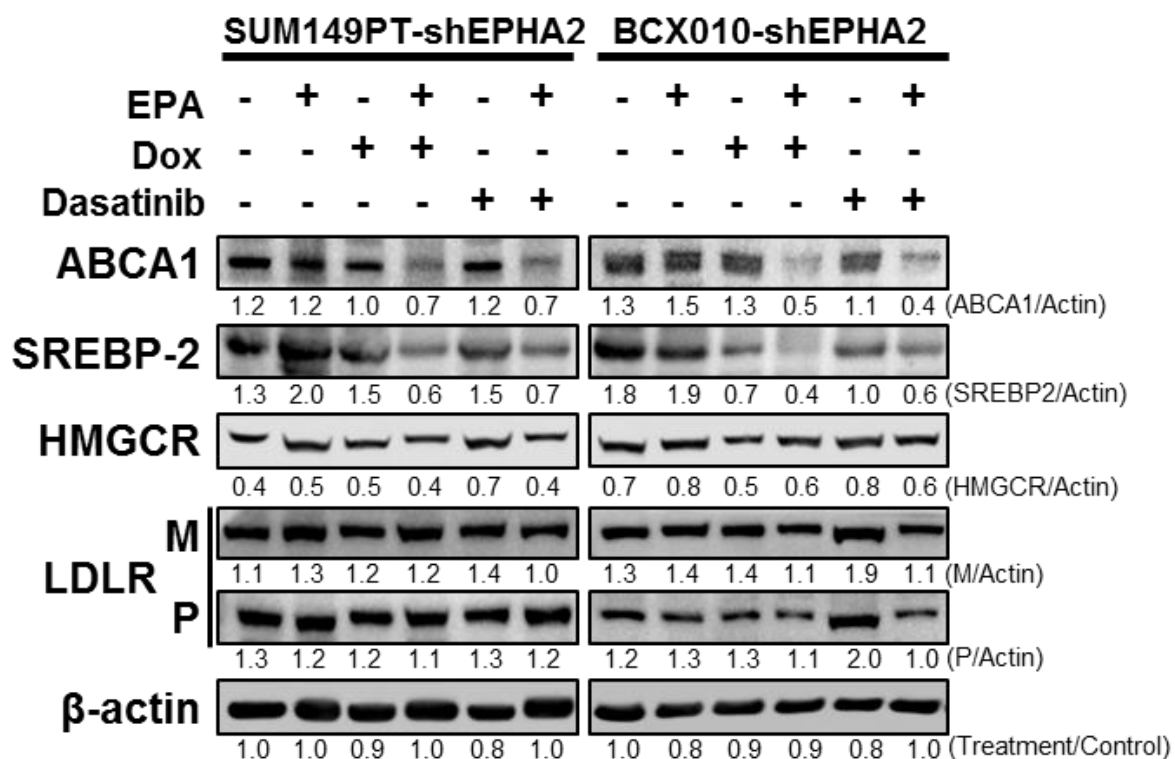


Figure 42. ABCA1 and SREBP-2 are inhibited following combination therapy of EPA and EPHA2-inhibition in TN-IBC cells. Immunoblotting assay of main cholesterol homeostasis regulating proteins: ABCA1, matured SREBP-2, HMG CoA Reductase (HMGCR), and LDL-Receptor (LDLR) matured (M) and precursor (P) forms after EPA in combination with EPHA2-shRNA (Dox), or dasatinib. Pixel density of proteins were quantified for each condition, and the ratios of protein/ β -actin or treatment/control are shown next to the blots; β -actin expression was used as a protein loading control.

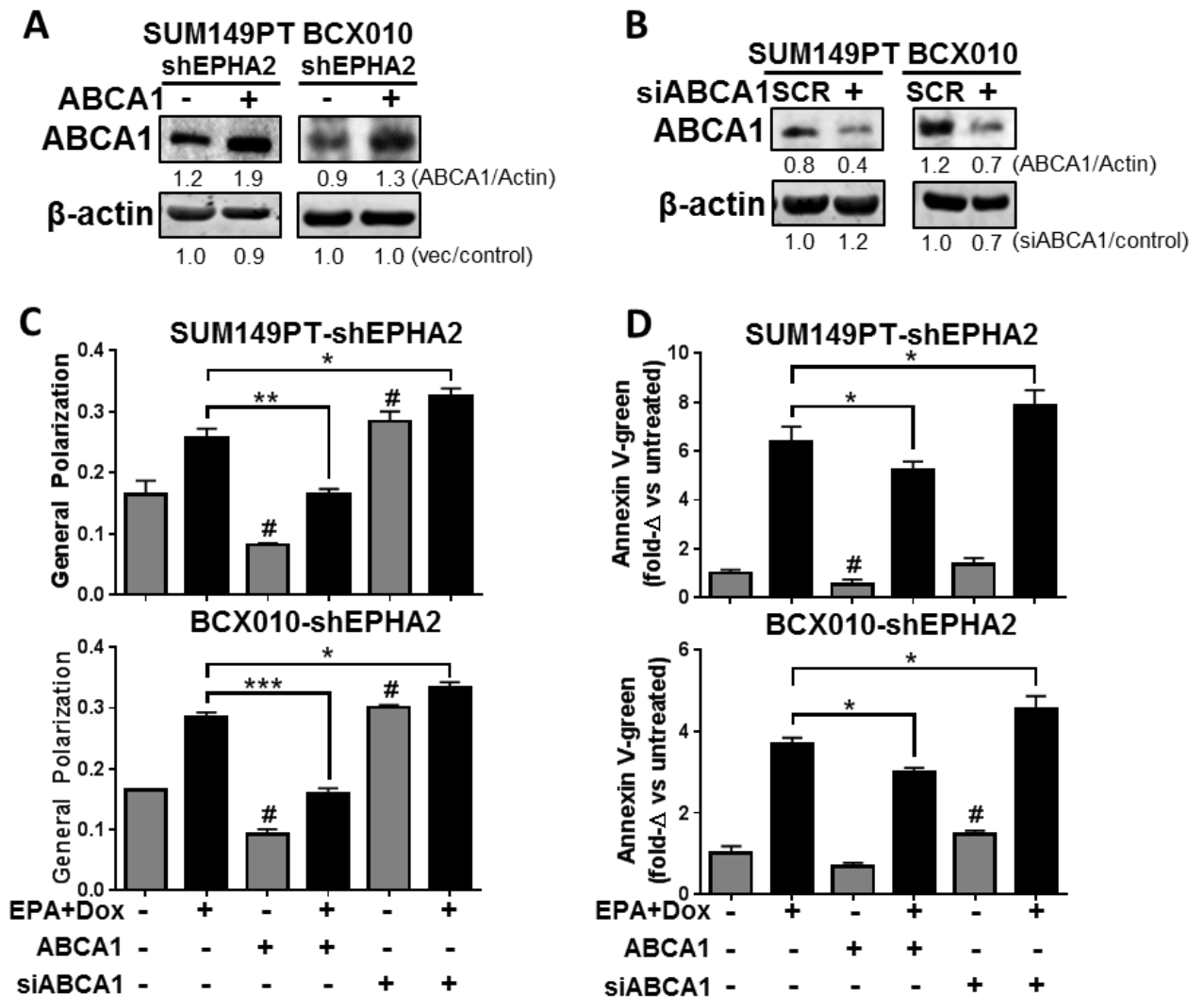


Figure 43. ABCA1 modulation is responsible for the induction of apoptosis following combination EPA and EPHA2-targeting therapy in TN-IBC cells. SUM149PT and BCX010 cells were transfected with either an ABCA1-expressing vector or empty control vector (**A**), or pooled ABCA1 (siABCA1) or Scrambled (SCR) siRNA (**B**). Pixel density of proteins were quantified for each condition, and the ratios of protein/β-actin or treatment/control are shown next to the blots; β-actin expression was used as a protein loading control. ABCA1 expression vector or siRNA transfection role in membrane general polarization (rigidity) (**C**), and fold-induction of apoptosis relative to untreated control (**D**), in TN-IBC cells after combination of EPA with EPHA2-shRNA (Dox), or dasatinib. Data were pooled from at least three independent experiments and presented as mean of fold-change compared to untreated control ± SD. Unpaired T-test: *, $P < 0.05$; **, $P < 0.001$; *** $P < 0.0001$; #, $P < 0.05$ compared to untreated control.

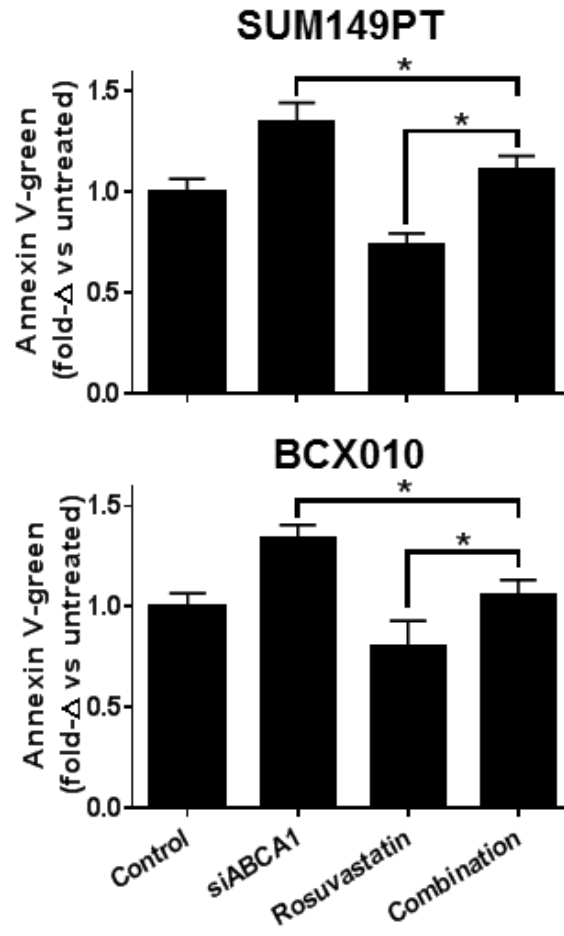


Figure 44. Cholesterol accumulation induces apoptosis following ABCA1-siRNA inhibition. TN-IBC cells were transfected with ABCA1 siRNA, alone or in combination with rosuvastatin, for analysis of apoptosis using annexin V-green. Data were pooled from at least three independent experiments and presented as mean of fold-change compared to untreated control \pm SD. Unpaired T-test: *, $P < 0.05$.

4.2.6 Inhibition of EPHA2 enhances the therapeutic action of EPA in TN-IBC xenograft models

Our *in vitro* data infers that EPA therapy combined with EPHA2 inhibition would be an effective therapy. We proceeded to determine whether inhibition of EPHA2, both by gene silencing and targeting drug dasatinib, could enhance EPA efficacy inhibiting tumor growth in preclinical xenograft models of TN-IBC. Mice bearing established (**Figure 45A-B**) SUM149PT-shEPHA2 or BCX010-shEPHA doxycycline-inducible tumor xenografts received *ad libitum* administration of EPA containing diets alone or in combination with doxycycline water. When compared to mice treated with control diets or single treatments, combination treated mice displayed a significant reduction in TN-IBC tumor growth ($P < 0.001$) (**Figure 46A**), and prolonged survival ($P < 0.001$) (**Figure 46B**). Immunostaining for markers of proliferation and apoptosis in tumors after combination treatment confirmed a significant reduction of Ki67, and an increase in cleaved caspase-3 ($P < 0.05$) (**Figure 46C-D**). As expected, our combination therapy inhibited EPHA2 leading to modified expression of cholesterol regulator ABCA1 compared to single and control groups ($P < 0.05$) (**Figure 47A-B**). These findings confirm the efficacy of specific EPHA2-inhibition sensitizing TN-IBC tumors to EPA treatment via inhibition of ABCA1 as a potential therapeutic approach for further preclinical development.

Supported by our findings on the efficacy of EPHA2 gene silencing enhancing EPA therapy *in vivo*, we proceeded to assess the ability of dasatinib sensitizing TN-IBC tumors to EPA. Similar to our previous animal study, mice bearing TN-IBC tumor xenografts received EPA alone or in combination with dasatinib. Combination treatment displayed inhibition of tumor growth ($P < 0.05$) (**Figure 48A**), as well as prolonged survival ($P < 0.001$) (**Figure 48B**), when compared to single treatment and untreated mice groups. Immunostaining of tumor tissues

following treatments confirmed a reduction in Ki67 proliferation marker, and increase in cleaved caspase-3 apoptosis marker following combination treatments in comparison to single and untreated controls ($P < 0.05$) (**Figure 49A-B**). Confirming our *in vitro* molecular studies, we identified a reduction of tumor EPHA2 protein expression following dasatinib treatment. Moreover, we identified inhibition of ABCA1 protein expression after combination treatment ($P < 0.05$) (**Figure 49C-D**). Together, these results provide evidence supporting the clinical development of an EPHA2-targeting therapy in combination with EPA against TN-IBC through a mechanism involving increased cell membrane rigidity mediated by ABCA1 inhibition.

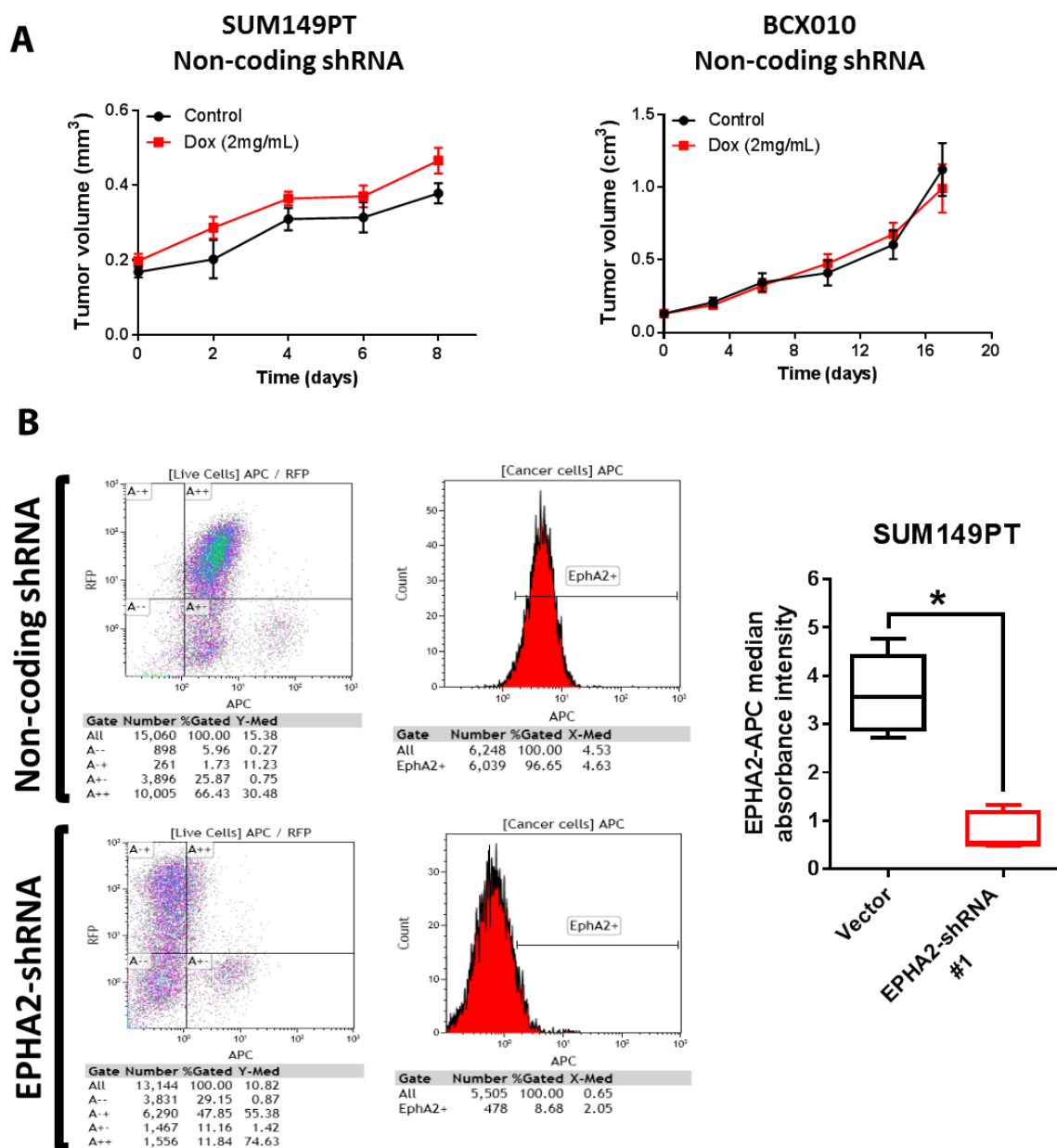


Figure 45. Establishment of inducible shRNA-RPHA2 TN-IBC cell lines in xenograft models. Doxycycline-inducible shRNA-EPHA2-GFP SUM149PT and BCX010 cell lines induction efficacy was assessed in tumor xenografts in mice. (A), Tumor volume measurements of non-coding shRNA SUM149PT and BCX010 tumor xenografts following treatment with doxycycline (Dox) in water (2 mg/mL; ad libitum). (B), Flow cytometry analysis using anti-EPHA2 APC-labeled antibody in Red Fluorescent Protein (RFP) positive cells derived from Dox treated mice bearing non-coding-, and EPHA2-targeting, shRNA-RFP inducible SUM149PT tumor xenografts. EPHA2 expression was quantified from five mice per treatment group. Data is presented as mean \pm maximum/minimum values. T-test: *, $P < 0.001$.

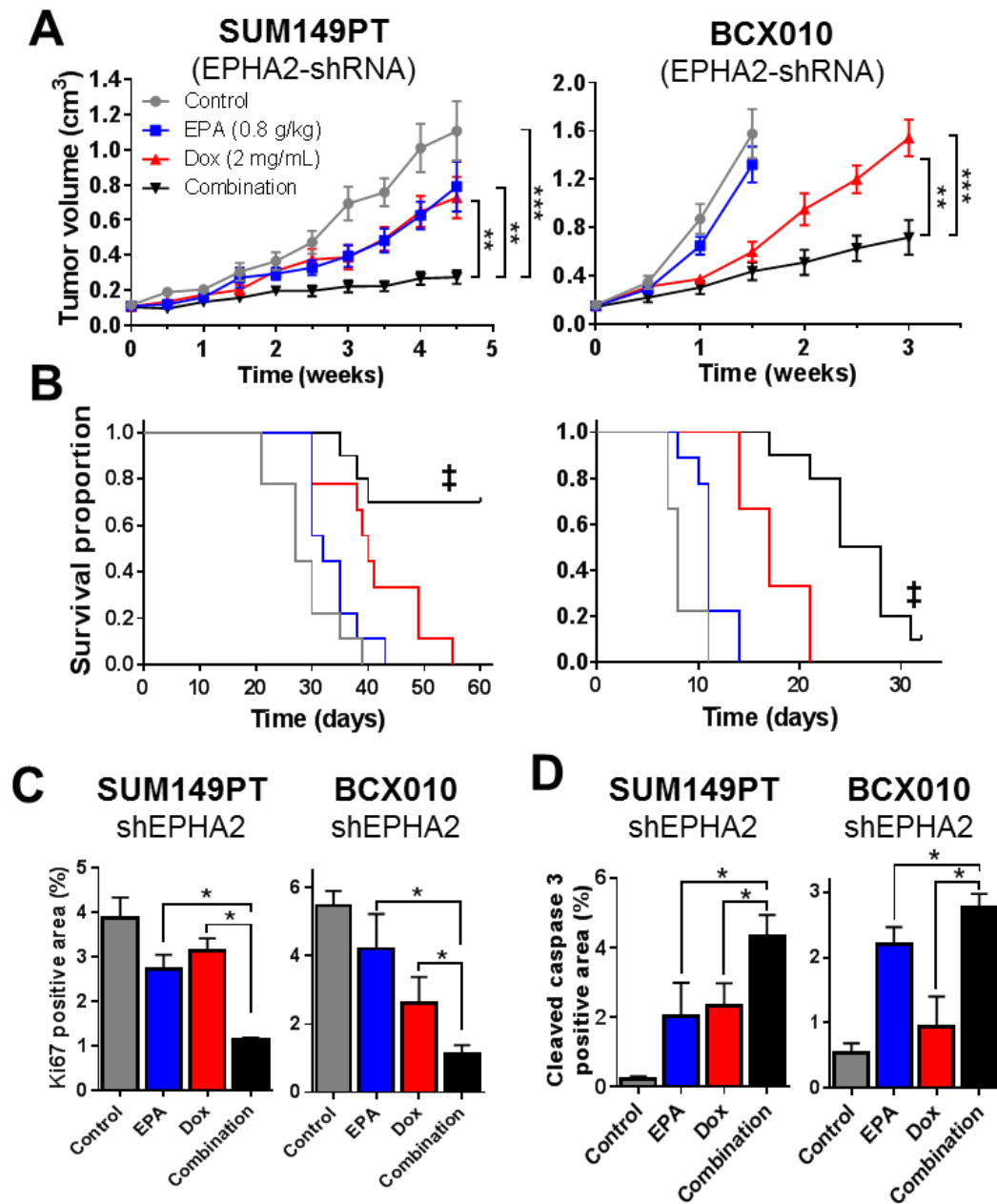


Figure 46. Gene silencing inhibition of EPHA2 acts synergistically with EPA against TN-IBC tumor xenografts. ShRNA-inducible EPHA2 inhibition enhances EPA efficacy in TN-IBC cell lines. Tumor volume measurements (**A**), and Kaplan-Meier survival curves to endpoint (tumor volume = 1,500 mm³) (**B**) for shEPHA2 inducible TN-IBC tumor xenograft-bearing mice following treatment with control diet, EPA diet (0.8 g/kg), and/or doxycycline (Dox) in water (2 mg/mL). Paraformaldehyde-fixed paraffin sections were quantified for proliferation (Ki67) (**C**), and apoptosis (Cleaved Caspase-3) (**D**), protein expression markers by immunohistochemistry (IHC) staining of three representative tumor samples from each treatment group of mice bearing tumor xenografts treated with control or treatments as indicated above. Images were converted using ImageJ software to accomplish the quantifications of Ki-67 and Cleaved Caspase-3 antibody staining. Data is represented as mean \pm SD. T-test or Log-Rank: *, $P < 0.05$; ‡, $P < 0.001$ combination treatment survival proportion compared to single treatment and untreated control groups.

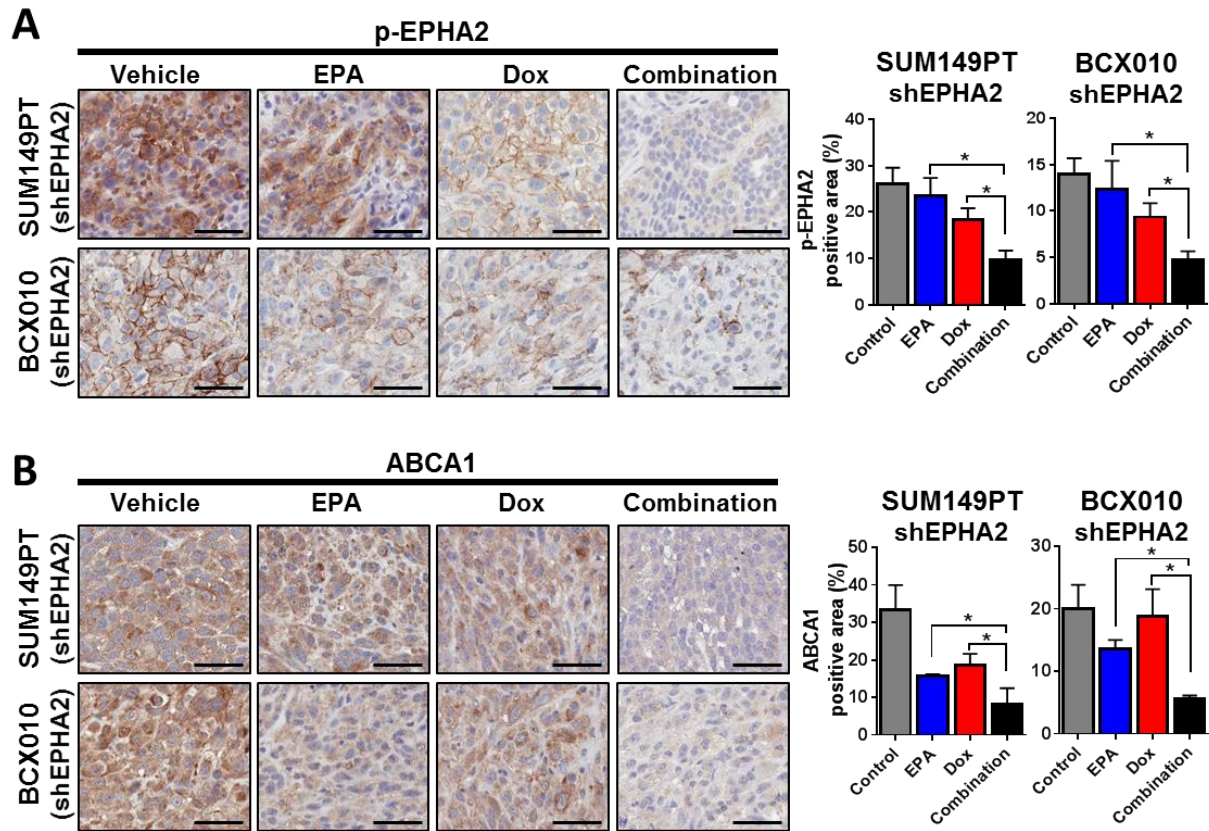


Figure 47. Inhibition of EPHA2 following gene silencing and EPA treatment inhibits ABCA1 in TN-IBC tumor xenografts. IHC staining and expression quantifications from shEPHA2 inducible TN-IBC tumor xenograft-bearing mice following treatment with control diet, EPA diet (0.8 g/kg), and/or doxycycline (Dox) in water (2 mg/mL), using anti-phospho-EPHA2 (p-EPHA2) (**A**), and anti-ABCA1 (**B**) antibodies. Representative images of three IHC staining experiments per treatment group are illustrated. Magnification, 20x. Images were converted using ImageJ software to accomplish the quantifications of p-EPHA2, and ABCA1 antibody staining. Data is represented as mean \pm SD. T-test: *, $P < 0.05$.

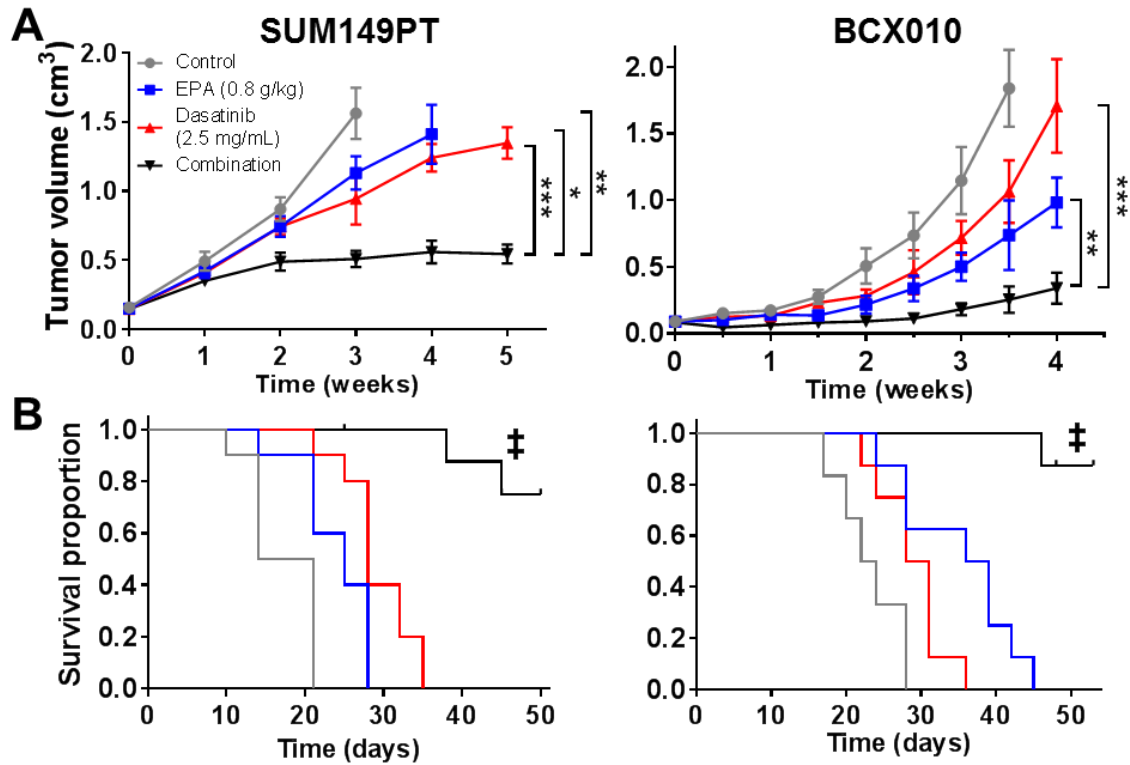


Figure 48. Dasatinib EPHA2-targeted inhibition enhances EPA therapy against TN-IBC tumor xenografts. EPHA2 inhibition by dasatinib is synergistic in combination with EPA therapy inhibiting tumor growth, and prolonging mice survival. Tumor volume measurements (**A**), and Kaplan-Meier survival curves to endpoint (tumor volume = 1,500 mm³) (**B**) for SUM149PT and BCX010 tumor xenograft-bearing mice following treatment with control diet, EPA diet (0.8 g/kg; ad libitum), and/or dasatinib (2.5 mg/mL; IP injection). Data is represented as mean \pm SD. T-test or Log-Rank: *, $P < 0.05$; **, $P < 0.001$; *** $P < 0.0001$; ‡, $P < 0.0001$ combination treatment survival proportion compared to single treatment and untreated control groups.

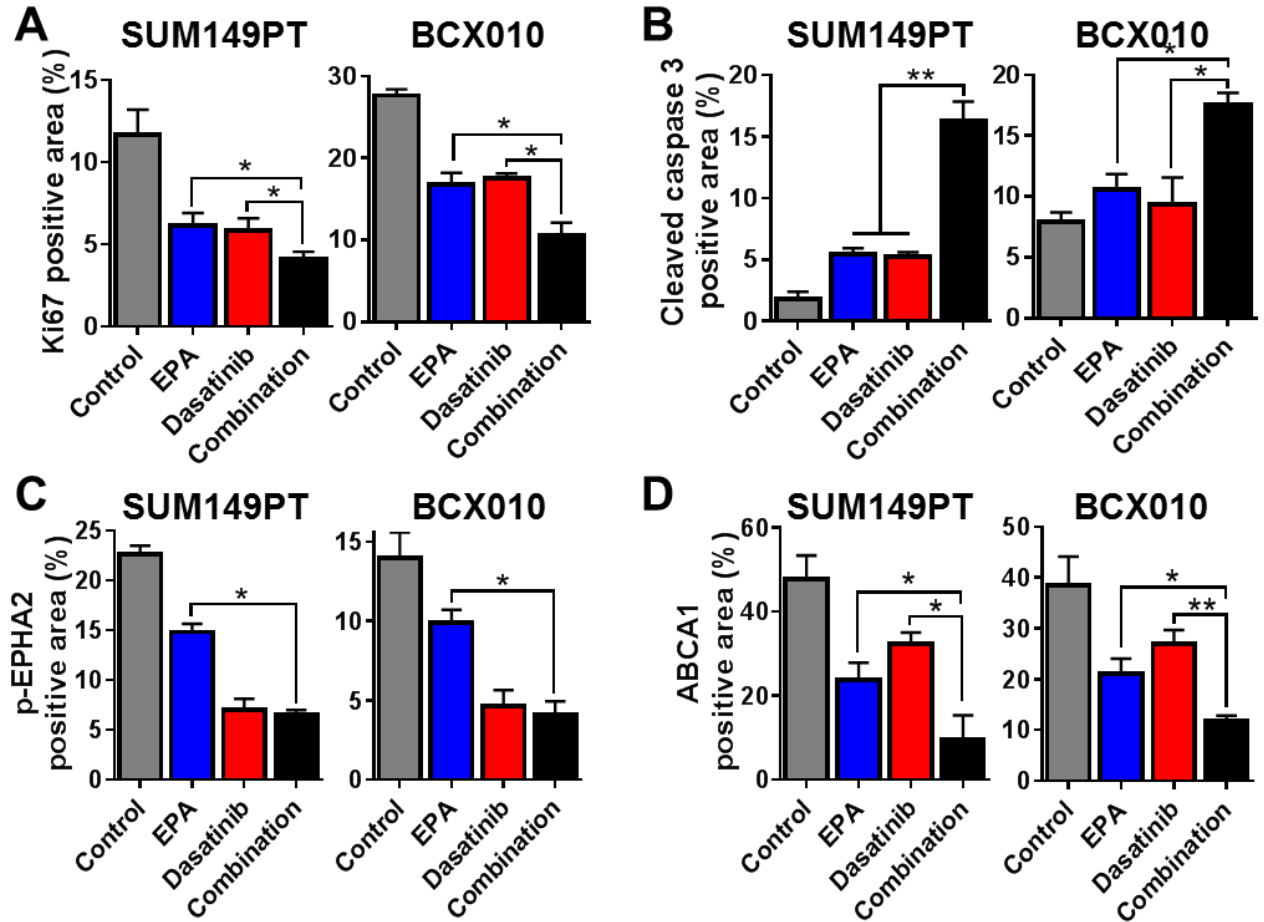


Figure 49. Inhibition of EPHA2 following dasatinib and EPA treatment inhibits ABCA1 and promotes apoptosis in TN-IBC tumor xenografts. Paraformaldehyde-fixed paraffin sections for SUM149PT and BCX010 tumor xenograft-bearing mice following treatment with control diet, EPA diet (0.8 g/kg; ad libitum), and/or dasatinib (2.5 mg/mL; IP injection), were quantified for proliferation (Ki67) (A), and apoptosis (Cleaved Caspase-3) (B) protein markers, as well as for mechanistic proteins: p-EPHA2 (C), and ABCA1 (D), by immunohistochemistry (IHC) staining of three representative tumor samples from each treatment group. Images were converted using ImageJ software to accomplish the quantifications of Ki-67, Cleaved Caspase-3, p-EPHA2, and ABCA1 antibodies staining. Data is represented as mean \pm SD. T-test or Log-Rank: *, $P < 0.05$; **, $P < 0.001$.

4.3 Discussion

The need to identify new biological therapeutic targets for TN-IBC is undisputed. Through this study, we have successfully unveiled a novel and clinically significant therapeutic approach against TN-IBC. Our screen for candidate genes that have synergistic antitumor activity with EPA in TN-IBC identified EPHA2 as a target that, when ablated, sensitized TN-IBC cells to EPA therapy. Suppression of EPHA2 through various approaches enhanced the antitumor effect of EPA, reducing TN-IBC cell growth and proliferation and promoting apoptosis. Similarly, combinations of EPA with EPHA2-inhibiting therapy reduced tumor growth in two *in vivo* xenograft models of TN-IBC.

EPHA2, a cell-surface receptor tyrosine kinase associated with proto-oncogene tyrosine-protein kinase Src (SRC) signaling, is aberrantly expressed in multiple cancer types, playing an important ligand-independent role in tumor growth and metastasis (108-110). The localization of cell surface receptor EPHA2 has been implicated in the modulation of gap junctions and cell plasma membrane fluidity, contributing to tumor invasion via increased cell motility (111-113). Modulating cancer cell motility is also one of the functions of omega-3 fatty acids such as EPA, which incorporate into the plasma membrane, where they modify lipid rafts, increase membrane compaction, modify intracellular signaling, and inhibit invasive features (100-102). Regulation of cancer cell plasma membrane fluidity has been implicated in the modulation of invasive and metastatic potential (116-118). Until now, however, there has been no evidence of increased membrane rigidity as a mechanism of apoptosis induction following combination therapy against TN-IBC. Furthermore, the inhibition of the cholesterol-exporting channel protein ABCA1, followed by accumulation of intracellular cholesterol, and increased membrane rigidity

preceding TN-IBC cell death in response to the EPA and EPHA2-inhibiting combinations is a previously unknown mode of action.

Our study has identified EPHA2 as a significant synergistic partner whose loss enhances EPA therapy, synergistically reducing tumorigenic potential by inducing apoptosis in preclinical models of TN-IBC. Further, in a retrospective analysis of breast cancer patients, we identified a significant and specific association between high-EPHA2 expression in tumors and shorter DFS outcomes in patients with TNBC/basal-like subtype, highlighting the clinical relevance of targeting EPHA2. Using proteomic and cellular biology assays, we demonstrated that the combination of EPHA2-inhibition and EPA was significantly associated with a previously unknown activity that precedes and induces TN-IBC cell death through inhibition of the cholesterol-exporting channel protein ABCA1 and subsequent increase of membrane cholesterol levels and membrane rigidity.

Other studies have demonstrated independent roles for EPA and EPHA2 in the modification of cell membrane fluidity (*101, 111*). Here, we have identified a direct connection whereby EPA induces the internalization of EPHA2 from the cell surface and, in concert with targeted inhibition of EPHA2, enhances cell membrane rigidity. Phospholipid profiling of cellular membranes provided evidence that membrane rigidity correlated with a significant increase in expression of longer phosphatidylcholine species (e.g. those with more carbons in the acyl chains) (data not shown). Cholesterol concentrations also were increased in cell membranes following combination treatments. Increased cholesterol concentration has been associated with greater cell membrane rigidity (*123, 124*). Major regulators of cholesterol homeostasis in cells include the cholesterol exporter ABCA1, the cholesterol importer LDLR,

and the cholesterol biosynthesis regulators SREBP2 and HMGCR (*125-128*). High cholesterol levels prevent SREBP2 activation, inhibiting the subsequent induction of HMGCR and maturation of LDLR (**Figure 50A**) (*129, 130*). Studies in human macrophages have observed that incorporation of EPA into the plasma membrane impairs ABCA1-dependent cholesterol efflux (*131, 132*), but our study is the first to report this phenomenon in cancer xenograft models. Here, we demonstrated that suppression of ABCA1 activity by the combination of EPA and EPHA2-inhibition induced the accumulation of cellular cholesterol contributing to increased membrane rigidity, inhibition of SREBP2, disruption of cellular lipid homeostasis, and apoptosis (**Figure 50B**).

EPA has been widely tested for its benefits as a dietary supplement or as neoadjuvant therapy in cancer because of its anti-inflammatory qualities and safe toxicity profile (*133-136*). This is the first report of its use in a synergistic therapeutic strategy in cancer, providing a safe and non-toxic approach for treating the highly aggressive breast cancer TN-IBC. These results provide a rationale for administering EPA in combination with FDA-approved EPHA2-targeting drugs such as dasatinib, as well as in combination with other specific targeted agents currently been tested in pre-clinical studies and in humans (e.g., NCT01591356) (*137, 138*), facilitating its clinical translation.

TN and IBC remain diseases without effective therapeutic strategies that can significantly improve patients' outcomes or survival. Our study is important as we report for the first time preclinical evidence of combined EPA and EPHA2-targeted therapy effectiveness against TN-IBC through a mechanism involving the induction of apoptosis by ABCA1 inhibition and subsequent regulation of cell membrane rigidity. Other studies have evaluated the

potential of ABCA1 inhibition and increased membrane rigidity in association to decreased metastatic potential, and enhanced efficacy of multiple anti-metastatic drugs (124). This would suggest that besides induction of apoptosis following ABCA1 inhibition, our combination therapy strategy could additionally have significant implications preventing metastasis of TN-IBC.

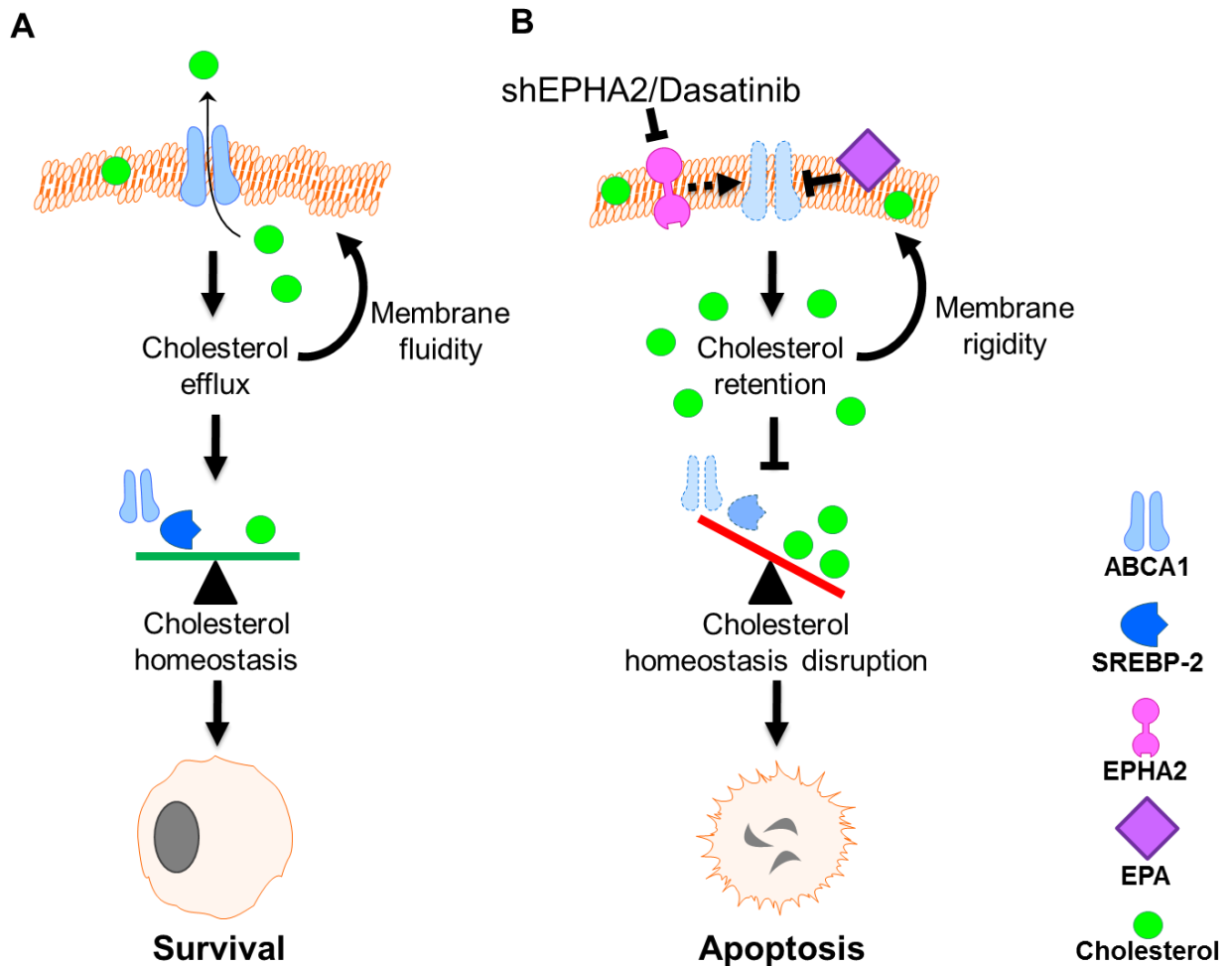


Figure 50. Summary of mechanistic action of EPA in combination with EPHA2-targeting via ABCA1 inhibition in TN-IBC cells. Proposed mechanism of action for increased cholesterol concentration and membrane rigidity mediated by ABCA1 inhibition following combination therapy. (A), Cellular cholesterol homeostasis is normally maintained by the balancing effects of the cholesterol efflux channel protein ABCA1, and cholesterol biosynthesis inducer SREBP-2. Their activity promote the maintained fluidity of the plasma cell membrane and cellular survival. (B), Following combination treatment of EPA and inhibition of EPHA2 from cells membrane, the plasma membrane structure is altered inhibiting the cholesterol exporting functions of ABCA1, this resulting in the accumulation of intracellular cholesterol and subsequent increase in plasma membrane rigidity status. This aberrant accumulation of intracellular/membrane cholesterol prevents the activity of cholesterol biosynthesis inducer proteins (e.g. SREBP-2), and disrupts cellular cholesterol homeostasis resulting in apoptosis.

CHAPTER 5: CONCLUSIONS AND FUTURE DIRECTIONS

5.1 Major findings

Through these projects, I have demonstrated the efficacy of combined HDAC inhibitor entinostat and MEK inhibitor pimasertib treatments blocking the progression of preclinical models of TNBC and IBC (**Figure 51A**). The effectiveness of this therapy has been significantly associated with the induction of tumor apoptosis regulated by NOXA-mediated MCL1 degradation. Also, I established the rationale for a novel EPA and EPHA2-targeting based combination therapy that displays efficacy in EPHA2 positive TN-IBC (**Figure 51B**). The

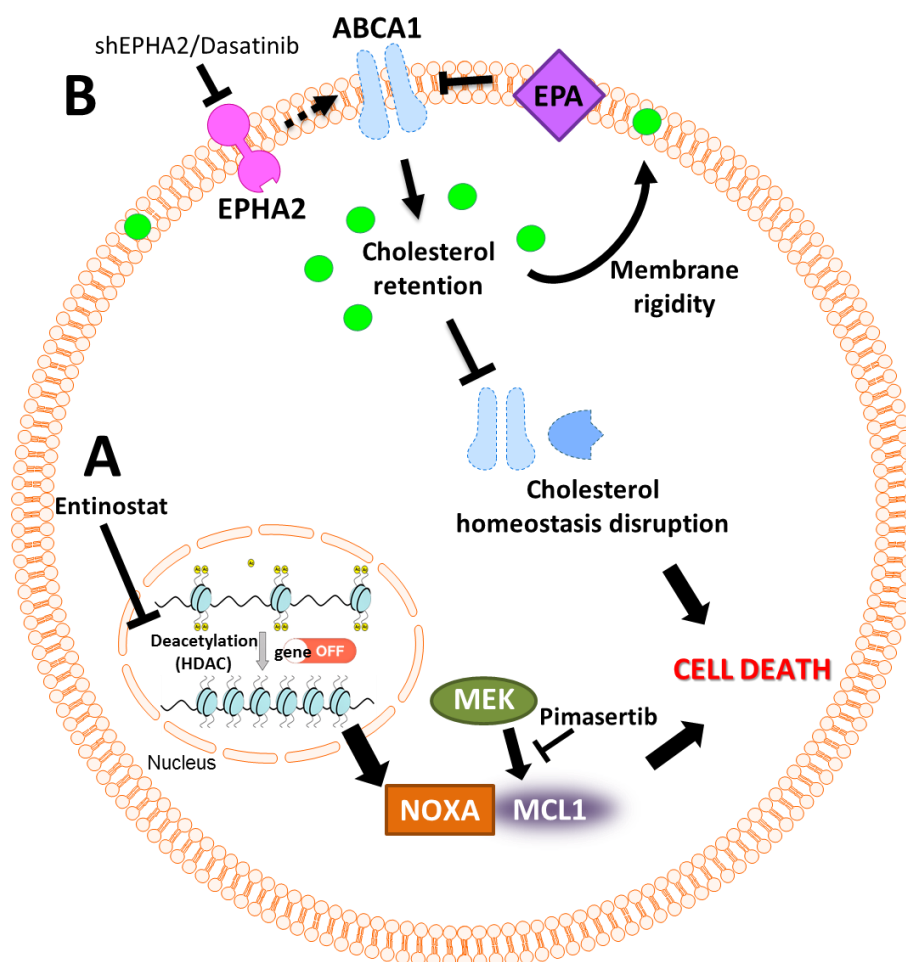


Figure 51. Diagram of major mechanisms of synergy involved in our newly discovered combinational therapies against TNBC and IBC: (A) entinostat and pimasertib, and (B) EPA with EPHA2-inhibition.

mechanism of action for EPA/EPHA2-inhibition based therapy relied on the induction of changes in the membrane of TN-IBC cells as a prelude to induction of cell death.

5.2 Significance

TNBC and IBC are the two most aggressive breast cancers, which still lack effective targeted therapy options that significantly inhibit tumor burden, or improve patient outcome. Therefore, the studies presented in this dissertation provide compelling evidence for the efficacy of novel combination therapies consisting of HDAC and MEK inhibitors, or EPA and EPHA2 inhibition, promoting TNBC and IBC cell death in translational xenograft models. The evidence developed in these projects additionally provide a strong rationale for the clinical testing of two novel therapeutic strategies against TNBC and IBC, as well as a basis for the development of predictive biomarkers for patient stratification and therapeutic response.

Besides breast cancer (*139*), overexpression of MCL1 has been associated with survival pathways, resistance, and poor prognosis in multiple cancers, such as melanoma (*71*), small-cell lung cancer (*140*), colorectal cancer (*141*), oral cancers (*142*), endometrial cancer (*143*), as well as multiple hematological malignancies (*72, 144*). Therefore, combination treatment of HDAC and MEK inhibitors may be effective in other cancers, increasing the significance of this study. However, further validation in clinically relevant models for each disease is needed. Others have reported data supporting the potential for the combination treatment of MCL1 inhibitors and inducers of NOXA, providing further evidence of the likely applicability of our combination treatment (*145, 146*). Furthermore, we observed sensitivity of IBC and TNBC cells to entinostat and pimasertib treatment within clinically relevant concentrations, providing a preclinical rationale for translation into a clinically appropriate dose.

Overexpression of EPHA2 has been associated with poor prognosis in multiple cancers, such as colorectal, lung, ovarian, endometrial, and pancreatic, among others (147-152). Moreover, ABCA1 overexpression was identified to be associated with poor prognosis in breast, ovarian, and hepatocellular carcinomas (124, 153-155). Therefore, our combination treatment may be effective in other cancers, thus broadening the importance of this study.

5.3 Future directions

To evaluate the clinical efficacy of the combinational treatment strategies proposed here, as well as to determine the validity of proposed biomarkers for treatment response and patient selection, we will translate our results into the development of clinical trials for therapeutic testing in humans following the reporting recommendations for tumor marker prognostic studies (REMARK) guidelines (156). The REMARK guidelines provide a standardized method for study design, development of hypotheses, patient and specimen characteristics, assay methods, and statistical analysis methods in addition to suggestions for data presentation and discussions. Complying with these guidelines, we have proposed a Phase 1b clinical trial protocol for the testing in humans of the HDAC inhibitor entinostat, and a MEK pathway inhibitor selumetinib, in metastatic breast cancer patients with tumors expressing high MCL1, and low NOXA protein levels. Detailed information on study design, as well as on specimen characteristic and assay methods for tumor biomarker studies, are illustrated in detail in **Figure 52**. This study, expected to start in late 2017 to early 2018, will be supported by the Cancer Therapy Evaluation Program (CTEP) of the National Cancer Institute at the National Institutes of Health, and conducted at The University of Texas MD Anderson Cancer Center in Houston, Texas, by Dr. Naoto T. Ueno and Dr. Bora Lim from the Department of Breast Medical Oncology and the Morgan Welsh Inflammatory Breast Cancer Research Program and Clinic.

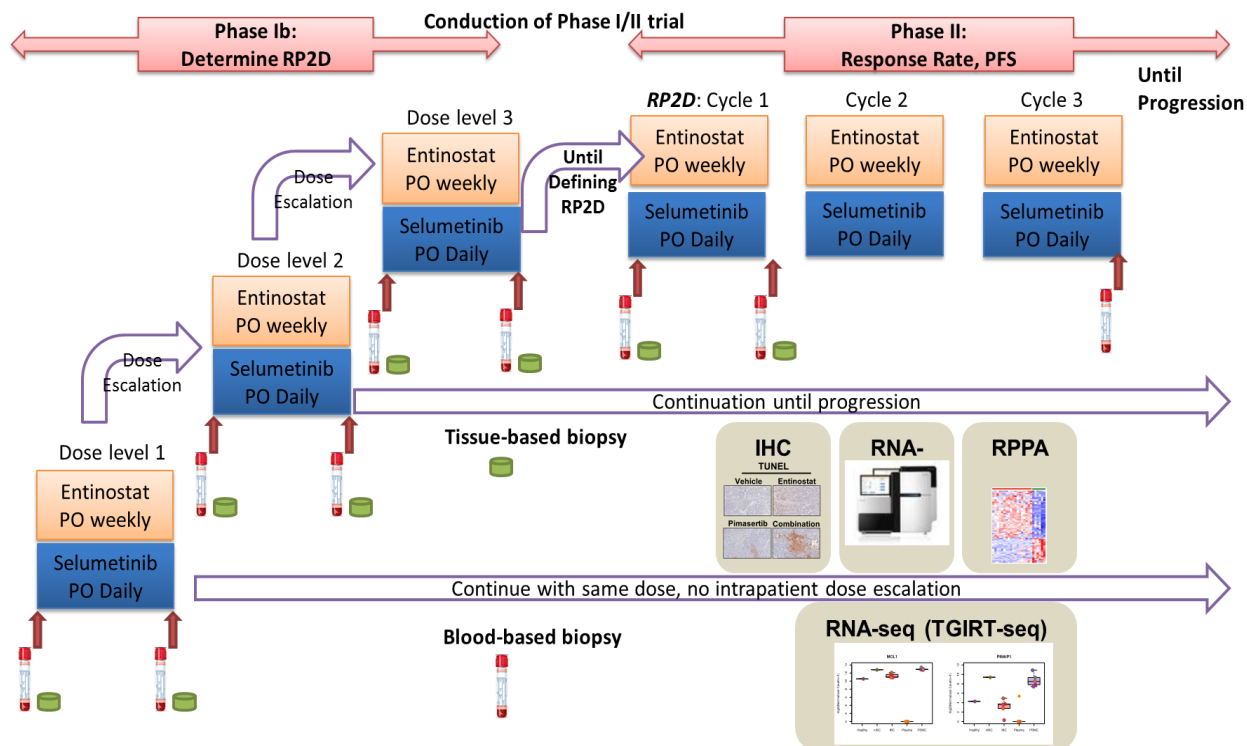


Figure 52. Schema of clinical trial for entinostat in combination with selumetinib including details of biological sample collection for biomarker analysis.

Remaining unclear are the specific reasons why select IBC and TNBC cell lines have increased NOXA mRNA expression, and *NOXA* promoter acetylation, in response to entinostat. Here we noted a tendency for *TP53*- and *BRCA1*-mutant cell lines to be unresponsive to treatment. *BRCA1* is a co-activator of *TP53* which subsequently induces apoptosis via NOXA, suggesting a possible escape mechanism when *BRCA1* and *TP53* are mutated (65). Additionally, we cannot rule out as possible contributing factors the potential differences in the intracellular metabolism of entinostat across cell lines, as well as other possible mechanisms by which entinostat could be modulating *NOXA* gene expression. Future investigation into the role of *TP53* and *BRCA1* mutation status and entinostat intracellular metabolism in association with NOXA expression and treatment response would be crucial, potentially enabling additional criteria for patient selection.

We will also initiate a Phase 1b study to evaluate the clinical efficacy of combination EPA and EPHA2-targeting therapy in human cancers. Through this second clinical trial, combination therapy will be tested in breast cancer patients with metastatic disease that have an elevated tumor expression of EPHA2, and ABCA1, proteins. We will submit this clinical trial protocol for support by the CTEP in early 2018, to be carried out at The University of Texas MD Anderson Cancer Center and Morgan Welsh Inflammatory Breast Cancer Research Program and Clinic in Houston, Texas, by Dr. Naoto T. Ueno and Dr. Bedrich Eckhardt.

Because cell sensitivity to EPA in combination with EPHA2-inhibition seems to be dependent on cell membrane accumulation of cholesterol, a potential challenge for the clinical application of our therapeutic strategy is the high percentage (49%) of adults in the U.S. population currently receiving therapy with cholesterol biosynthesis inhibitors (i.e., statins), which could reduce the efficacy of EPA and EPHA2-targeting therapy (*157-159*). However, statins have been reported to have both tumorigenic and anti-tumorigenic roles, probably due to their pleiotropic effects. Therefore, the efficacy of the EPA and EPHA2-inhibiting combinations in patients receiving a statin should be evaluated, together with ABCA1 and EPHA2 protein expression measurements; such investigations have the potential to provide robust predictive biomarkers of treatment response to EPA and EPHA2-targeted combination therapy.

The results from these clinical trials would further support the initiation of a Phase II and III trials for testing the efficacy of these combination treatment strategies in patients with TNBC and IBC, but also potentially on patients with cancer types that overexpress MCL1, or EPHA2 and ABCA1, respectively (**Figure 53**). Additionally, the clinically relevant doses tested in our preclinical models would potentially allow for a significantly decreased toxicity to patients,

compared to that of cytotoxic chemotherapy and other non-targeting approaches with higher toxicities.

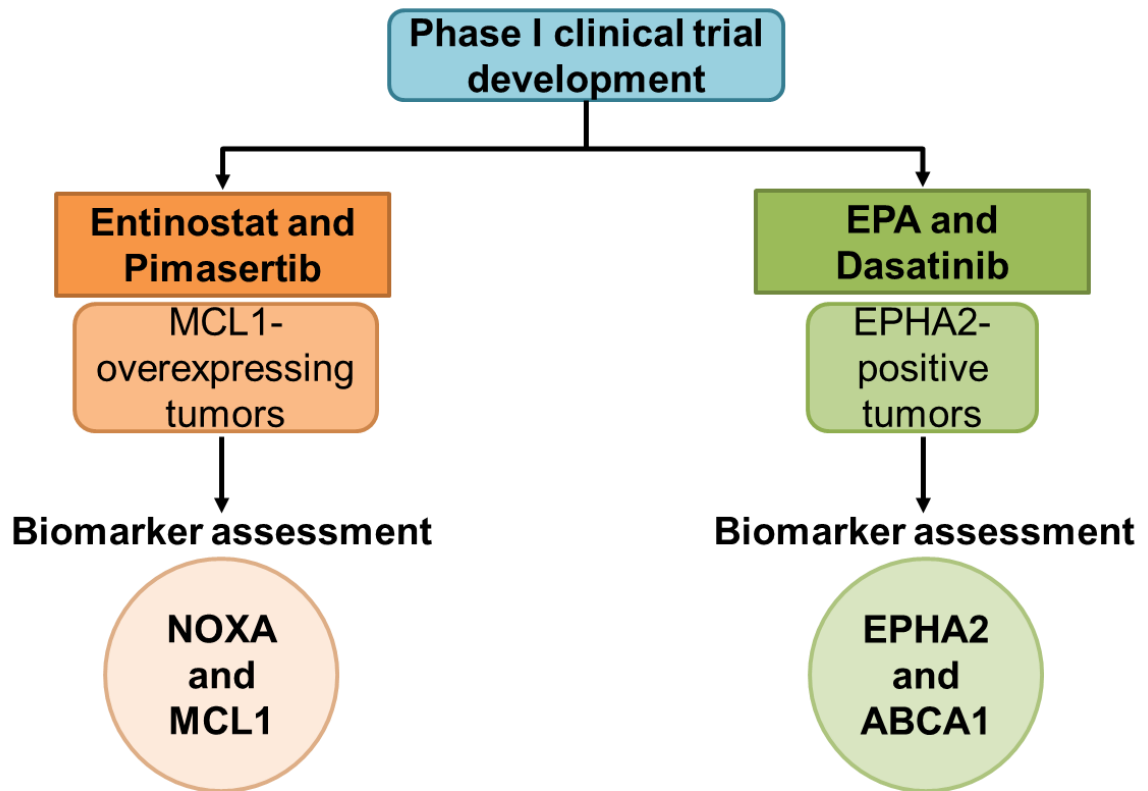


Figure 53. Summarized overview of clinical trials and biomarker development for proposed combination therapy strategies in patients with invasive breast cancers.

BIBLIOGRAPHY

1. R. L. Siegel, K. D. Miller, A. Jemal, Cancer Statistics, 2017. *CA Cancer J Clin* **67**, 7-30 (2017).
2. R. R. Bastien, A. Rodriguez-Lescure, M. T. Ebbert, A. Prat, B. Munarriz, L. Rowe, P. Miller, M. Ruiz-Borrego, D. Anderson, B. Lyons, I. Alvarez, T. Dowell, D. Wall, M. A. Segui, L. Barley, K. M. Boucher, E. Alba, L. Pappas, C. A. Davis, I. Aranda, C. Fauron, I. J. Stijleman, J. Palacios, A. Anton, E. Carrasco, R. Caballero, M. J. Ellis, T. O. Nielsen, C. M. Perou, M. Astill, P. S. Bernard, M. Martin, PAM50 breast cancer subtyping by RT-qPCR and concordance with standard clinical molecular markers. *BMC Med Genomics* **5**, 44 (2012).
3. T. Sorlie, C. M. Perou, R. Tibshirani, T. Aas, S. Geisler, H. Johnsen, T. Hastie, M. B. Eisen, M. van de Rijn, S. S. Jeffrey, T. Thorsen, H. Quist, J. C. Matese, P. O. Brown, D. Botstein, P. E. Lonning, A. L. Borresen-Dale, Gene expression patterns of breast carcinomas distinguish tumor subclasses with clinical implications. *Proc Natl Acad Sci U S A* **98**, 10869-10874 (2001).
4. X. Dai, T. Li, Z. Bai, Y. Yang, X. Liu, J. Zhan, B. Shi, Breast cancer intrinsic subtype classification, clinical use and future trends. *Am J Cancer Res* **5**, 2929-2943 (2015).
5. C. M. Perou, T. Sorlie, M. B. Eisen, M. van de Rijn, S. S. Jeffrey, C. A. Rees, J. R. Pollack, D. T. Ross, H. Johnsen, L. A. Akslen, O. Fluge, A. Pergamenschikov, C. Williams, S. X. Zhu, P. E. Lonning, A. L. Borresen-Dale, P. O. Brown, D. Botstein, Molecular portraits of human breast tumours. *Nature* **406**, 747-752 (2000).
6. T. Sorlie, R. Tibshirani, J. Parker, T. Hastie, J. S. Marron, A. Nobel, S. Deng, H. Johnsen, R. Pesich, S. Geisler, J. Demeter, C. M. Perou, P. E. Lonning, P. O. Brown, A. L. Borresen-Dale, D. Botstein, Repeated observation of breast tumor subtypes in

- independent gene expression data sets. *Proc Natl Acad Sci U S A* **100**, 8418-8423 (2003).
7. M. C. Cheang, S. K. Chia, D. Voduc, D. Gao, S. Leung, J. Snider, M. Watson, S. Davies, P. S. Bernard, J. S. Parker, C. M. Perou, M. J. Ellis, T. O. Nielsen, Ki67 index, HER2 status, and prognosis of patients with luminal B breast cancer. *J Natl Cancer Inst* **101**, 736-750 (2009).
 8. C. S. Vallejos, H. L. Gomez, W. R. Cruz, J. A. Pinto, R. R. Dyer, R. Velarde, J. F. Suazo, S. P. Neciosup, M. Leon, M. A. de la Cruz, C. E. Vigil, Breast cancer classification according to immunohistochemistry markers: subtypes and association with clinicopathologic variables in a peruvian hospital database. *Clin Breast Cancer* **10**, 294-300 (2010).
 9. C. Sotiriou, S. Y. Neo, L. M. McShane, E. L. Korn, P. M. Long, A. Jazaeri, P. Martiat, S. B. Fox, A. L. Harris, E. T. Liu, Breast cancer classification and prognosis based on gene expression profiles from a population-based study. *Proc Natl Acad Sci U S A* **100**, 10393-10398 (2003).
 10. J. D. Brenton, L. A. Carey, A. A. Ahmed, C. Caldas, Molecular classification and molecular forecasting of breast cancer: ready for clinical application? *J Clin Oncol* **23**, 7350-7360 (2005).
 11. J. S. Parker, M. Mullins, M. C. Cheang, S. Leung, D. Voduc, T. Vickery, S. Davies, C. Fauron, X. He, Z. Hu, J. F. Quackenbush, I. J. Stijleman, J. Palazzo, J. S. Marron, A. B. Nobel, E. Mardis, T. O. Nielsen, M. J. Ellis, C. M. Perou, P. S. Bernard, Supervised risk predictor of breast cancer based on intrinsic subtypes. *J Clin Oncol* **27**, 1160-1167 (2009).

12. S. Y. Bae, S. Kim, J. H. Lee, H. C. Lee, S. K. Lee, W. H. Kil, S. W. Kim, J. E. Lee, S. J. Nam, Poor prognosis of single hormone receptor- positive breast cancer: similar outcome as triple-negative breast cancer. *BMC Cancer* **15**, 138 (2015).
13. C. Criscitiello, H. A. Azim, Jr., P. C. Schouten, S. C. Linn, C. Sotiriou, Understanding the biology of triple-negative breast cancer. *Ann Oncol* **23 Suppl 6**, vi13-18 (2012).
14. C. Fan, D. S. Oh, L. Wessels, B. Weigelt, D. S. Nuyten, A. B. Nobel, L. J. van't Veer, C. M. Perou, Concordance among gene-expression-based predictors for breast cancer. *N Engl J Med* **355**, 560-569 (2006).
15. L. A. Carey, C. M. Perou, C. A. Livasy, L. G. Dressler, D. Cowan, K. Conway, G. Karaca, M. A. Troester, C. K. Tse, S. Edmiston, S. L. Deming, J. Geradts, M. C. Cheang, T. O. Nielsen, P. G. Moorman, H. S. Earp, R. C. Millikan, Race, breast cancer subtypes, and survival in the Carolina Breast Cancer Study. *JAMA* **295**, 2492-2502 (2006).
16. B. D. Lehmann, J. A. Bauer, X. Chen, M. E. Sanders, A. B. Chakravarthy, Y. Shyr, J. A. Pietenpol, Identification of human triple-negative breast cancer subtypes and preclinical models for selection of targeted therapies. *J Clin Invest* **121**, 2750-2767 (2011).
17. S. Dawood, N. T. Ueno, V. Valero, W. A. Woodward, T. A. Buchholz, G. N. Hortobagyi, A. M. Gonzalez-Angulo, M. Cristofanilli, Differences in survival among women with stage III inflammatory and noninflammatory locally advanced breast cancer appear early: a large population-based study. *Cancer* **117**, 1819-1826 (2011).
18. S. Chang, S. L. Parker, T. Pham, A. U. Buzdar, S. D. Hursting, Inflammatory breast carcinoma incidence and survival: the surveillance, epidemiology, and end results program of the National Cancer Institute, 1975-1992. *Cancer* **82**, 2366-2372 (1998).

19. W. F. Anderson, C. Schairer, B. E. Chen, K. W. Hance, P. H. Levine, Epidemiology of inflammatory breast cancer (IBC). *Breast Dis* **22**, 9-23 (2005).
20. J. Li, A. M. Gonzalez-Angulo, P. K. Allen, T. K. Yu, W. A. Woodward, N. T. Ueno, A. Lucci, S. Krishnamurthy, Y. Gong, M. L. Bondy, W. Yang, J. S. Willey, M. Cristofanilli, V. Valero, T. A. Buchholz, Triple-negative subtype predicts poor overall survival and high locoregional relapse in inflammatory breast cancer. *Oncologist* **16**, 1675-1683 (2011).
21. N. Chaher, H. Arias-Pulido, N. Terki, C. Qualls, K. Bouzid, C. Verschraegen, A. M. Wallace, M. Royce, Molecular and epidemiological characteristics of inflammatory breast cancer in Algerian patients. *Breast Cancer Res Treat* **131**, 437-444 (2012).
22. J. A. Zell, W. Y. Tsang, T. H. Taylor, R. S. Mehta, H. Anton-Culver, Prognostic impact of human epidermal growth factor-like receptor 2 and hormone receptor status in inflammatory breast cancer (IBC): analysis of 2,014 IBC patient cases from the California Cancer Registry. *Breast Cancer Res* **11**, R9 (2009).
23. H. Matsumoto, S. L. Koo, R. Dent, P. H. Tan, J. Iqbal, Role of inflammatory infiltrates in triple negative breast cancer. *J Clin Pathol* **68**, 506-510 (2015).
24. L. T. Steward, F. Gao, M. A. Taylor, J. A. Margenthaler, Impact of radiation therapy on survival in patients with triple-negative breast cancer. *Oncol Lett* **7**, 548-552 (2014).
25. F. M. Robertson, M. Bondy, W. Yang, H. Yamauchi, S. Wiggins, S. Kamrudin, S. Krishnamurthy, H. Le-Petross, L. Bidaut, A. N. Player, S. H. Barsky, W. A. Woodward, T. Buchholz, A. Lucci, N. T. Ueno, M. Cristofanilli, Inflammatory breast cancer: the disease, the biology, the treatment. *CA Cancer J Clin* **60**, 351-375 (2010).
26. I. A. Jaiyesimi, A. U. Buzdar, G. Hortobagyi, Inflammatory breast cancer: a review. *J Clin Oncol* **10**, 1014-1024 (1992).

27. E. Charafe-Jauffret, C. Tarpin, P. Viens, F. Bertucci, Defining the molecular biology of inflammatory breast cancer. *Semin Oncol* **35**, 41-50 (2008).
28. A. M. Gonzalez-Angulo, G. N. Hortobagyi, F. J. Esteva, Adjuvant therapy with trastuzumab for HER-2/neu-positive breast cancer. *Oncologist* **11**, 857-867 (2006).
29. N. T. Ueno, A. U. Buzdar, S. E. Singletary, F. C. Ames, M. D. McNeese, F. A. Holmes, R. L. Theriault, E. A. Strom, B. J. Wasaff, L. Asmar, D. Frye, G. N. Hortobagyi, Combined-modality treatment of inflammatory breast carcinoma: twenty years of experience at M. D. Anderson Cancer Center. *Cancer Chemother Pharmacol* **40**, 321-329 (1997).
30. F. Bertucci, N. T. Ueno, P. Finetti, P. Vermeulen, A. Lucci, F. M. Robertson, M. Marsan, T. Iwamoto, S. Krishnamurthy, H. Masuda, P. Van Dam, W. A. Woodward, M. Cristofanilli, J. M. Reuben, L. Dirix, P. Viens, W. F. Symmans, D. Birnbaum, S. J. Van Laere, Gene expression profiles of inflammatory breast cancer: correlation with response to neoadjuvant chemotherapy and metastasis-free survival. *Ann Oncol* **25**, 358-365 (2014).
31. A. M. Gonzalez-Angulo, B. T. Hennessy, K. Broglio, F. Meric-Bernstam, M. Cristofanilli, S. H. Giordano, T. A. Buchholz, A. Sahin, S. E. Singletary, A. U. Buzdar, G. N. Hortobagyi, Trends for inflammatory breast cancer: is survival improving? *Oncologist* **12**, 904-912 (2007).
32. H. Yamauchi, W. A. Woodward, V. Valero, R. H. Alvarez, A. Lucci, T. A. Buchholz, T. Iwamoto, S. Krishnamurthy, W. Yang, J. M. Reuben, G. N. Hortobagyi, N. T. Ueno, Inflammatory breast cancer: what we know and what we need to learn. *Oncologist* **17**, 891-899 (2012).

33. J. A. Niemiec, A. Adamczyk, A. Ambicka, A. Mucha-Malecka, W. M. Wysocki, B. Biesaga, M. Ziobro, I. Cedrych, A. Grela-Wojewoda, M. Domagala-Haduch, J. Wysocka, J. Rys, B. Sas-Korczynska, Prognostic role of lymphatic vessel density and lymphovascular invasion in chemotherapy-naïve and chemotherapy-treated patients with invasive breast cancer. *Am J Transl Res* **9**, 1435-1447 (2017).
34. E. S. Steinskog, S. J. Sagstad, M. Wagner, T. V. Karlsen, N. Yang, C. E. Markhus, S. Yndestad, H. Wiig, H. P. Eikesdal, Impaired lymphatic function accelerates cancer growth. *Oncotarget* **7**, 45789-45802 (2016).
35. I. J. Suarez-Arroyo, Y. R. Feliz-Mosquea, J. Perez-Laspiur, R. Arju, S. Giashuddin, G. Maldonado-Martinez, L. A. Cubano, R. J. Schneider, M. M. Martinez-Montemayor, The proteome signature of the inflammatory breast cancer plasma membrane identifies novel molecular markers of disease. *Am J Cancer Res* **6**, 1720-1740 (2016).
36. J. S. Tomlinson, M. L. Alpaugh, S. H. Barsky, An intact overexpressed E-cadherin/alpha,beta-catenin axis characterizes the lymphovascular emboli of inflammatory breast carcinoma. *Cancer Res* **61**, 5231-5241 (2001).
37. N. Cabioglu, Y. Gong, R. Islam, K. R. Broglio, N. Sneige, A. Sahin, A. M. Gonzalez-Angulo, P. Morandi, C. Bucana, G. N. Hortobagyi, M. Cristofanilli, Expression of growth factor and chemokine receptors: new insights in the biology of inflammatory breast cancer. *Ann Oncol* **18**, 1021-1029 (2007).
38. S. Dawood, K. Broglio, Y. Gong, W. T. Yang, M. Cristofanilli, S. W. Kau, F. Meric-Bernstam, T. A. Buchholz, G. N. Hortobagyi, A. M. Gonzalez-Angulo, G. Inflammatory Breast Cancer Research, Prognostic significance of HER-2 status in women with inflammatory breast cancer. *Cancer* **112**, 1905-1911 (2008).

39. C. G. Kleer, K. L. van Golen, S. D. Merajver, Molecular biology of breast cancer metastasis. Inflammatory breast cancer: clinical syndrome and molecular determinants. *Breast Cancer Res* **2**, 423-429 (2000).
40. J. Lee, C. Bartholomeusz, O. Mansour, J. Humphries, G. N. Hortobagyi, P. Ordentlich, N. T. Ueno, A class I histone deacetylase inhibitor, entinostat, enhances lapatinib efficacy in HER2-overexpressing breast cancer cells through FOXO3-mediated Bim1 expression. *Breast Cancer Res Treat* **146**, 259-272 (2014).
41. B. Gerber, S. Loibl, H. Eidtmann, M. Rezai, P. A. Fasching, H. Tesch, H. Eggemann, I. Schrader, K. Kittel, C. Hanusch, R. Kreienberg, C. Solbach, C. Jackisch, G. Kunz, J. U. Blohmer, J. Huober, M. Hauschild, V. Nekljudova, M. Untch, G. von Minckwitz, I. German Breast Group, Neoadjuvant bevacizumab and anthracycline-taxane-based chemotherapy in 678 triple-negative primary breast cancers; results from the geparquinto study (GBG 44). *Ann Oncol* **24**, 2978-2984 (2013).
42. K. D. Amos, B. Adamo, C. K. Anders, Triple-negative breast cancer: an update on neoadjuvant clinical trials. *Int J Breast Cancer* **2012**, 385978 (2012).
43. K. Ha, W. Fiskus, D. S. Choi, S. Bhaskara, L. Cerchietti, S. G. Devaraj, B. Shah, S. Sharma, J. C. Chang, A. M. Melnick, S. Hiebert, K. N. Bhalla, Histone deacetylase inhibitor treatment induces 'BRCAness' and synergistic lethality with PARP inhibitor and cisplatin against human triple negative breast cancer cells. *Oncotarget* **5**, 5637-5650 (2014).
44. I. Beuvink, A. Boulay, S. Fumagalli, F. Zilbermann, S. Ruetz, T. O'Reilly, F. Natt, J. Hall, H. A. Lane, G. Thomas, The mTOR inhibitor RAD001 sensitizes tumor cells to DNA-damaged induced apoptosis through inhibition of p21 translation. *Cell* **120**, 747-759 (2005).

45. N. Berrada, S. Delaloge, F. Andre, Treatment of triple-negative metastatic breast cancer: toward individualized targeted treatments or chemosensitization? *Ann Oncol* **21 Suppl 7**, vii30-35 (2010).
46. J. Harding, B. Burtneess, Cetuximab: an epidermal growth factor receptor chemeric human-murine monoclonal antibody. *Drugs Today (Barc)* **41**, 107-127 (2005).
47. H. A. Wahba, H. A. El-Hadaad, Current approaches in treatment of triple-negative breast cancer. *Cancer Biol Med* **12**, 106-116 (2015).
48. B. D. Lehmann, J. A. Pietenpol, Identification and use of biomarkers in treatment strategies for triple-negative breast cancer subtypes. *J Pathol* **232**, 142-150 (2014).
49. S. J. Van Laere, N. T. Ueno, P. Finetti, P. Vermeulen, A. Lucci, F. M. Robertson, M. Marsan, T. Iwamoto, S. Krishnamurthy, H. Masuda, P. van Dam, W. A. Woodward, P. Viens, M. Cristofanilli, D. Birnbaum, L. Dirix, J. M. Reuben, F. Bertucci, Uncovering the molecular secrets of inflammatory breast cancer biology: an integrated analysis of three distinct affymetrix gene expression datasets. *Clin Cancer Res* **19**, 4685-4696 (2013).
50. S. F. Madden, C. Clarke, P. Gaule, S. T. Aherne, N. O'Donovan, M. Clynes, J. Crown, W. M. Gallagher, BreastMark: an integrated approach to mining publicly available transcriptomic datasets relating to breast cancer outcome. *Breast Cancer Res* **15**, R52 (2013).
51. A. H. Klopp, L. Lacerda, A. Gupta, B. G. Debeb, T. Solley, L. Li, E. Spaeth, W. Xu, X. Zhang, M. T. Lewis, J. M. Reuben, S. Krishnamurthy, M. Ferrari, R. Gaspar, T. A. Buchholz, M. Cristofanilli, F. Marini, M. Andreeff, W. A. Woodward, Mesenchymal stem cells promote mammosphere formation and decrease E-cadherin in normal and malignant breast cells. *PLoS One* **5**, e12180 (2010).

52. J. Kurebayashi, T. Otsuki, C. K. Tang, M. Kurosumi, S. Yamamoto, K. Tanaka, M. Mochizuki, H. Nakamura, H. Sonoo, Isolation and characterization of a new human breast cancer cell line, KPL-4, expressing the Erb B family receptors and interleukin-6. *Br J Cancer* **79**, 707-717 (1999).
53. F. Ye, J. A. Bauer, J. A. Pietenpol, Y. Shyr, Analysis of high-throughput RNAi screening data in identifying genes mediating sensitivity to chemotherapeutic drugs: statistical approaches and perspectives. *BMC Genomics* **13 Suppl 8**, S3 (2012).
54. E. Sezgin, D. Waither, J. Bernardino de la Serna, C. Eggeling, Spectral imaging to measure heterogeneity in membrane lipid packing. *Chemphyschem* **16**, 1387-1394 (2015).
55. J. Folch, M. Lees, G. H. Sloane Stanley, A simple method for the isolation and purification of total lipides from animal tissues. *J Biol Chem* **226**, 497-509 (1957).
56. Y. Y. Fan, K. S. Ramos, R. S. Chapkin, Dietary gamma-linolenic acid enhances mouse macrophage-derived prostaglandin E1 which inhibits vascular smooth muscle cell proliferation. *J Nutr* **127**, 1765-1771 (1997).
57. R. S. Chapkin, K. J. Coble, Remodeling of Mouse Kidney Phospholipid Classes and Subclasses by Diet. *J Nutr Biochem* **2**, 158-164 (1991).
58. S. Pounds, S. W. Morris, Estimating the occurrence of false positives and false negatives in microarray studies by approximating and partitioning the empirical distribution of p-values. *Bioinformatics* **19**, 1236-1242 (2003).
59. A. M. Torres-Adorno, J. Lee, T. Kogawa, P. Ordentlich, D. Tripathy, B. Lim, N. T. Ueno, Histone Deacetylase Inhibitor Enhances the Efficacy of MEK Inhibitor through NOXA-Mediated MCL1 Degradation in Triple-Negative and Inflammatory Breast Cancer. *Clin Cancer Res*, (2017).

60. M. Mottamal, S. Zheng, T. L. Huang, G. Wang, Histone deacetylase inhibitors in clinical studies as templates for new anticancer agents. *Molecules* **20**, 3898-3941 (2015).
61. A. Saito, T. Yamashita, Y. Mariko, Y. Nosaka, K. Tsuchiya, T. Ando, T. Suzuki, T. Tsuruo, O. Nakanishi, A synthetic inhibitor of histone deacetylase, MS-27-275, with marked in vivo antitumor activity against human tumors. *Proc Natl Acad Sci U S A* **96**, 4592-4597 (1999).
62. D. A. Yardley, R. R. Ismail-Khan, B. Melichar, M. Lichinitser, P. N. Munster, P. M. Klein, S. Cruickshank, K. D. Miller, M. J. Lee, J. B. Trepel, Randomized phase II, double-blind, placebo-controlled study of exemestane with or without entinostat in postmenopausal women with locally recurrent or metastatic estrogen receptor-positive breast cancer progressing on treatment with a nonsteroidal aromatase inhibitor. *J Clin Oncol* **31**, 2128-2135 (2013).
63. N. N. Danial, BCL-2 family proteins: critical checkpoints of apoptotic cell death. *Clin Cancer Res* **13**, 7254-7263 (2007).
64. P. Fritsche, B. Seidler, S. Schuler, A. Schnieke, M. Gottlicher, R. M. Schmid, D. Saur, G. Schneider, HDAC2 mediates therapeutic resistance of pancreatic cancer cells via the BH3-only protein NOXA. *Gut* **58**, 1399-1409 (2009).
65. S. Inoue, J. Riley, T. W. Gant, M. J. Dyer, G. M. Cohen, Apoptosis induced by histone deacetylase inhibitors in leukemic cells is mediated by Bim and Noxa. *Leukemia* **21**, 1773-1782 (2007).
66. C. M. Goodwin, O. W. Rossanese, E. T. Olejniczak, S. W. Fesik, Myeloid cell leukemia-1 is an important apoptotic survival factor in triple-negative breast cancer. *Cell Death Differ* **22**, 2098-2106 (2015).

67. Y. Mei, W. Du, Y. Yang, M. Wu, Puma(*)Mcl-1 interaction is not sufficient to prevent rapid degradation of Mcl-1. *Oncogene* **24**, 7224-7237 (2005).
68. P. E. Czabotar, E. F. Lee, M. F. van Delft, C. L. Day, B. J. Smith, D. C. Huang, W. D. Fairlie, M. G. Hinds, P. M. Colman, Structural insights into the degradation of Mcl-1 induced by BH3 domains. *Proc Natl Acad Sci U S A* **104**, 6217-6222 (2007).
69. C. Ploner, R. Kofler, A. Villunger, Noxa: at the tip of the balance between life and death. *Oncogene* **27 Suppl 1**, S84-92 (2008).
70. C. Mitchell, A. Yacoub, H. Hossein, A. P. Martin, M. D. Bareford, P. Eulitt, C. Yang, K. P. Nephew, P. Dent, Inhibition of MCL-1 in breast cancer cells promotes cell death in vitro and in vivo. *Cancer Biol Ther* **10**, 903-917 (2010).
71. N. Chetoui, K. Sylla, J. V. Gagnon-Houde, C. Alcaide-Loridan, D. Charron, R. Al-Daccak, F. Aoudjit, Down-regulation of mcl-1 by small interfering RNA sensitizes resistant melanoma cells to fas-mediated apoptosis. *Mol Cancer Res* **6**, 42-52 (2008).
72. M. Konopleva, M. Milella, P. Ruvolo, J. C. Watts, M. R. Ricciardi, B. Korchin, T. McQueen, W. Bornmann, T. Tsao, P. Bergamo, D. H. Mak, W. Chen, J. McCubrey, A. Tafuri, M. Andreeff, MEK inhibition enhances ABT-737-induced leukemia cell apoptosis via prevention of ERK-activated MCL-1 induction and modulation of MCL-1/BIM complex. *Leukemia* **26**, 778-787 (2012).
73. C. Bartholomeusz, A. M. Gonzalez-Angulo, P. Liu, N. Hayashi, A. Lluch, J. Ferrer-Lozano, G. N. Hortobagyi, High ERK protein expression levels correlate with shorter survival in triple-negative breast cancer patients. *Oncologist* **17**, 766-774 (2012).
74. A. A. Adjei, R. B. Cohen, W. Franklin, C. Morris, D. Wilson, J. R. Molina, L. J. Hanson, L. Gore, L. Chow, S. Leong, L. Maloney, G. Gordon, H. Simmons, A. Marlow, K. Litwiler, S. Brown, G. Poch, K. Kane, J. Haney, S. G. Eckhardt, Phase I

- pharmacokinetic and pharmacodynamic study of the oral, small-molecule mitogen-activated protein kinase kinase 1/2 inhibitor AZD6244 (ARRY-142886) in patients with advanced cancers. *J Clin Oncol* **26**, 2139-2146 (2008).
75. C. Bartholomeusz, T. Oishi, H. Saso, U. Akar, P. Liu, K. Kondo, A. Kazansky, S. Krishnamurthy, J. Lee, F. J. Esteva, J. Kigawa, N. T. Ueno, MEK1/2 inhibitor selumetinib (AZD6244) inhibits growth of ovarian clear cell carcinoma in a PEA-15-dependent manner in a mouse xenograft model. *Mol Cancer Ther* **11**, 360-369 (2012).
 76. K. Kim, S. Y. Kong, M. Fulciniti, X. Li, W. Song, S. Nahar, P. Burger, M. J. Rumizen, K. Podar, D. Chauhan, T. Hideshima, N. C. Munshi, P. Richardson, A. Clark, J. Ogden, A. Goutopoulos, L. Rastelli, K. C. Anderson, Y. T. Tai, Blockade of the MEK/ERK signalling cascade by AS703026, a novel selective MEK1/2 inhibitor, induces pleiotropic anti-myeloma activity in vitro and in vivo. *Br J Haematol* **149**, 537-549 (2010).
 77. A. D. Awada, J.P.; Houede, N.; Lebbe, C.; Lesimple, T.; Schellens, J.H.M.; Rottey, S.; Kefford, R.; Rejeb, N.; Raymond, E., in *AACR Symposium on Molecular Targets and Cancer Therapeutics*, E. Ltd., Ed. (European Journal of Cancer, 2012), vol. 48, pp. 185-186.
 78. F. Catalanotti, D. B. Solit, M. P. Pulitzer, M. F. Berger, S. N. Scott, T. Iyriboz, M. E. Lacouture, K. S. Panageas, J. D. Wolchok, R. D. Carvajal, G. K. Schwartz, N. Rosen, P. B. Chapman, Phase II trial of MEK inhibitor selumetinib (AZD6244, ARRY-142886) in patients with BRAFV600E/K-mutated melanoma. *Clin Cancer Res* **19**, 2257-2264 (2013).
 79. J. Farley, W. E. Brady, V. Vathipadiekal, H. A. Lankes, R. Coleman, M. A. Morgan, R. Mannel, S. D. Yamada, D. Mutch, W. H. Rodgers, M. Birrer, D. M. Gershenson,

- Selumetinib in women with recurrent low-grade serous carcinoma of the ovary or peritoneum: an open-label, single-arm, phase 2 study. *Lancet Oncol* **14**, 134-140 (2013).
80. C. Bartholomeusz, X. Xie, M. K. Pitner, K. Kondo, A. Dadbin, J. Lee, H. Saso, P. D. Smith, K. N. Dalby, N. T. Ueno, MEK Inhibitor Selumetinib (AZD6244; ARRY-142886) Prevents Lung Metastasis in a Triple-Negative Breast Cancer Xenograft Model. *Mol Cancer Ther* **14**, 2773-2781 (2015).
 81. L. Zhou, V. R. Ruvolo, T. McQueen, W. Chen, I. J. Samudio, O. Conneely, M. Konopleva, M. Andreeff, HDAC inhibition by SNDX-275 (Entinostat) restores expression of silenced leukemia-associated transcription factors Nur77 and Nor1 and of key pro-apoptotic proteins in AML. *Leukemia* **27**, 1358-1368 (2013).
 82. M. Baou, S. L. Kohlhaas, M. Butterworth, M. Vogler, D. Dinsdale, R. Walewska, A. Majid, E. Eldering, M. J. Dyer, G. M. Cohen, Role of NOXA and its ubiquitination in proteasome inhibitor-induced apoptosis in chronic lymphocytic leukemia cells. *Haematologica* **95**, 1510-1518 (2010).
 83. T. R. Singh, S. Shankar, R. K. Srivastava, HDAC inhibitors enhance the apoptosis-inducing potential of TRAIL in breast carcinoma. *Oncogene* **24**, 4609-4623 (2005).
 84. P. Gomez-Bougie, E. Menoret, P. Juin, C. Dousset, C. Pellat-Deceunynck, M. Amiot, Noxa controls Mule-dependent Mcl-1 ubiquitination through the regulation of the Mcl-1/USP9X interaction. *Biochem Biophys Res Commun* **413**, 460-464 (2011).
 85. R. R. Rosato, J. A. Almenara, S. Grant, The histone deacetylase inhibitor MS-275 promotes differentiation or apoptosis in human leukemia cells through a process regulated by generation of reactive oxygen species and induction of p21CIP1/WAF1 1. *Cancer Res* **63**, 3637-3645 (2003).

86. R. L. Carpenter, H. W. Lo, Regulation of Apoptosis by HER2 in Breast Cancer. *J Carcinog Mutagen* **2013**, (2013).
87. K. Milde-Langosch, A. M. Bamberger, G. Rieck, D. Grund, G. Hemminger, V. Muller, T. Loning, Expression and prognostic relevance of activated extracellular-regulated kinases (ERK1/2) in breast cancer. *Br J Cancer* **92**, 2206-2215 (2005).
88. G. Wei, A. A. Margolin, L. Haery, E. Brown, L. Cucolo, B. Julian, S. Shehata, A. L. Kung, R. Beroukhim, T. R. Golub, Chemical genomics identifies small-molecule MCL1 repressors and BCL-xL as a predictor of MCL1 dependency. *Cancer Cell* **21**, 547-562 (2012).
89. D. Hanahan, R. A. Weinberg, Hallmarks of cancer: the next generation. *Cell* **144**, 646-674 (2011).
90. A. Korniluk, O. Koper, H. Kemon, V. Dymicka-Piekarska, From inflammation to cancer. *Ir J Med Sci* **186**, 57-62 (2017).
91. B. Trabert, R. C. Eldridge, R. M. Pfeiffer, M. S. Shiels, T. J. Kemp, C. Guillemette, P. Hartge, M. E. Sherman, L. A. Brinton, A. Black, A. K. Chaturvedi, A. Hildesheim, S. I. Berndt, M. Safaeian, L. Pinto, N. Wentzensen, Prediagnostic circulating inflammation markers and endometrial cancer risk in the prostate, lung, colorectal and ovarian cancer (PLCO) screening trial. *Int J Cancer* **140**, 600-610 (2017).
92. R. J. Hung, C. M. Ulrich, E. L. Goode, Y. Brhane, K. Muir, A. T. Chan, L. L. Marchand, J. Schildkraut, J. S. Witte, R. Eeles, P. Boffetta, M. R. Spitz, J. G. Poirier, D. N. Rider, B. L. Fridley, Z. Chen, C. Haiman, F. Schumacher, D. F. Easton, M. T. Landi, P. Brennan, R. Houlston, D. C. Christiani, J. K. Field, H. Bickeboller, A. Risch, Z. Kote-Jarai, F. Wiklund, H. Gronberg, S. Chanock, S. I. Berndt, P. Kraft, S. Lindstrom, A. A. Al Olama, H. Song, C. Phelan, N. Wentzensen, U. Peters, M. L. Slattery, Gecco, T. A.

- Sellers, Foci, G. Casey, S. B. Gruber, Corect, D. J. Hunter, Drive, C. I. Amos, B. Henderson, G.-O. Network, Cross Cancer Genomic Investigation of Inflammation Pathway for Five Common Cancers: Lung, Ovary, Prostate, Breast, and Colorectal Cancer. *J Natl Cancer Inst* **107**, (2015).
93. J. Todoric, L. Antonucci, M. Karin, Targeting Inflammation in Cancer Prevention and Therapy. *Cancer Prev Res (Phila)* **9**, 895-905 (2016).
 94. A. H. Lee, L. C. Happerfield, R. R. Millis, L. G. Bobrow, Inflammatory infiltrate in invasive lobular and ductal carcinoma of the breast. *Br J Cancer* **74**, 796-801 (1996).
 95. P. M. Rothwell, F. G. Fowkes, J. F. Belch, H. Ogawa, C. P. Warlow, T. W. Meade, Effect of daily aspirin on long-term risk of death due to cancer: analysis of individual patient data from randomised trials. *Lancet* **377**, 31-41 (2011).
 96. E. J. Ramos, F. A. Middleton, A. Laviano, T. Sato, I. Romanova, U. N. Das, C. Chen, Y. Qi, M. M. Meguid, Effects of omega-3 fatty acid supplementation on tumor-bearing rats. *J Am Coll Surg* **199**, 716-723 (2004).
 97. A. Laviano, S. Rianda, A. Molfino, F. Rossi Fanelli, Omega-3 fatty acids in cancer. *Curr Opin Clin Nutr Metab Care* **16**, 156-161 (2013).
 98. E. A. Brinton, R. P. Mason, Prescription omega-3 fatty acid products containing highly purified eicosapentaenoic acid (EPA). *Lipids Health Dis* **16**, 23 (2017).
 99. C. Vors, J. Allaire, J. Marin, M. C. Lepine, A. Charest, A. Tchernof, P. Couture, B. Lamarche, Inflammatory gene expression in whole blood cells after EPA vs. DHA supplementation: Results from the ComparED study. *Atherosclerosis* **257**, 116-122 (2017).

100. P. A. Corsetto, G. Montorfano, S. Zava, I. E. Jovenitti, A. Cremona, B. Berra, A. M. Rizzo, Effects of n-3 PUFAs on breast cancer cells through their incorporation in plasma membrane. *Lipids Health Dis* **10**, 73 (2011).
101. P. A. Corsetto, A. Cremona, G. Montorfano, I. E. Jovenitti, F. Orsini, P. Arosio, A. M. Rizzo, Chemical-physical changes in cell membrane microdomains of breast cancer cells after omega-3 PUFA incorporation. *Cell Biochem Biophys* **64**, 45-59 (2012).
102. C. C. Mandal, T. Ghosh-Choudhury, T. Yoneda, G. G. Choudhury, N. Ghosh-Choudhury, Fish oil prevents breast cancer cell metastasis to bone. *Biochem Biophys Res Commun* **402**, 602-607 (2010).
103. E. B. Pasquale, Eph-ephrin bidirectional signaling in physiology and disease. *Cell* **133**, 38-52 (2008).
104. S. D. Funk, A. W. Orr, Ephs and ephrins resurface in inflammation, immunity, and atherosclerosis. *Pharmacol Res* **67**, 42-52 (2013).
105. N. W. Gale, S. J. Holland, D. M. Valenzuela, A. Flenniken, L. Pan, T. E. Ryan, M. Henkemeyer, K. Strebhardt, H. Hirai, D. G. Wilkinson, T. Pawson, S. Davis, G. D. Yancopoulos, Eph receptors and ligands comprise two major specificity subclasses and are reciprocally compartmentalized during embryogenesis. *Neuron* **17**, 9-19 (1996).
106. D. Arvanitis, A. Davy, Eph/ephrin signaling: networks. *Genes Dev* **22**, 416-429 (2008).
107. E. B. Pasquale, Eph receptor signalling casts a wide net on cell behaviour. *Nat Rev Mol Cell Biol* **6**, 462-475 (2005).
108. J. E. Park, A. I. Son, R. Zhou, Roles of EphA2 in Development and Disease. *Genes (Basel)* **4**, 334-357 (2013).
109. M. L. Taddei, M. Parri, A. Angelucci, F. Bianchini, C. Marconi, E. Giannoni, G. Rauei, M. Bologna, L. Calorini, P. Chiarugi, EphA2 induces metastatic growth regulating

- amoeboid motility and clonogenic potential in prostate carcinoma cells. *Mol Cancer Res* **9**, 149-160 (2011).
110. H. Miao, D. Q. Li, A. Mukherjee, H. Guo, A. Petty, J. Cutter, J. P. Basilion, J. Sedor, J. Wu, D. Danielpour, A. E. Sloan, M. L. Cohen, B. Wang, EphA2 mediates ligand-dependent inhibition and ligand-independent promotion of cell migration and invasion via a reciprocal regulatory loop with Akt. *Cancer Cell* **16**, 9-20 (2009).
 111. N. Sugiyama, E. Gucciardo, K. Lehti, EphA2 bears plasticity to tumor invasion. *Cell Cycle* **12**, 2927-2928 (2013).
 112. J. Huang, D. Xiao, G. Li, J. Ma, P. Chen, W. Yuan, F. Hou, J. Ge, M. Zhong, Y. Tang, X. Xia, Z. Chen, EphA2 promotes epithelial-mesenchymal transition through the Wnt/beta-catenin pathway in gastric cancer cells. *Oncogene* **33**, 2737-2747 (2014).
 113. K. Salaita, P. M. Nair, R. S. Petit, R. M. Neve, D. Das, J. W. Gray, J. T. Groves, Restriction of receptor movement alters cellular response: physical force sensing by EphA2. *Science* **327**, 1380-1385 (2010).
 114. E. R. Rayburn, S. J. Ezell, R. Zhang, Anti-Inflammatory Agents for Cancer Therapy. *Mol Cell Pharmacol* **1**, 29-43 (2009).
 115. M. J. Thun, S. J. Henley, C. Patrono, Nonsteroidal anti-inflammatory drugs as anticancer agents: mechanistic, pharmacologic, and clinical issues. *J Natl Cancer Inst* **94**, 252-266 (2002).
 116. I. Nakazawa, M. Iwaizumi, A role of the cancer cell membrane fluidity in the cancer metastases: an ESR study. *Tohoku J Exp Med* **157**, 193-198 (1989).
 117. R. Zeisig, T. Koklic, B. Wiesner, I. Fichtner, M. Sentjurs, Increase in fluidity in the membrane of MT3 breast cancer cells correlates with enhanced cell adhesion in vitro and

- increased lung metastasis in NOD/SCID mice. *Arch Biochem Biophys* **459**, 98-106 (2007).
118. A. Sade, S. Tuncay, I. Cimen, F. Severcan, S. Banerjee, Celecoxib reduces fluidity and decreases metastatic potential of colon cancer cell lines irrespective of COX-2 expression. *Biosci Rep* **32**, 35-44 (2012).
 119. J. Wykosky, W. Debinski, The EphA2 receptor and ephrinA1 ligand in solid tumors: function and therapeutic targeting. *Mol Cancer Res* **6**, 1795-1806 (2008).
 120. R. M. Neve, K. Chin, J. Fridlyand, J. Yeh, F. L. Baehner, T. Fevr, L. Clark, N. Bayani, J. P. Coppe, F. Tong, T. Speed, P. T. Spellman, S. DeVries, A. Lapuk, N. J. Wang, W. L. Kuo, J. L. Stilwell, D. Pinkel, D. G. Albertson, F. M. Waldman, F. McCormick, R. B. Dickson, M. D. Johnson, M. Lippman, S. Ethier, A. Gazdar, J. W. Gray, A collection of breast cancer cell lines for the study of functionally distinct cancer subtypes. *Cancer Cell* **10**, 515-527 (2006).
 121. M. Y. van der Wulp, H. J. Verkade, A. K. Groen, Regulation of cholesterol homeostasis. *Mol Cell Endocrinol* **368**, 1-16 (2013).
 122. M. S. Jaureguiberry, M. A. Tricerri, S. A. Sanchez, G. S. Finarelli, M. A. Montanaro, E. D. Prieto, O. J. Rimoldi, Role of plasma membrane lipid composition on cellular homeostasis: learning from cell line models expressing fatty acid desaturases. *Acta Biochim Biophys Sin (Shanghai)* **46**, 273-282 (2014).
 123. W. K. Subczynski, M. Pasenkiewicz-Gierula, J. Widomska, L. Mainali, M. Raguz, High Cholesterol/Low Cholesterol: Effects in Biological Membranes Review. *Cell Biochem Biophys*, (2017).

124. W. Zhao, S. Prijic, B. C. Urban, M. J. Tisza, Y. Zuo, L. Li, Z. Tan, X. Chen, S. A. Mani, J. T. Chang, Candidate Antimetastasis Drugs Suppress the Metastatic Capacity of Breast Cancer Cells by Reducing Membrane Fluidity. *Cancer Res* **76**, 2037-2049 (2016).
125. T. F. Osborne, Sterol regulatory element-binding proteins (SREBPs): key regulators of nutritional homeostasis and insulin action. *J Biol Chem* **275**, 32379-32382 (2000).
126. H. Shimano, I. Shimomura, R. E. Hammer, J. Herz, J. L. Goldstein, M. S. Brown, J. D. Horton, Elevated levels of SREBP-2 and cholesterol synthesis in livers of mice homozygous for a targeted disruption of the SREBP-1 gene. *J Clin Invest* **100**, 2115-2124 (1997).
127. J. D. Horton, J. L. Goldstein, M. S. Brown, SREBPs: activators of the complete program of cholesterol and fatty acid synthesis in the liver. *J Clin Invest* **109**, 1125-1131 (2002).
128. S. Nandi, L. Ma, M. Denis, J. Karwatsky, Z. Li, X. C. Jiang, X. Zha, ABCA1-mediated cholesterol efflux generates microparticles in addition to HDL through processes governed by membrane rigidity. *J Lipid Res* **50**, 456-466 (2009).
129. A. R. Miserez, P. Y. Muller, L. Barella, S. Barella, H. B. Staehelin, E. Leitersdorf, J. D. Kark, Y. Friedlander, Sterol-regulatory element-binding protein (SREBP)-2 contributes to polygenic hypercholesterolaemia. *Atherosclerosis* **164**, 15-26 (2002).
130. K. Ma, P. Malhotra, V. Soni, O. Hedroug, F. Annaba, A. Dudeja, L. Shen, J. R. Turner, E. A. Khramtsova, S. Saksena, P. K. Dudeja, R. K. Gill, W. A. Alrefai, Overactivation of intestinal SREBP2 in mice increases serum cholesterol. *PLoS One* **9**, e84221 (2014).
131. N. Fournier, S. Tardivel, J. F. Benoist, B. Védie, D. Rousseau-Ralliard, M. Nowak, F. Allaoui, J. L. Paul, Eicosapentaenoic acid membrane incorporation impairs ABCA1-dependent cholesterol efflux via a protein kinase A signaling pathway in primary human macrophages. *Biochim Biophys Acta* **1861**, 331-341 (2016).

132. Y. W. Hu, X. Ma, X. X. Li, X. H. Liu, J. Xiao, Z. C. Mo, J. Xiang, D. F. Liao, C. K. Tang, Eicosapentaenoic acid reduces ABCA1 serine phosphorylation and impairs ABCA1-dependent cholesterol efflux through cyclic AMP/protein kinase A signaling pathway in THP-1 macrophage-derived foam cells. *Atherosclerosis* **204**, e35-43 (2009).
133. M. Makarewicz-Wujec, G. Parol, A. Parzonko, M. Kozłowska-Wojciechowska, Supplementation with omega-3 acids after myocardial infarction and modification of inflammatory markers in light of the patients' diet: a preliminary study. *Kardiol Pol*, (2017).
134. J. F. Ferguson, C. K. Mulvey, P. N. Patel, R. Y. Shah, J. Doveikis, W. Zhang, J. Tabita-Martinez, K. Terembula, M. Eiden, A. Koulman, J. L. Griffin, N. N. Mehta, R. Shah, K. J. Propert, W. L. Song, M. P. Reilly, Omega-3 PUFA supplementation and the response to evoked endotoxemia in healthy volunteers. *Mol Nutr Food Res* **58**, 601-613 (2014).
135. D. P. Rose, J. M. Connolly, M. Coleman, Effect of omega-3 fatty acids on the progression of metastases after the surgical excision of human breast cancer cell solid tumors growing in nude mice. *Clin Cancer Res* **2**, 1751-1756 (1996).
136. O. Ciftci, A. Cetin, M. Aydin, K. Kaya, F. Oguz, Fish oil, contained in eicosapentaenoic acid and docosahexaenoic acid, attenuates testicular and spermatological damage induced by cisplatin in rats. *Andrologia* **46**, 1161-1168 (2014).
137. H. Shen, C. Rodriguez-Aguayo, R. Xu, V. Gonzalez-Villasana, J. Mai, Y. Huang, G. Zhang, X. Guo, L. Bai, G. Qin, X. Deng, Q. Li, D. R. Erm, B. Aslan, X. Liu, J. Sakamoto, A. Chavez-Reyes, H. D. Han, A. K. Sood, M. Ferrari, G. Lopez-Berestein, Enhancing chemotherapy response with sustained EphA2 silencing using multistage vector delivery. *Clin Cancer Res* **19**, 1806-1815 (2013).

138. M. J. Wagner, R. Mitra, M. J. McArthur, W. Baze, K. Barnhart, S. Wu, C. Rodriguez-Aguayo, X. Zhang, R. L. Coleman, G. Lopez-Berestein, A. K. Sood, Preclinical mammalian safety studies of EPHARNA (DOPC nanoliposomal EphA2-targeted siRNA). *Mol Cancer Ther*, (2017).
139. J. M. Balko, J. M. Giltane, K. Wang, L. J. Schwarz, C. D. Young, R. S. Cook, P. Owens, M. E. Sanders, M. G. Kuba, V. Sanchez, R. Kurupi, P. D. Moore, J. A. Pinto, F. D. Doimi, H. Gomez, D. Horiuchi, A. Goga, B. D. Lehmann, J. A. Bauer, J. A. Pietenpol, J. S. Ross, G. A. Palmer, R. Yelensky, M. Cronin, V. A. Miller, P. J. Stephens, C. L. Arteaga, Molecular profiling of the residual disease of triple-negative breast cancers after neoadjuvant chemotherapy identifies actionable therapeutic targets. *Cancer Discov* **4**, 232-245 (2014).
140. P. Hauck, B. H. Chao, J. Litz, G. W. Krystal, Alterations in the Noxa/Mcl-1 axis determine sensitivity of small cell lung cancer to the BH3 mimetic ABT-737. *Mol Cancer Ther* **8**, 883-892 (2009).
141. A. R. Mattoo, J. Zhang, L. A. Espinoza, J. M. Jessup, Inhibition of NANOG/NANOGP8 downregulates MCL-1 in colorectal cancer cells and enhances the therapeutic efficacy of BH3 mimetics. *Clin Cancer Res* **20**, 5446-5455 (2014).
142. V. Palve, S. Mallick, G. Ghaisas, S. Kannan, T. Teni, Overexpression of Mcl-1L splice variant is associated with poor prognosis and chemoresistance in oral cancers. *PLoS One* **9**, e111927 (2014).
143. Y. Konno, P. Dong, Y. Xiong, F. Suzuki, J. Lu, M. Cai, H. Watari, T. Mitamura, M. Hosaka, S. J. Hanley, M. Kudo, N. Sakuragi, MicroRNA-101 targets EZH2, MCL-1 and FOS to suppress proliferation, invasion and stem cell-like phenotype of aggressive endometrial cancer cells. *Oncotarget* **5**, 6049-6062 (2014).

144. D. L. Hermanson, S. G. Das, Y. Li, C. Xing, Overexpression of Mcl-1 confers multidrug resistance, whereas topoisomerase II β downregulation introduces mitoxantrone-specific drug resistance in acute myeloid leukemia. *Mol Pharmacol* **84**, 236-243 (2013).
145. P. Geserick, J. Wang, M. Feoktistova, M. Leverkus, The ratio of Mcl-1 and Noxa determines ABT737 resistance in squamous cell carcinoma of the skin. *Cell Death Dis* **5**, e1412 (2014).
146. J. Yan, N. Zhong, G. Liu, K. Chen, X. Liu, L. Su, S. Singhal, Usp9x- and Noxa-mediated Mcl-1 downregulation contributes to pemetrexed-induced apoptosis in human non-small-cell lung cancer cells. *Cell Death Dis* **5**, e1316 (2014).
147. D. P. Zelinski, N. D. Zantek, J. C. Stewart, A. R. Irizarry, M. S. Kinch, EphA2 overexpression causes tumorigenesis of mammary epithelial cells. *Cancer Res* **61**, 2301-2306 (2001).
148. P. D. Dunne, S. Dasgupta, J. K. Blayney, D. G. McArt, K. L. Redmond, J. A. Weir, C. A. Bradley, T. Sasazuki, S. Shirasawa, T. Wang, S. Srivastava, C. W. Ong, K. Arthur, M. Salto-Tellez, R. H. Wilson, P. G. Johnston, S. Van Schaeybroeck, EphA2 Expression Is a Key Driver of Migration and Invasion and a Poor Prognostic Marker in Colorectal Cancer. *Clin Cancer Res* **22**, 230-242 (2016).
149. M. S. Kinch, M. B. Moore, D. H. Harpole, Jr., Predictive value of the EphA2 receptor tyrosine kinase in lung cancer recurrence and survival. *Clin Cancer Res* **9**, 613-618 (2003).
150. P. H. Thaker, M. Deavers, J. Celestino, A. Thornton, M. S. Fletcher, C. N. Landen, M. S. Kinch, P. A. Kiener, A. K. Sood, EphA2 expression is associated with aggressive features in ovarian carcinoma. *Clin Cancer Res* **10**, 5145-5150 (2004).

151. A. A. Kamat, D. Coffey, W. M. Merritt, E. Nugent, D. Urbauer, Y. G. Lin, C. Edwards, R. Broaddus, R. L. Coleman, A. K. Sood, EphA2 overexpression is associated with lack of hormone receptor expression and poor outcome in endometrial cancer. *Cancer* **115**, 2684-2692 (2009).
152. S. V. Mudali, B. Fu, S. S. Lakkur, M. Luo, E. E. Embuscado, C. A. Iacobuzio-Donahue, Patterns of EphA2 protein expression in primary and metastatic pancreatic carcinoma and correlation with genetic status. *Clin Exp Metastasis* **23**, 357-365 (2006).
153. H. Hou, Y. Kang, Y. Li, Y. Zeng, G. Ding, J. Shang, miR-33a expression sensitizes Lgr5+ HCC-CSCs to doxorubicin via ABCA1. *Neoplasia* **64**, 81-91 (2017).
154. J. L. Chou, R. L. Huang, J. Shay, L. Y. Chen, S. J. Lin, P. S. Yan, W. T. Chao, Y. H. Lai, Y. L. Lai, T. K. Chao, C. I. Lee, C. K. Tai, S. F. Wu, K. P. Nephew, T. H. Huang, H. C. Lai, M. W. Chan, Hypermethylation of the TGF-beta target, ABCA1 is associated with poor prognosis in ovarian cancer patients. *Clin Epigenetics* **7**, 1 (2015).
155. E. L. Hedditch, B. Gao, A. J. Russell, Y. Lu, C. Emmanuel, J. Beesley, S. E. Johnatty, X. Chen, P. Harnett, J. George, G. Australian Ovarian Cancer Study, R. T. Williams, C. Flemming, D. Lambrechts, E. Despierre, S. Lambrechts, I. Vergote, B. Karlan, J. Lester, S. Orsulic, C. Walsh, P. Fasching, M. W. Beckmann, A. B. Ekici, A. Hein, K. Matsuo, S. Hosono, T. Nakanishi, Y. Yatabe, T. Pejovic, Y. Bean, F. Heitz, P. Harter, A. du Bois, I. Schwaab, E. Hogdall, S. K. Kjaer, A. Jensen, C. Hogdall, L. Lundvall, S. A. Engelholm, B. Brown, J. Flanagan, M. D. Metcalf, N. Siddiqui, T. Sellers, B. Fridley, J. Cunningham, J. Schildkraut, E. Iversen, R. P. Weber, A. Berchuck, E. Goode, D. D. Bowtell, G. Chenevix-Trench, A. deFazio, M. D. Norris, S. MacGregor, M. Haber, M. J. Henderson, ABCA transporter gene expression and poor outcome in epithelial ovarian cancer. *J Natl Cancer Inst* **106**, (2014).

156. L. M. McShane, D. G. Altman, W. Sauerbrei, S. E. Taube, M. Gion, G. M. Clark, N. C. I. E. W. G. o. C. D. Statistics Subcommittee of the, REporting recommendations for tumour MARKer prognostic studies (REMARK). *Br J Cancer* **93**, 387-391 (2005).
157. M. J. Pencina, A. M. Navar-Boggan, R. B. D'Agostino, Sr., K. Williams, B. Neely, A. D. Sniderman, E. D. Peterson, Application of new cholesterol guidelines to a population-based sample. *N Engl J Med* **370**, 1422-1431 (2014).
158. F. Cortese, M. Gesualdo, A. Cortese, S. Carbonara, F. Devito, A. Zito, G. Ricci, P. Scicchitano, M. M. Ciccone, Rosuvastatin: Beyond the cholesterol-lowering effect. *Pharmacol Res* **107**, 1-18 (2016).
159. S. M. Hoy, Pitavastatin: A Review in Hypercholesterolemia. *Am J Cardiovasc Drugs* **17**, 157-168 (2017).

VITA

Angie Marie Torres-Adorno was born in Bayamón, Puerto Rico on October 22, 1988, the daughter of Luis Angel Torres-Quñones and María Magdalena Adorno-Ríos. After completing her studies at Miguel de Cervantes Saavedra High School in Bayamón, Puerto Rico in 2006, she entered The University of Puerto Rico at Bayamón in Bayamón, Puerto Rico. She received the degree of Bachelor of Science with a major in General Biology, minor in Biotechnology, from the University of Puerto Rico at Bayamón in June, 2011. In August of 2011 she entered The University of Texas MD Anderson Cancer Center UTHealth Graduate School of Biomedical Sciences to pursue her Ph.D. degree in Cancer Biology and Experimental Therapeutics.